Student thesis series INES nr 443

Humpback whale (*Megaptera novaeangliae*) location in Southeast Alaska: modeling the influence of mesoscale krill (*Euphausiacea*) patch depth and size

Christine Walder

2018
Department of
Physical Geography and Ecosystem Science
Lund University
Sölvegatan 12
S-223 62 Lund
Sweden

Christine Walder (2018).
Humpback whale (*Megaptera novaeangliae*) location in Southeast Alaska: modeling the influence of mesoscale krill (*Euphausiacea*) patch depth and size
Lokalisering av knölvalar (*Megaptera novaeangliae*) i sydöstra Alaska: vikten av krillstims (*Euphausiacea*) djup och storlek inom modellering
Master degree thesis, 30 credits in *Physical Geography and Ecosystem Analysis*
Department of Physical Geography and Ecosystem Science, Lund University

Level: Master of Science (MSc)

Course duration: *September* 2017 until *January* 2018

Disclaimer

Photographic credits: cover photograph taken by Christine Walder under NOAA research permit #18529. It depicts a large group of bubble-netting humpback whales in Chatham Strait, Southeast Alaska, USA.

Humpback whale (*Megaptera novaeangliae*) location in Southeast Alaska: modeling the influence of mesoscale krill (*Euphausiacea*) patch depth and size

---

Christine Walder

Master thesis, 30 credits, in *Physical Geography and Ecosystem Analysis*

Jonathan Seaquist, PhD
Lund University, Department of Physical Geography and Ecosystem Science

Andrew Szabo, PhD
The Alaska Whale Foundation

Exam committee:
Paul Miller, PhD
Lund University Department of Physical Geography and Ecosystem Science

Martin Berggren, PhD
Lund University Department of Physical Geography and Ecosystem Science

ABSTRACT

Humpback whales (*Megaptera novaeangliae*) require dense prey aggregations due to the high energetic cost of their feeding methods. Modeling studies have shown that when whales are on their feeding grounds, they are closely associated with high prey concentrations. These studies collapse the prey field into a two dimensional measure of prey abundance in horizontal space. However, patchiness is one of the dominant characteristics of marine systems. The three-dimensional structure of prey is known to affect rorqual whale (family *Balaenopteridae*) feeding kinematics and prey patchiness affects the foraging decisions of central-based marine predators.

This study aims to assess how spatial and temporal patterns in krill distribution affect the distribution of humpback whales across the feeding area of Frederick Sound and Lower Stephens Passage, Southeast Alaska, from 2006-2008. Data from hydroacoustic surveys were used to identify prey patches, and statistics related to their depth, size and backscatter intensity were calculated. These statistics, along with measures of prey hot spots for each survey, persistent prey hot spots, bathymetry and season were used in a spatially explicit Generalized Additive Model (GAM) to explain humpback whale distribution.

The model showed that whales preferred large, dense prey patches that occurred persistently. Whales were rarely found at patches covering less than 22 000 square meters vertically. With regards to depth, shallower patches at 40 meters depth were preferred. However, patches located at depths of approximately 90 meters were larger, occurred frequently, and were favored by whales as well. There was some indication that whales were more likely to be located at persistent prey hot spots.

A comparison of the prey patch explicit model and a model built using horizontal prey densities indicated that incorporating measures of prey depth and patch size greatly improved models of humpback whale distribution. The patch explicit model explained 59% of whale counts, while the horizontally averaged prey model explained 35%. Incorporating patch-explicit variables can be used to improve future modeling efforts for rorqual whale species abundance and distribution.

Keywords: physical geography and ecosystem analysis, humpback whales, krill, patchiness, vertical distribution, Generalized Additive Models (GAMs), spatial modeling

TABLE OF CONTENTS

1 INTRODUCTION

The main patterns and drivers of *Megaptera novaeangliae* (humpback whale) movement on a global scale are fairly well understood: whales undertake long annual migrations between nutrient rich summer feeding grounds and warm, predator-poor winter breeding grounds. Distinct subpopulations travel to defined feeding grounds, with low levels of travel between different feeding grounds by members of each subpopulation (Calambokidis et al. 2008). Within these feeding grounds, however, the drivers of whale movements are not well understood. The animals devote a large percentage of their time to feeding with the aim of building up lipid stores for subsequent migrations. They feed mainly on euphausiids (commonly referred to as krill, of the order *Euphausiacea*) and small schooling fish species (Clapham and Mead 1999).

For a species that spends more than half of its summer time feeding (Kennedy et al. 2014), prey is expected to play a large role in shaping the distribution of humpback whales. Indeed, large-scale modeling studies for several rorqual whale species (family *Balaenopteridae,* having baleen plates) have shown that both krill and fish abundance are important explanatory variables for whale location (Piatt and Methven 1992; Reid et al. 2000; Croll et al. 2005; Friedlaender et al. 2006; Brower et al. 2017). Humpback whales were found in association with geographically recurring krill hotspots. These krill retention zones occurred due to the interaction between prevailing currents and bathymetric features (Santora et al. 2010). The same association was seen in blue whales, which feed on the densest available euphausiid patches at the edge of an underwater canyon (Croll et al. 2005). Friedlaender et al (2006) found that krill density from 25 to 100 meters consistently had the greatest influence on whale abundance, while deeper krill were of minimal importance. This is the only study to make any distinction by depth. In an examination of the effect of scale on modeling, Reid et al. (2000) found that whales are positively associated with krill density at large spatial scales. However, this relationship weakens at smaller scales. These studies support the theory that prey density is an important determinant of whale location.

Because of their focus on large-scale patterns, these studies are unable to answer more specific questions about the three-dimensional environment in which whales forage. A series of studies have equipped foraging whales with acoustic tags (called D-tags) that detect whale motion, based on the level of sound generated by swimming at different speeds, as well as depth to better understand foraging behavior on the micro-scale. They have answered questions about the energetic costs and gains of feeding and have begun to identify depths and krill densities at which whales feed. Foraging whales seek out the densest krill layer, regardless of its depth (Goldbogen et al. 2011; Goldbogen et al. 2015; Burrows et al. 2016), although whales may feed within the shallowest portion of the densest layer (Goldbogen et al. 2008). The energetic cost of a lunge, the motion by which a whale engulfs prey, is high and makes a feeding dive much more costly than other dive types (Goldbogen et al. 2008). Indeed, feeding efficiency is strongly dependent on prey density rather than prey depth (Goldbogen et al. 2011). It may be that the energy gained from feeding on a patch at depth is offset if that patch is of sufficient density.

According to optimal foraging theory, overall krill patch characteristics related to the size of a patch, as well as its density and depth, are expected to be highly relevant to feeding whales. The energy gained from feeding on a dense patch must be weighed against the cost of finding a patch, which is related to its size and predictability. In addition, the transitory cost

of traveling between patches as well as traveling between a patch and the surface must be considered (Charnov 1976; Dolphin 1988).

Both Friedlaender et al. (2006) and Santora et al. (2010) have expressed a need to investigate how krill patch depth, density, shape, and volume on a fine-scale of less than one kilometer affect whale distribution. In a study on marine birds and fur seals, Benoit-Bird et al. (2013) characterized krill and pollock patches and found that patch depth, density and spacing were successful predictors of these marine predators' distributions. By contrast, averaged prey densities over the horizontal study area were not. This suggests that predator-prey relationships in pelagic marine environments are regulated by patchiness, and that this patchiness must be defined to accurately model marine predator distribution.

There is a gap in the literature with regards to how spatial and temporal patterns in small-scale krill aggregations of hundreds of meters affect large baleen whale distribution. Large-scale modeling studies have averaged patchy prey data into two-dimensional horizontal space, and micro-scale studies on whale foraging kinematics have disregarded ecosystem-wide conditions. Little work has been done to characterize krill patches and investigate their effect on the distribution of foraging whales.

This study aimed to fill this research gap by looking at the relationship between krill patch characteristics and foraging humpback whales. It focused on the confluence of Frederick Sound and Stephens Passage, a remote area in Southeast Alaska (SEAK). This is a fjordal marine environment characterized by inner channels and bays. Hydroacoustic surveys were used to sample the area during 2006-2008 for krill while simultaneously locating whales. Krill patches were identified and characterized using the sonar data.

This thesis aims to build a spatially explicit explanatory model describing humpback whale locations using krill, bathymetric and temporal variables. The research question to be answered is:

> *How do spatial and temporal patterns in krill distribution help to explain humpback whale location?*

The null hypothesis, H_0, that whales were distributed independently of krill, was tested against several alternative hypotheses, which are as follows:

> H_1: patch quality measures related to the depth, density and size of krill patches are weighed by feeding whales because these factors affect the whales' energy budget.
>
> H_2: spatial trends in krill distribution (i.e. clustering and hot spots) affect the location of foraging whales, since the travel costs between patches within a hot spot are lower.
>
> H_3: trends in krill distribution over time (i.e. persistent hot spots) affect whale distribution, since these whales are long-lived, return to the same areas year after year, and presumably have a good memory for where food has been available in the past (Weinrich 1998).

The model results were evaluated against these hypotheses to determine how spatial and temporal trends in krill patch distribution were related to humpback whale locations.

2 BACKGROUND

2.1 Marine Patchiness

"*It is now almost a platitude that variability in the ocean occurs throughout a hierarchical spectrum of space and time scales, of which only a fraction can be resolved by any single model, sampling method or observational program*" (Mackas et al. 1985).

Marine ecosystems have long been recognized for their patchiness, a phenomenon that is particularly evident in plankton communities. It is, in fact, rare for a single individual to live out its entire life under 'average' conditions. Patchiness occurs along a hierarchy of spatial and temporal scales, with different mechanisms forming the dominant drivers of patchiness at each scale (Mackas et al. 1985).

By following a small patch of water that has been 'stirred' by an eddy, the variation in the marine environment can be imagined. This patch has a unique set of chemical and biological properties. As the water is stirred and the patch moves, it is stretched and twisted until it is dispersed into smaller and smaller patches with new physical and chemical properties that result from mixing with the surrounding water. One large patch that has been stirred in such a way will break up into smaller and smaller patches with greater separation between each. However, biological systems are not static and organisms grow, reproduce, are eaten and move around within this context of ocean patchiness.

2.2 Krill and Patchiness

Euphausiids (order *Euphausiacea*), commonly known as krill, are small crustacean zooplankton that are found in all of the world's major oceans. See Figure 1 for a drawing of the krill species *Euphausia pacifica*. Krill form an important link in oceanic trophic systems (Miller et al. 2010). Different krill species feed on zooplankton, phytoplankton, and detritus (Mauchline 1980; Simmard et al. 1986). In turn, krill are eaten by other krill, fish, birds, seals, and the world's largest predators, baleen whales. Baleen plates line a whale's upper jaw and are used to filter out small prey from water. Many species of krill form dense swarms or schools, which present predators with a concentrated energy source (Nicol and Endo 1999). At the same time, the formation of krill patches is believed to be a protective mechanism, where individuals in the center of the patch are relatively protected from predation and predators are visually confused by the movement of the school (Hamner 1995; Hamner and Hamner 2000).

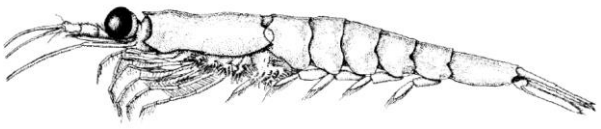

Figure 1. Drawing of *Euphausia pacifica*, one of the krill species found in the study site. Source: Brinton and Wyllie (1976).

The temporal and spatial scales of patch formation in Antarctic krill follow the general patterns seen in marine patchiness, with fine-scale swarms 1-100 meters in diameter and hours to days in duration, aggregated patches of swarms with 1-100 kilometer diameters and day to month-long durations, and finally concentrations of patches on the scale of hundreds of kilometers and months (Murphy et al. 1988). The formation of euphausiid aggregations is a result of complex interactions between oceanographic processes, biological processes and the limited movements that individuals are capable of.

2.2.1 Biological productivity

While predators may exert influence on zooplankton communities, it is more often the case that bottom-up processes are the major determinants of zooplankton abundance (Moloney et al. 2010). A number of processes are important to the water movement and nutrient mixing of coastal ecosystems, which in turn affect plankton aggregations. Upwelling, the process by which nutrient rich deep waters are brought to the surface, is an important driver of productivity. Wind-driven coastal upwelling occurs when winds blow parallel to shore This causes water to move offshore at a 90 degree angle due to Ekman transport and deeper water moves up to replace it. Tide-driven vertical exchange occurs when strong currents move along a shallow bottom and cause vertical stirring. Alongshore currents can cause upwelling along the continental shelf edge because of strong velocity shears (Hsuesh and O'Brien 1971). In fjordal systems, freshwater input through runoff plays a large role in structuring water flow patterns; it creates strong stratification in the water column, establishes fronts, and drives estuarine-like circulation within fjords and channels (Weingartner et al. 2009).

The temporal and spatial scale of an upwelling event will determine its impact on productivity. Upwelling is an important biological enhancement factor above large-scale features such as shelf breaks, where residence time is sufficient to lead to increased productivity and to propagate up the food web (Genin 2004). For smaller topographic features, upwelling can be an important mechanism for biological enhancement downstream of the feature, as short-term pulses of upwelling will be mixed into the photic layer downstream of the feature (Genin 2004).

2.2.2 Vertical Diel Migration

Krill exhibit vertical diel migration, in which they spend daylight hours at depth and swim to the surface at night (Heywood 1996; Sourisseau et al. 2008; Cohen and Forward 2016). During daylight hours, krill are located in layers at 50-300 meters depth (Simmard et al. 1986; Nicol and Endo 1999) where there is little light and visual predators cannot locate the krill as easily (Lampert 1989). These layers tend to be the densest aggregations formed by krill. At dusk, krill swim to the surface to feed. When they are satisfied, they will swim deeper again, sometimes forming an intermediate layer at night. A second feeding interval can take place before dawn, when krill will once again swim to the surface. When dawn breaks, the krill swim back to depth to escape visual predators (Sourisseau et al. 2008).

Although vertical diel migration is believed to be a predatory evasion mechanism in most krill species, this behavior has other implications. Water currents at different depths often have different velocities. Despite their ability to swim at a rate of 2-6 m/s (Heywood 1996), krill are planktonic organisms and are carried around by their surrounding environments' currents. This means that while at depth, krill will be transported at a different rate and potentially different direction from the plankton patch at the surface upon which they were feeding. Daily relocation can bring euphausiids to new prey patches, although this can also be disadvantageous if they are brought to an area with poor food conditions.

Euphausiids influence their distribution by actively swimming and by changing their position in the water column. Euphausiids use their vertical position to change which currents they are affected by, and this is often ontogenetic behavior that changes with life cycle transitions (Pillar et al. 1989; Tarling et al. 1999; Woodson and McManus 2007). Krill retention within an area is highly dependent on the proportion of time they spend at the surface, as surface and deep water flow is often highly variable and can result in different transport patterns (Sourisseau et al. 2006; Woodson and McManus 2007). Krill have the ability to remain within algal patches by swimming (Price 1989), and in at least some species schools are highly mobile and reactive to disturbances and food sources (Hamner 1984).

Local topography can directly influence the formation of mobile zooplankton aggregations. On a daily scale, shallow to intermediate depth seamounts (approximately 100-300 meters deep) or other features block the downward migration of zooplankton so that they are trapped above the bottom (Isaacs and Schwartzlose 1965; Genin 2004). Prey sources can be renewed daily through horizontal transport above such features, and zooplanktivorous fish have been known to concentrate over seamounts because of this topographic blockage mechanism (Fock et al. 2002). In response to vertical currents, zooplankton will swim vertically to maintain their depth and avoid the euphotic zone during daylight hours, thus aggregating in thin horizontal strips (Franks 1992). Krill can also be pushed against bathymetric features, resulting in local aggregations (Cotté and Simard 2005).

2.3 Humpback Whales (*Megaptera novaeangliae*)

2.3.1 Biology and Foraging Behavior

Rorqual whales, of the family *Balaenopteridae,* include nine extant species ranging in size from the minke whale (*Balaenoptera acutorostrata,* eight meters long) to the blue whale (*Balaenoptera musculus,* thirty meters long). They are characterized by baleen plates that grow from their upper jaw and pleats on their lower jaw that extend along their belly, and about a quarter of their body length is composed of the mouth region (Goldbogen et al. 2010). These whales use baleen to filter small fish and krill from water that they engulf. The humpback whale, *Megaptera novaeangliae,* is a rorqual whale found in the world's major oceans. It is an average of fourteen meters in length.

Rorqual whales must invest a high amount of energy into feeding. Whales dive below the surface to reach their prey, lunge a number of times, and then swim back to the surface to breathe (Simon et al. 2012). During a lunge, the whale will swim at high speeds and then open its mouth so that the hinged lower jaw expands to a 90-degree angle. Water hits the large surface area created by the opened jaw and expands the whale's buccal pouch. The whale then closes its mouth and water is filtered past the baleen plates, retaining any prey that was suspended in the engulfed water mass (Pivorunas 1979). The volume of water engulfed in each lunge is roughly equal to the body mass of the animal (Goldbogen et al. 2010). It is determined mechanistically and is not believed to be controlled by the whale; instead, engulfment volume is a constant value (Simon et al. 2012). Lunging suspends the whale's momentum almost completely, and it must accelerate from a near stand-still following each lunge (Simon et al. 2012; Cade et al. 2016). This repeated stop-and-go motion requires a large energy investment and makes it costly for rorqual whales to feed.

While all lunging is costly, prey distribution and movement have a modifying effect on lunging energetics. Lunges are normally done at an approximately 45 degree angle upwards, so that prey is attacked from below (Simon et al. 2012; Goldbogen et al. 2015; Cade et al. 2016). Whales have been shown to favor vertically distributed fish schools over those that are thin and stretched horizontally, presumably because it is easier to feed on them (Hazen et al. 2009). Lunges are often associated with a roll, which allows the whale to aim its lunge and account for the escape response of its prey (Goldbogen et al. 2013). The gymnastic maneuvers of the whale increase with prey agility, so that animals feeding on small fish with a quick escape response or more sparse krill patches must expend more energy to capture prey (Goldbogen et al. 2015; Cade et al. 2016). Because of this, a lunge on less agile prey species with favorable distributions requires less energy.

Little is known about humpback whales' ability to navigate and locate prey. Mothers travel with their calves to potential feeding grounds during the calves' first year of life, and visit a high number of feeding grounds even when prey quality is low (Weinrich 1998). This is believed to teach the calf where to feed in the future, and most calves show a preference for

sites they were exposed to as a calf (Weinrich 1998). They will also learn from experience and by locating other feeding whales, thereby building up a store of knowledge for potential feeding grounds and times to visit them (Weinrich 1998).

Humpback whales that have been tagged on their feeding grounds show great individual variation in movement patterns. Some whales remain in one area for weeks at a time, while others undertake long trips between different feeding areas. A tagging study based from the Aleutian Islands in Alaska tracked a whale that traveled over 2,800 kilometers over the course of 26 days, undertaking a journey of approximately 1,500 kilometers from the Aleutian Islands to Chukotka, Russia. On average, however, whales in this study traveled 46 kilometers a day and visited six feeding locations per day. They spent 62% of their time foraging and 13% of their time traveling, while 25% of their behavior could not be classified. However, the individual variation in this breakdown was quite large (Kennedy et al. 2014). Dalla Rosa et al. (2008) tagged whales on their feeding ground at the Antarctic Peninsula and found similarly high individual variation between whales and an average daily travel distance of 36 kilometers. These studies indicate that foraging whales travel distances on the order of 10s of kilometers each day, although individual behavior varies drastically.

On a smaller scale it also unclear how whales locate their prey. Researchers in the field say that whales will swim to prey patches that are tens of kilometers away (Hazen et al. 2009). Whales may use visual cues, and their eyes can be extended out from the body and rotated. They also have sensory hairs, much like vibrissae, on their snout which are activated by small currents or contact and indicate when prey densities are high (Ogawa and Shida 1950; Slijper and Harrison 1979; Friedlaender et al. 2009). There are even some reports of sonar/echolocation-like sound production during nighttime foraging bouts (Stimpert et al. 2007). Much still remains to be learned about how whales locate prey.

2.4 Optimal Foraging Theory

Optimal foraging theory states that animals foraging in a patchy environment must consider the costs and benefits associated with feeding on and traveling between different patches of differing quality (Charnov 1976).

2.4.1 Prey Density and Quality

Krill are calorically rich on a per-gram basis, making them an attractive food source. To survive seasonal periods of food scarcity, krill in high latitudes convert their energetic intake to lipid reserves in the form of waxes or fats (Falk-Petersen et al. 2000). Areas with high krill density are hotspots for other predators such as fish and birds (Falk-Petersen et al. 1990; Healey et al. 1990; Santora et al. 2009). However, krill are small (20-50 mm long) and many individual organisms must be consumed.

Krill live for several years and go through multiple life stages, which affects their quality as prey. As krill develop, their increasing size makes them more caloric but also allows them to swim faster. Krill growth is a function of size and maturity but also a function of food availability and temperature (Murphy et al. 2007). Different marine predators are known to target different size classes (Santora et al. 2010). In addition, diverse species have alternative spawning times, growth patterns, lipid levels, and lipid compositions (Falk-Petersen et al. 2000; Szabo and Batchelder 2014). Krill swarms may have distinct structures depending on the life stage of the krill. Swarms of immature krill are large and tightly packed, while smaller, more diffuse swarms are composed of more mature krill (Tarling et al. 2009). Ontogenetic migration, which is when particular life stages of a species migrate into discrete habitats, is seen in krill and can affect their spatial distribution (Trathan et al. 1993). Krill dynamics are quite complex and researchers are only now beginning to understand

them. However, spatial and temporal distribution, size, maturity, life stage, and previous conditions are all important in determining krill quality as a food source.

Because lunging is energetically costly, there is a threshold at which it is no longer cost-effective to feed. If the energetic cost of the lunge is not offset by the energetic gain associated with the captured prey, the whale will be losing energy (Goldbogen et al. 2011). This threshold behavior has been difficult to elucidate in the wild, and the exact prey density threshold at which whales will no longer forage is not known. Burrows et al. (2016) observed a potential value of 9 434 krill per m^3 or 1 223 grams/m^3 and Goldbogen et al. (2011) calculated a value of 100 grams/m^3 for blue whales.

Despite the high cost of a lunge, there is potential for very high energetic gain. At normal prey densities, feeding by rorqual whales results in net gains similar to those seen in other marine mammals (i.e. seals, porpoises, etc.). However, when high prey densities are available, the potential gain for a lunge feeder can be several orders of magnitude greater than that of any other marine predator (Goldbogen et al. 2011). Prey density therefore plays a large role in determining the quality of a prey patch for a rorqual whale.

2.4.2 Prey Patchiness

In addition to the high cost of a lunge, whales must weigh the transitory costs of feeding. There are two types of transitory costs: those associated with diving down to prey patches, and those associated with traveling between prey patches. According to optimal foraging theory, a whale that has to choose between a deep or a shallow prey patch of equivalent density will choose the shallow patch because transition costs are lower (Charnov 1976).

The advent of acoustic tags, or DTags, has triggered a series of studies looking at the fine-scale kinematics of whale diving behavior. DTags measure the acoustic noise in a whale's surroundings, and can be used to extrapolate the swimming speed of the whale and even identify lunges. Additional devices measuring depth, pitch and heading are associated with the tags and these data can be combined to build a three-dimensional track of the whale (Goldbogen et al. 2013).

The effect of prey depth on rorqual whale foraging behavior is entangled with other depth-dependent variables. While depth plays an important role in whale diving behavior, its exact implications are not known. Studies have shown that whales generally feed on the densest prey layer, regardless of its depth (Goldbogen et al. 2015), although some evidence suggests that whales will feed on the shallowest part of this layer (Goldbogen et al. 2008). Whether this occurs or not may depend on how thick the layer is (Burrows et al. 2016).

Feeding on shallow prey may optimize breathing patterns. When feeding on shallow prey (less than 25 m depth), whales will lunge once, then return to the surface to breathe (Ware et al. 2011). This optimizes the handling time required to process prey once it has been engulfed by combining it with returning to the (relatively nearby) surface to breathe. With dives below 100 meters, whales lunged many more times before returning to the surface to breathe. Deep dives are associated with increased surface time and increased ventilation, which indicates that they require more energy. However, this may be a result of the number of lunges undertaken rather than the depth of the dive, since dense prey patches are often located at depth (Goldbogen et al. 2008; Ware et al. 2011). Whales may dive at their physiological depth and duration limits when prey patch quality is at its highest and maximum exploitation is desired, despite its added cost (Goldbogen et al. 2008).

2.5 Background on General Additive Models (GAMs)

2.5.1 General Information

General Additive Models (GAMs) have become popular in the literature because they are easy to interpret, flexible, nonparametric, and do not require linear relationships between independent and dependent variables. They can be used to uncover new relationships, as their form does not need to be specified *a priori*. Instead, they fit a smooth function to the existing data in whichever shape provides the best fit. Endless combinations of complex model forms are therefore possible with GAMs.

In the field of marine spatial modeling, GAMs have been used by a number of studies to investigate the relationship of cetaceans to various explanatory variables. They have uncovered relationships between whales and krill density, where whale abundance is positively related to krill density at low values and plateaus at higher values (Friedlaender et al. 2006). They have also been used to show the relationship between whale abundance and other environmental variables (Dalla Rosa et al. 2012). GAMs have been selected as the tool of choice in building a large-scale predictive model of cetacean abundance covering the entire west coast of the United States (Barlow et al. 2009). Because of their applications to a number of research questions, they are widely accepted in the field of marine modeling.

Despite their many advantages, the results of a GAM must be treated with caution because they are known to overfit data. The output of a GAM may appear to explain much of the variance in the data, but the relationships can be difficult to interpret ecologically. Therefore, it is important to either restrict the model form by limiting its degrees of freedom or to keep in mind the tendency to overfit when interpreting results (Zuur et al. 2011).

2.5.2 Theory

A GAM is based on the idea that the relationship between predictor and dependent variables is a smooth function. The shape of the relationship does not need to be known beforehand, but is instead determined by the model. The relationships for all predictor variables are estimated simultaneously and then added to create a predictive model of the dependent variable. One or many link functions are used to connect the expected value to the predictor variables. The smoothness of the predictor functions can be controlled by penalizing model complexity. Model complexity can be seen as the 'wiggliness' of the model fit. Several packages are available to build a GAM in R, but the *mgcv* package is used most widely in the literature.

A Generalized Additive Model (GAM) is a form of linear modelling that has relaxed many of the assumptions of a traditional linear model. GAMs take the form of

$$g(\mu_i) = X_i^*\theta + f_1(x_{1i}) + f_2(x_{2i}) + f_3(x_{3i}, x_{4i}) + \ldots$$

where

$$\mu_i \equiv E(Y_i) \text{ and } Y_i \sim \text{some exponential family distribution}$$

μ_i is the average of the response variable, while Y_i are the individual responses. $g(\mu_i)$ is a monotonic, smooth link function where μ_i generally belongs to some exponential family distribution. Examples of the link function include a log, identity, or square root. Some exponential family distributions are gamma, Poisson, normal, and Gaussian. The X_i^* is a row of the matrix of all parametric predictor variables, and θ is the parameter vector. The f_j are smooth functions of the predictor variable covariates x_j. The j notation refers to the covariate used (x_j) to make the smoothing function (f_j) (Wood 2006). Unlike a traditional linear model, the final model function of a GAM does not include traditional constants since the

smooth functions that make up a GAM cannot be represented by traditional equations. This makes it more difficult to interpret both the direction and magnitude of each variables' contribution to the overall model performance.

Using smoothing equations introduces the issues of how to represent the equations and how to decide on the degree of smoothness to use. A number of smoothing basis equations can be used in a GAM, including thin plate regression splines with or without shrinkage, cubic regression splines with or without shrinkage, cyclic cubic regression splines and p-splines. Two smoothing functions are available in the *mgcv* package. Tensor product smoothing is invariant to the linear rescaling of covariates but not to rotation of covariate space, while thin plate regression spline (TPRS) smoothing is invariant to the rotation of covariate space but not the rescaling of covariates. It is therefore common to use tensor product smoothing for spatial coordinates. Tensor product smoothing is in general good for modeling the smooth interactions of quantities that have been measured with different units or when the interactions may require very different degrees of scaling. They are also computationally inexpensive. TPRS smoothing is good for modeling the smooth interactions of variables with the same units, although computational costs can be high. With a good model, however, the type of smoothing that is used should not influence the general form of the model.

The prediction error of the model is estimated to optimize selection of a smoothing parameter. If the scale parameter of the model is known, the expected mean square error (MSE) of the model is represented by the Un-Biased Risk Estimator (UBRE). If the scale parameter is unknown, smoothness penalization is achieved by using cross validation. In this approach, one datum is iteratively dropped from the dataset, the square error is calculated for this new dataset, and then the average square error for all iterations is taken as the GCV score (Wood 2006).

2.5.3 Model Selection and Evaluation

Model selection using a GAM is similar to model selection with a traditional linear model. Once the model has been run, variables can be removed through stepwise selection (forward or backward) or shrinkage. Forward stepwise selection involves adding each variable one by one to the model, and proceeding with the variable that contributes most to the model. This is repeated in an iterative process until no new variables can be added. In backwards stepwise selection, the variable that contributes least to the model is removed and the model is re-run. This is repeated until no additional variables can be removed. The contribution of a variable to the model can be assessed using a combination of AIC scores, *p*-values, and visual assessment of the form of the smooth function and model residuals. Shrinkage works by shrinking the coefficients of variables to near 0 instead of removing them from the model completely as is done in a stepwise approach. Models can be compared using GCV or UBRE scores, adjusted R-squared values, and AIC scores.

The *p*-values that are calculated for the explanatory variables of a GAM have been shown to be unreliable in some situations. They are calculated using an F-test. If the degrees of freedom of a smoothing spline have been estimated, the uncertainty of this estimation is not incorporated in the calculation of the *p*-values. Based on simulations, *p*-values that are close to 0.05 may be incorrect. When the null hypothesis is true, *p*-values may be around half their correct value. This means that a *p*-value between 0.001 and 0.05 should be treated with caution, while values outside this range can generally be accepted (Wood 2006).

Hypothesis testing can be performed using GAMs to compare two models and determine which performs best. However, this must be treated with caution due to the uncertainty attached to *p*-values. If *p*-values are near the threshold for rejecting a hypothesis, it is better to use un-penalized GAMs and to limit the basis dimension for smoothing

equations. This will result in a smoother, less powerful, but more correct model. When scale parameters of the model are unknown, an F-ratio test can be used to test hypotheses against each other. The maximum penalized likelihood estimate and effective degrees of freedom of the model are used in place of maximum likelihood estimates and real degrees of freedom, respectively (Wood 2006).

Remaining spatial or temporal autocorrelation in the residuals of a model indicates that some spatial or temporal patterns have not been captured by the model and must be dealt with. The spatial autocorrelation of the model residuals can be tested using Moran's I to make sure that spatial patterns do not exist in the residuals. If they do, the model may be missing an explanatory variable which has a spatial component. If no additional variables are available, the latitude and longitude of data may be entered directly into the model so that spatial effects are considered. If this is not sufficient, mixed effects modeling using i.e. General Additive Mixed Models (GAMMs) may need to be considered. A spatial autocorrelation structure can be added directly to the model using GAMMs. The same can be done with a temporal autocorrelation structure (Zuur et al 2009). This allows for a flexible way to deal with spatial or temporal autocorrelation in the model.

3 DATA AND METHODS

Data on whales and backscatter conditions (a proxy for krill, see discussion for explanation) were collected in the study area from 2006-2008. Backscatter data were used to locate and analyze patches in the study area. They were also used to locate momentary and persistent krill hot spots. These variables were used in a generalized additive model (GAM) to explain whale locations as a function of backscatter and bathymetry.

These data, along with net samples of euphausiids, were collected for a PhD dissertation to assess life history and abundance patterns in euphausiids, seasonal shifts in whale abundance, and patterns of humpback whale location relative to prey (Szabo 2011). The whale data were formerly used in a publication on humpback preference for adult krill (Szabo 2015). However, no spatially explicit results using either the whale or the sonar data have been published and the sonar data have not been published at all. The analyses of the sonar data within Szabo (2011)'s dissertation were not as robust as the approach presented here, and did not take into account patch depth or density. This thesis presents a new approach to analyzing the sonar data.

3.1 Study Area

This study was carried out at the confluence of Frederick Sound and Lower Stephen's Passage in Southeast Alaska (56° to 57° N, 133° to 134° W). These are inside waters that are characterized by a series of fjordal channels and protected bays, abundant streams and rivers, and strong tidal currents (Figure 2). Mean daily tidal oscillation at The Brothers Islands is, on average, 4.5 meters (National Ocean Services 2017). High annual precipitation levels contribute to substantial freshwater runoff, especially during the spring snowmelt (Weingartner et al. 2009). A paucity of information remains about the area, particularly with respect to oceanography, marine biogeography and marine biology. However, it is a known hotspot for humpback whales feeding on krill (Dahlheim et al. 2009).

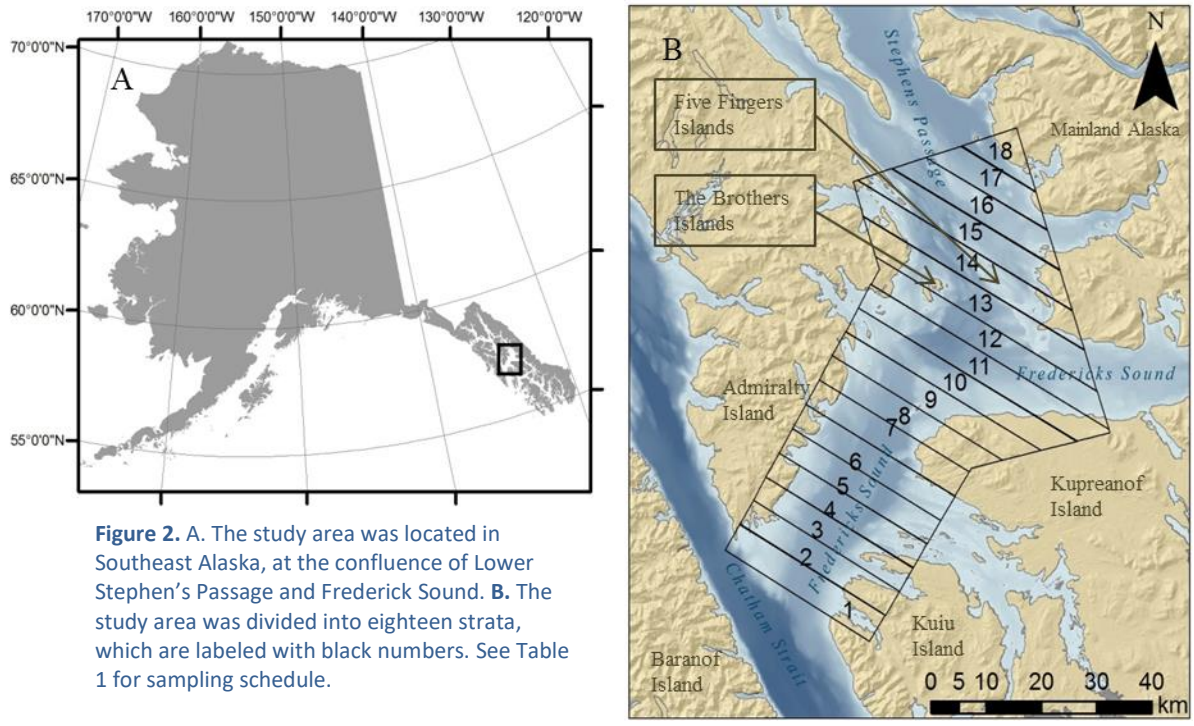

Figure 2. A. The study area was located in Southeast Alaska, at the confluence of Lower Stephen's Passage and Frederick Sound. **B.** The study area was divided into eighteen strata, which are labeled with black numbers. See Table 1 for sampling schedule.

3.2 Hydroacoustic (Sonar) Data

Sonar is widely used in fisheries research to assess the abundance or distribution of organisms in the water column. Hydroacoustic (sonar) surveys were completed in Frederick Sound and Lower Stephen's Passage between May and September in 2006 (n=5), 2007 (n=3) and 2008 (n=6) (Table 1). Surveys were completed approximately every 20 days during 2008, the most complete year. The study area was divided into 18 strata, each approximately 4.8 km wide (Figure 2). A stratified random sampling design was used, where the location of the transect line within each stratum was randomly decided for each survey (see Appendix S1, Figure S1for locations of transect lines).

A 120 KHz split-beam echosounder (Simrad EK60) sonar device was towed behind a research vessel traveling at 8-10 km/hr during daylight hours. The 120 KHz frequency was chosen to optimize detection of krill and small fish (MacLennan and Simmonds 2013). Sonar operates on the principle that objects in the water column reflect sound back towards the transmitting device. This returns a decibel output, calculated as the log of the ratio of the amount of energy received divided by the amount of energy sent out. For statistical purposes, the log values were back-transformed to a linear measure called the Nautical Area Scattering Coefficient (NASC). NASC is the backscattered sound, standardized by the volume of the insonified water, and extended to the area of one nautical mile (MacLennan and Simmonds 2013).

Sonar data were processed using the EchoView software suite. Data were processed using four different threshold levels: -75dB, -65dB, -60dB, and -55dB. Signals below the decibel threshold were removed from the data to eliminate weak signals. Data were binned into 10-meter vertical by 100-meter horizontal (measured by the distance traveled by the boat) blocks. Signals below 150 meters were eliminated due to deterioration in signal quality. The upper two meters of the water column were removed to eliminate surface noise. One meter directly above the bottom was also excluded to eliminate errors in automated sonar bottom detection and other strong, bottom associated targets. The contribution to NASC from single targets presumed to be too large to be whale prey (e.g., large fish) were removed (see Appendix S2 for methodology). After examining the sonar data, there appeared to be some issues in the -75dB data. The -65dB data allowed for flexibility in determining the importance of NASC values across a dynamic range and was used for all further analyses.

I received .csv files of each processed sonar file, and conducted the single target correction and comparison of processing thresholds myself.

3.3 Whale Data

In 2006 and 2007, a second whale survey vessel traveled along the center of every other stratum. In 2008, the whale spotters were located on the sonar vessel and thus surveyed every stratum. The observer was located at the bow of the vessel and scanned continuously for whales. Once spotted, the vessel's GPS chart-plotter was used to place the whale relative to reference points and then calculate the range and bearing to the whale from the ship's location. Spotters were regularly trained in accurate distance estimation on the water using buoys, fixed targets, and a radar device to validate their estimations. Spotters noted during data collection if a whale was believed to be a resight and referred to the time of the original whale sighting to link the two individuals or groups in the dataset.

Whale data were then corrected for a variety of issues. To deal with errors in range estimation that placed whales on land, whales were moved closer to the boat's location until they were no longer on land. Location data was filtered so that only whales spotted within the stratum being surveyed were retained for further analysis. Resighted whales were also included only once in the dataset; the most recent sighting was retained when possible. See Appendix S1, Figure S2 for the filtered results of the whale surveys and maps of the strata

sampled during each survey. I received a .csv file of all whale spotting events and conducted all data cleaning and correction myself.

Table 1. Sampling effort of Frederick Sound and Lower Stephens Passage, Southeast Alaska. In 2006 and 2007, whale spotting was done from a separate boat from that of the sonar survey. In 2008, the sonar and whale survey were conducted from the same boat and were therefore always done on the same day. 2008 represents the most complete dataset. See Figure 2 for the study area strata, Figure S1 of Appendix S4 for transect location and Figure S2 of Appendix S4 for whale location.

Survey	Year	Sonar Date	Whale Date	Sonar Strata	Whale Strata
Y6s1	2006	5/20-5/26	5/21-5/25	1-11, 13-18	1, 3, 5,7, 9, 11, 13, 15, 17
Y6s2	2006	6/5-6/11	6/8-6/10	1-4, 7-8, 10-17	1, 3, 5,7, 9, 11, 13, 15, 17
Y6s3	2006	7/29- 8/10	7/30-8/7	1-4, 6-18	1, 3, 5,7, 9, 11, 13, 15, 17
Y6s4	2006	8/23-8/30	8/24-8/28	1-18	1, 3, 5,7, 9, 11, 13, 15, 17
Y6s5	2006	9/13-9/16	9/14-9/15	12-18	11, 13, 15, 17
Y7s1	2007	7/19-7/21	7/22	11-18	11, 13, 15, 17
Y7s2	2007	8/13-8/15	8/15	11-17	11, 13, 15, 17
Y7s3	2007	9/12-9/14	9/13	11-16	11, 13, 15, 17
Y8s1	2008	5/22-5/27			1-18
Y8s2	2008	6/8-6/13			1-18
Y8s3	2008	6/27- 7/3			1-18
Y8s4	2008	7/15-7/22			1-18
Y8s5	2008	8/5-8/10			1-18
Y8s6	2008	8/27-8/31			1-17

3.4 Grid cells

The study area was divided into grid cells to be used in statistical analyses. The tradeoff between choosing an ecologically significant versus a statistically optimal size was assessed. A 4.8km width was necessitated by the survey design, and a 6.5km length was chosen to create grid cells that contained a sufficient number of whale points per grid cell and captured patterns in backscatter. Grid cells were drawn in ArcGIS by placing the beginning of a grid cell along the coast and including all sonar and whale points; the side where the sections were begun was alternated so that the grid cells bordering the coasts were not unfairly optimized for one side of the study area. The area was divided into 100 grid cells, but only 78 of these contained data from the same whale and sonar survey at least once.

3.5 Backscatter Patch Definition

The sonar blocks (100m horizontal x 10m vertical) were viewed in two-dimensional space with distance along the transect line on the x-axis and depth on the y-axis. Patches were defined within this space. All blocks within a patch were above a cutoff NASC value and within a set vertical and horizontal linkage distance from each other.

NASC cutoff values of 50,100,150 and 200 were tested in the model (Figure 3A). There were insufficient data to convert NASC to krill density. Therefore, this data could not be compared to the potential prey density thresholds proposed by Burrows et al (2016).

Literature values were used to determine the vertical and horizontal linkage distances for a patch. Published studies showing whale dive profiles indicate that the usual vertical distance between lunges ranges from 10-30 meters (Goldbogen et al. 2008; Goldbogen et al. 2015; Burrows et al. 2016). The horizontal distance traveled during a dive was approximately 300-500 meters. These values were collected as part of a focal follow study undertaken concomitantly with the hydroacoustic habitat surveys from 2006-2008. Individual whales were followed for several hours and their movement tracks were recorded. On

average, a humpback whale's dive resulted in 300m horizontal displacement (unpublished data, D. Derrick). Because of this, vertical and horizontal distances between blocks belonging to the same patch were set at 30m and 300m, respectively.

The NASC cutoff value and linkage distances were used to build custom code in R to identify patches (see Appendix S3A). Patches were identified within each grid cell, such that patches spanning two grid cells were cut at the grid cell boundary (Figure 3B). The distance along the transect line and the depth of the center of the block were used as spatial coordinates for each 100m x 10m block. Patches were identified automatically using hierarchical clustering analysis with a single linkage method. Hierarchical clustering takes a set of points and assigns each point to its own cluster. The closest clusters are then grouped together, and this process is repeated until there are no nearby groups. The single linkage method combines nearby groups in a 'friends of friends' approach. Groups that are within the linkage distance in either the x or y direction are combined. A scaling factor was applied to the depth of each sonar block so that the horizontal and vertical distance thresholds between blocks were equivalent and could be clustered using hierarchical clustering. Hierarchical clustering was run on all blocks above the cutoff NASC value using the R package *stats* (R Core Team 2014).

The original values used in the NASC layer definition were based closely on known whale diving behavior. However, after inspecting the results, other distance threshold values were also tested to build an optimal NASC layer definition to be used in the final model. Grid cells with zero NASC values were dropped from the model because there was no way to represent the depth of the patch; therefore, to reduce the occurrence of zero values lower NASC cutoffs were tested.

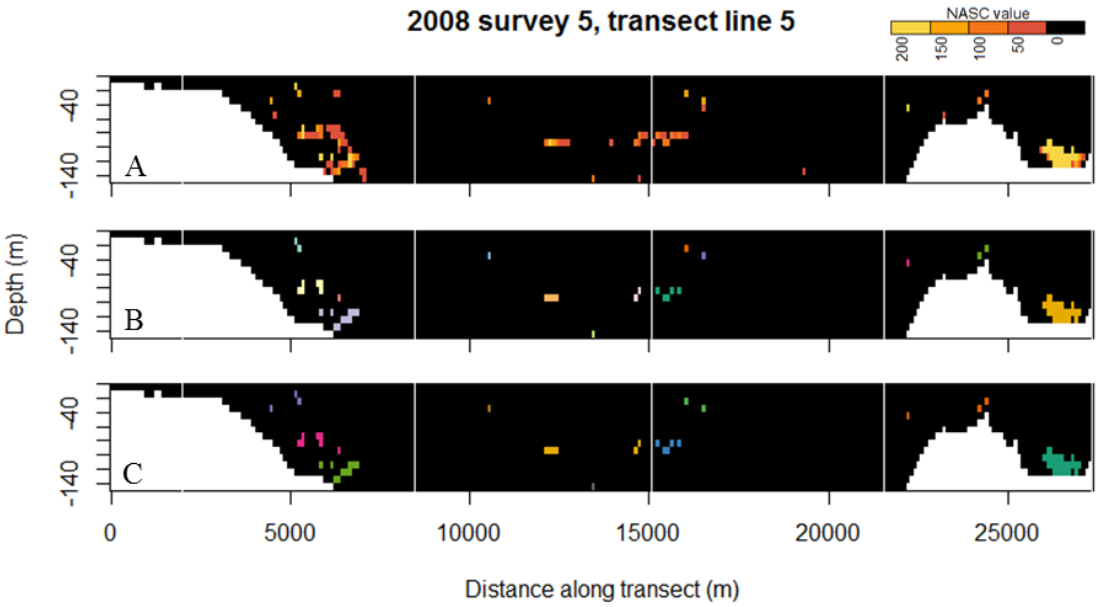

Figure 3. Example of patch identification and grouping. Results for transect line five of the fifth survey of 2008 are shown. Each pixel represents an averaged 100 meter horizontal by 10 meter vertical block of sonar data, collected at 120 KHz and processed at the -65dB threshold. White vertical lines represent grid cell boundaries. **A.** Visualization of NASC values separated by increments of 50. All values above 200 were grouped together (max= 20 761). **B.** Each patch, which was defined as blocks with a NASC value of 100 or greater within 400 meters horizontally and 20 meters vertically of each other, is represented by a different color. **C.** These patches were then grouped by depth, with each group represented by a different color.

Because there were many small patches within a grid cell, it was deemed important to combine patches into a more meaningful unit representative of overall conditions on the spatial scale of the analysis. Patches were thus grouped according to depth using custom code in R (Figure 3C, and see Appendix S3B). Groups were comprised of patches in a grid cell

with a depth range of no more than 35 meters. This was chosen based on whale diving behavior and was believed to preserve patch depth. Statistics were calculated for each group: mean depth, mean NASC, mean thickness, total area, total length, and number of patches within the group. When calculating means, each patch was weighted by its area. These methods were a simplification of the methods described by Barange (1994).

3.6 Analysis of Patches

Backscatter patches were analyzed for trends in depth and time. The patch variables that were assessed were the total NASC above 100 in each grid cell, the average depth of all patches in each grid cell, the total area of patches in each grid cell, and the average NASC values across all patches in a grid cell (see Table 2). Trends in depth were assessed by binning patches into depths of 0-10, 10-30, 30-50, 50-70, 70-90, 90-110, 110-130, and 130-150 meters. A one-way ANOVA was used to test the effect of depth on backscatter and patch area. A Tukey's honestly significant differences post-hoc test was applied to determine which depths were significantly different from each other. Seasonal trends were assessed by binning all patches into 20-day segments beginning at the 120^{th} day of the year and ending at the 260^{th}. These segments corresponded to the dates of the six surveys of 2008. A repeated-measures ANOVA, with habitat grid cells as the repeated measure, was used to assess the effect of season on patch depth and total backscatter. A Tukey contrasts multiple comparisons of means post-hoc test was used to determine which time periods were significantly different from each other.

3.7 Modelling

3.7.1 Explanatory Variables

A. Bathymetric and Oceanographic Variables

The mean depth, slope, and aspect of each grid cell were calculated using 40x40 meter resolution bathymetric data. The bathymetric data was derived from the sonar surveys, which detected bottom depth, and then kriged over the study area. This data was given to me as a raster file. The circular mean of 0-360° aspect data for each grid cell was calculated in R using the *circular* package. Rugosity, or 2D:3D surface area, was calculated to represent the bottom area that was actually exposed to the water and over which water flowed and interacted with using the equations:

$$\text{2D:3D Surface Area} = \textit{3D Area} \div \textit{2D Area}$$
$$\text{Where } \textit{3D Area} = \textit{2D Area} \div \cos(\textit{slope})$$

2D Area was the area of a single raster cell (1600 m^2), *slope* was the 40x40meter resolution slope, and *3D Area* was the resultant 40x40meter resolution area of exposed surface area. A ratio close to 1 meant that the bottom was essentially flat, while higher numbers were indicative of a rougher surface. The distance to the closest point on land was measured from the center of each grid cell.

The direction of water flow through the study area was derived using the conceptual circulation scheme for Southeast Alaskan shelf waters proposed by Weingartner et al (2009). I drew the water flow direction for each grid cell in ArcGIS. The grid cell aspect, ranging from $0\text{-}359^0$, was subtracted from these values, also ranging from $0\text{-}359^0$, to give the direction of water flow relative to bottom aspect, which ranged from -359 to 359^0. To put this in context, water flowing north over a northward facing slope had an output of 0^0, water flowing south over a northward facing slope had a value of 180^0, and water flowing north

over a south-facing slope had a value of -180^0. All calculations were carried out in ArcGIS (Version 10.5) unless otherwise stated.

B. Temporal Variables

Time of day (TOD) was calculated as the number of hours past midnight at which the sonar passed over the center of the grid cell. Krill undertake vertical diel migration, which affects the depth and density of krill patches. Time of day may thus influence the quality of prey patches. Day of year (DOY) was the number of days past January 1st. The time from high tide, given as a range of -6 to 6 hours, was calculated as the difference between the average time of when a whale was spotted in a grid cell and the time of high tide. Tide data distributed by NOAA (National Ocean Services 2017) was used for the Brothers Islands (57.295N, -133.797W).

C. Backscatter Variables (NASC)

To begin to answer some of the questions about whether depth, volume, or density of prey were most important to foraging whales, **(1)** the shallowest, largest, and most dense group of patches within each grid cell were identified. For grid cells with only one patch group, the same patch was used multiple times. The mean NASC, total vertical area, mean depth, total length and mean thickness were calculated for each of these patch groups. **(2)** Averaged values representing all patches in each grid cell were also calculated. The mean depth, mean thickness, mean NASC, total area, and total length for all patches as well as the number of patches were calculated for each grid cell. In addition, **(3)** the total NASC above 100 was calculated for each grid cell. This represented the total available NASC in each grid cell.

D. Hot Spot Analysis

A hot spot analysis was run to evaluate if momentary and persistent hot spots were present in the study area. Mean NASC values were used for each grid cell per survey. Mean NASC was calculated by summing the NASC value of all sonar blocks in a grid cell and dividing by the number of sonar blocks. The Getis-Ord Gi* was used with equal weights for all neighbors within 8 and 15km of each grid cell. The output of the hot spot analysis is a Z-score that is standardized and comparable across analyses.

Fourteen *momentary* hot spot analyses were conducted, showing where high and low backscattering values were clustered in space for each survey. A hot spot, with a z-value greater than zero, indicates that the grid cell is located in an area with higher mean NASC values than the average conditions over the entire study site. A cold spot, with a z-value less than zero, indicates that the conditions around the grid cell are lower than the average of the study site.

The mean of all z-scores for each grid cell was calculated to evaluate if there were *persistent* hot or cold spots. When the mean of the hot spot analysis was greater than or less than zero, it indicated that the conditions in that area were typically hot or cold, respectively. The hot spot analysis was carried out in RStudio using the *spdep* package (Bivand et al. 2013; Bivand and Piras 2015).

E. Spotter Bias

Whale spotters recorded visibility, wave height and wind speed. These measures can directly or indirectly affect the probability that a whale is detected and were therefore included in the model. The time between whale detection and the sonar survey was calculated as *whale time – sonar time* (ws_hours) and averaged for each grid cell. This was a proxy for the distance of the whale from the spotting vessel for the 2008 data and was therefore included as a spotter bias variable.

Table 2. All variables generated for the modeling analysis. Variables were calculated for conditions in each grid cell. The last column shows if the variables were included in the initial modeling, where all non-collinear variables were used. Collinear bathymetric variables were dropped, and collinear backscatter variables were not included in the same model.

	Variable	Unit	Trans-formation	Abbreviation	Included
Whales	Whale count	Number	None	nwhales	Yes
	Whale group count	Number	None	nwhales_grp	No
Bathymetry	Depth	Meters	None	depth	Yes
	Slope	Degrees	None	slope	No
	Aspect	Degrees	None	aspect	No
	Water flow direction	Degrees	None	wflow	No
	Water flow direction with respect to bottom aspect	Degrees, -360 to 360	None	asp_wflow	Yes
	Rugosity (2D:3D area), mean	ratio	None	asprat_mean	Yes
	Rugosity (2D:3D area), standard deviation	ratio	None	asprat_sd	No
	Distance to land	Meters	None	dis	No
Time	Time of day	Hours	None	TOD	Yes
	Day of year	Days past Jan 1st	None	DOY	Yes
	Time of sonar survey – time of high tide	Hours	None	Tide	Yes
Backscatter (NASC)	Momentary hot/cold spots (Getis G^*_i)	Z-score	None	locZ	Yes
	Persistent hot/cold spots (Getis G^*_i mean)	Z-score	None	meanZ	Yes
	Total backscatter within all patches	NASC	ln(NASC)	tNASC	Yes
	Backscatter, area-weighted average of all patches	NASC	ln(NASC)	NASC_av	Yes
	Patch depth, area-weighted average of all patches	Meters	None	depth_av	Yes
	Patch area, total of all patches	$Meters^2$	ln(area)	area_av	Yes
	Total number of patches in grid cell	Integer	None	npatch	Yes
	Total length of patches in grid cell	Meters	None	len	No
	Area-weighted average thickness of patches in grid cell	Meters	None	thick	No
	Mean backscatter of the shallowest group	NASC	ln(D_NASC)	D_NASC	Yes
	Mean patch depth, the shallowest group	Meters	None	D_depth	Yes
	Total patch area, the shallowest group	$Meters^2$	ln(D_area)	D_area	Yes
	Mean backscatter of the densest group	NASC	ln(K_NASC)	K_area	Yes
	Mean patch depth, the densest group	Meters	None	K_depth	Yes
	Total patch area, the densest group	$Meters^2$	ln(K_area)	K_NASC	Yes
	Mean backscatter of the largest group	NASC	ln(V_NASC)	V_area	Yes
	Mean patch depth, the largest group	Meters	None	V_depth	Yes
	Total patch area, the largest group	$Meters^2$	ln(V_area)	V_NASC	Yes
Spotter Bias	Visibility	0-10	None	Vis	Yes
	Wave height	Feet	None	Waveheight	Yes
	Wind speed	Knots	None	Windspeed	Yes
	Time of sonar survey – time of whale survey	Hours	None	ws_hours	Yes

F. Variable Checking and Selection

All model variables were assessed for outliers, data spread, and collinearity. Model variables were inspected for outliers using boxplots. Patch area and NASC variables were log-transformed to attain an even spread. Model variables were inspected for collinearity using the variance inflation factor (VIF). Collinear variables often have similar explanatory power in a model, thus masking significant ecological relationships. A backwards stepwise procedure was used to remove collinear variables with a VIF greater than 3 (Zuur et al. 2010). The variables were then visually examined using pair plots and inspected for Pearson's correlation coefficients greater than 0.75 to ensure independence. Variables are listed in Table 2. Collinear variables were not included in the model.

Grid cells with poor data quality or coverage were dropped from the modeling analysis. Grid cells with less than 500 meters of sonar survey effort were dropped. If there was more than four hours between the whale and the sonar survey, the grid cell was also dropped. This eliminated much of the data from 2006 and 2007, since the whales and hydroacoustic surveys were conducted from separate boats with different sampling schedules. The filtered 2006 and 2007 data was deemed to be sampled in an equivalent method to that of 2008 and was therefore included in the model. The model was therefore built on a multi-year data set, which eliminates bias related to year-specific phenomena and makes it more general. Grid cells with no patches were also dropped from the analysis (n=15) because there was no accurate way to represent the depth of the backscatter and GAMs require a value for every variable associated with a data point for it to be included in the model. A total of 480 grid cells were used to build the model. All of these grid cells had complete data and were deemed to be sampled in an equivalent manner.

3.7.2 Statistical Model

Whale counts were modeled using a Poisson distribution and a log-link function:

$$\ln(E[n_i]) = \sum_k s_k(z_{ik}) + \text{offset}(\ln[gridcell\ area]_i) + \alpha$$

Where n_i was the whale count in grid cell i and $E[n_i]$ was the expected count of whales. Additional models were run to explain the number of whale groups in each grid cell. The smoothing functions were s_k for the k explanatory covariates, z_i, of the conditions in the grid cells. The smoothing function for each explanatory covariate represents the linear contribution of that covariate to modeled whale counts and can be visualized to represent the relationship of the covariate to whale counts. These s_k smoothing functions are all added together to create the final model output (see Figure 8 for an example). The intercept was α. The area of each grid cell was used as an offset to allow for modeling of count data.

Two models were built. The first model, the simple model, used total backscatter within each grid cell as a predictor variable. The second model, the patch-explicit model, used all of the backscatter variables to build a model with the highest explanatory power of whale counts. Initial modeling of a base, shallowest, densest and largest models was used to help inform which variables to include. The 'base' model used all patches within a grid cell, and took the average depth, average NASC and total area for the patches. The 'shallowest', 'densest' and 'largest' models took the patch within each grid cell that was shallowest, densest, or largest, respectively. There was some repetition of these patches depending on how many were present in the grid cell.

Penalized isotropic thin plate regression splines were used for model smoothing and smoothing parameters were chosen using UBRE scores during the model fitting process. Lambda was set to 1.4 to help against overfitting (Kim and Gu 2004). A basis dimension

parameter of k=5 was used for single model terms to control for model complexity, which limited each model term's maximum degrees of freedom to four.

A forward stepwise procedure was used in model selection. Each unused term was added to the model individually and the term that resulted in the lowest AIC score and was significant at the p=0.05 level was added to the model. This process was repeated until no new variables contributed to the model. Interaction terms were included first in the model, and then were simplified if possible after model selection was complete.

All modeling was carried out in RStudio using the *mgcv* package (Wood 2011).

A. Model Evaluation

The residuals of the model were checked for homogeneity by visually examining plots of residuals versus fitted values for patterns. The residuals were also plotted against unused explanatory variables to check that no patterns had been excluded from the final model. The residuals were checked for normality using the Pearson Chi-square test for normality. They were examined for spatial autocorrelation using variograms with the *gstat* package (Pebesma 2004). The model was also evaluated for overdispersion using the *AER* package in R (Zeileis and Kleiber 2008). The Poisson distribution assumes that the mean of the predicted values is equal to the variance of the predicted values. The dispersion test evaluates whether the variance is equal to the mean, and a significant α value greater than zero indicates that the data is overdispersed, with variance equal to the mean plus α.

Models were evaluated for temporal autocorrelation using nested Generalized Additive Mixed Models (GAMMs). GAMMs contain an additional random effects term which can be explicitly included to model residual autocorrelation using a simple model. Using a GAMM implies that the response variable is not independent, and includes a stochastic structure to account for this. One GAMM of the exact form of the original model was built, and another GAMM with an additional first-order autocorrelation structure with time, represented as seconds past 1970, was built. The AIC scores for these two models were compared to determine if including a temporal correlation structure improved model performance. In addition, temporal trends in backscatter variables were assessed visually.

B. Model assumptions

1. Whales were assumed to be feeding. This was unlikely to always be true, but due to time constraints it was not possible to ascertain that all sighted whale were feeding. In spite of this, it is expected that whales' location would still be strongly connected to feeding sites. Kennedy et al (2014) concluded that whales observed on their feeding ground in northern Alaska spent 62% of their time feeding, and most of the remaining time was spent traveling.
2. It was assumed that the conditions remained constant for four hours on either side of the time of sampling. This assumption was statistically necessary. Technically, both whales and krill are moving targets. Whales travel an average of 30-40 kilometers a day while on their feeding grounds. Krill are strongly affected by water currents and actively change their vertical position in the water column, although this happens mostly at night. Surveys were conducted only during daylight.
3. It was assumed that backscatter conditions along the transect line were representative of conditions for the entire grid cell.
4. It was assumed that zeros in the dataset represented an actual absence of whales or prey. All grid cells included in the analysis were sampled for both whales and krill. It is unlikely that spotters failed to locate whales within a sampled grid cell, since the maximum distance from the boat to the outermost edge of the stratum was 4.8 km and

whales are visible at this distance. Humpback whales surface in seven-minute cycles, on average, giving spotters multiple opportunities to spot each whale.

C. Model Sensitivity to Whale Location

Error in whale location was estimated using published studies quantifying the error in range estimation at sea. Although few published studies exist, the literature suggests that distance estimates are usually off by 15-25% (Baird and Burkhart 2000; Williams et al. 2007; Mateos et al. 2010). The mean error in whale location was calculated by multiplying the estimated distance from the spotter to the whale by 0.15. A conservative estimate of error was chosen because spotters were regularly trained under the study period to improve their distance estimation accuracy.

One hundred iterations of randomized whale points were created, where each whale location was offset in the x and y direction by a randomized value between 0 and 0.15 times the distance of the whale from the spotting vessel. These points were used in the base model to test the model's sensitivity to error in whale location.

3.8 Software

All data analyses were carried out in RStudio Version 0.99.491 (R Core Team 2014) unless otherwise stated. ArcGIS Version 10.5.1 was also used for some analyses (ESRI 2017).

4 RESULTS

4.1 Whale and Hydroacoustic Surveys

Over the course of the study, a total of 809 whales were spotted. Known whale resights were removed from this count, so this number represents unique whale sightings. Of these individuals, the locations of 556 whales were used in the model. There were many grid cells in the model where no whales were spotted (n=278 out of 480).

A total of 829 grid cells were surveyed with the sonar, as can be seen in Figure 7. Although information from all surveys was used for the hot spot analysis, many of these cells were not used directly in the model.

Due to temporal mismatches between whale and sonar surveys in 2006 and 2007, a limited number of samples was used in the model for these years. Thirty-four samples were included from the 2006 surveys and seven samples from the 2007 surveys. Most data was from 2008 (n=439).

4.2 Bathymetric variables

Only water flow direction and three bathymetric variables were determined to be independent of each other: water depth, bottom rugosity (2D:3D area) and bottom aspect (Figure 4). The center channel of the study area was generally deepest. Much of the area had a fairly smooth bottom, although the northern area of the study site was more rugose. Although the direction in which water interacts with the bottom is difficult to interpret, there is a clear divide between the southern and northwestern half of the study area regarding the direction of water flow.

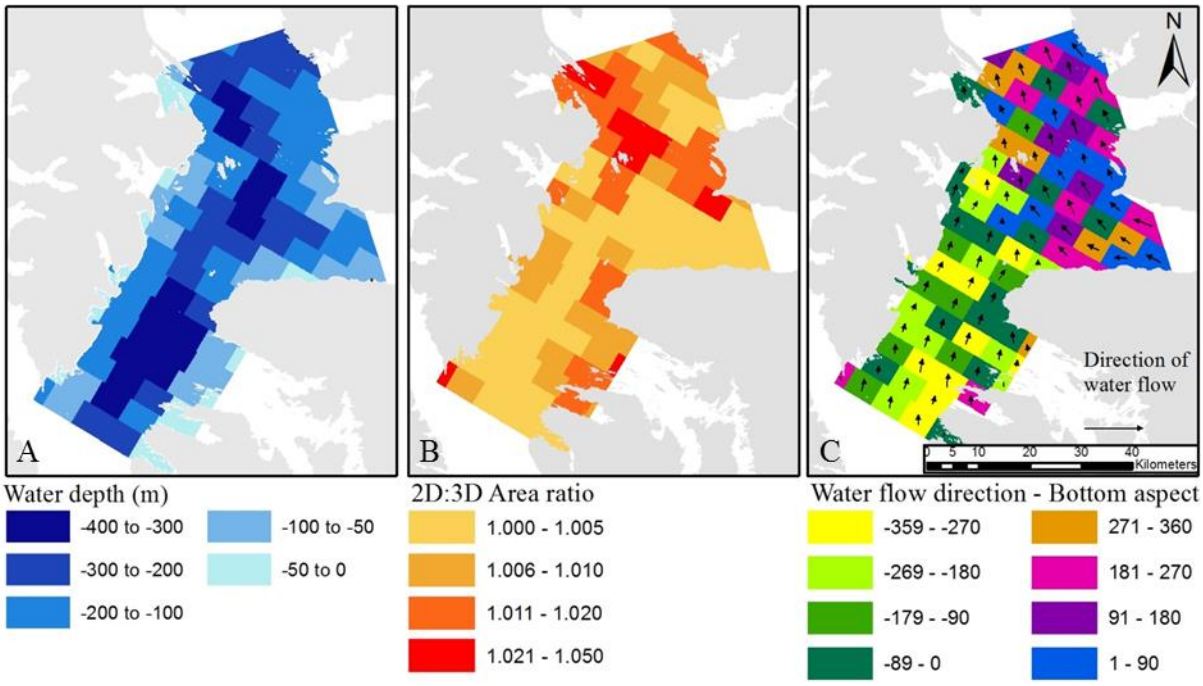

Figure 4. Bathymetric variables retained for modeling analysis. Depth, 2D:3D area, and aspect are all mean values for each grid cell. **A.** Water depth presents the depth of the bottom. **B.** 2D:3D area ratio represents the area of the bottom surface that was exposed to water and thus had the potential to affect water flow patterns. **C.** Water flow direction and aspect were from 0 to 360^{o}, with 0^{o} representing a north-facing slope and also northward-flowing water. This variable represents how water flow direction interacted with the bottom. N=100 grid cells.

4.3 Patch Definition Results

The results of the models using different patch definitions indicated that the distance and NASC threshold values used gave widely varying results. The cutoff NASC value was the most important variable in determining these differences. Model performance was very similar for the base model at the four NASC cutoff values regardless of the horizontal and vertical thresholds that were used (Table 3). For the other three models—densest, shallowest and largest—there was more variation in model performance across different NASC thresholds. In general, models with the same NASC cutoff performed similarly even if the distance cutoffs changed. The most notable exception to this was the densest model, which varied quite a bit across NASC values 100 and 200. The shallowest model varied most at NASC values of 50 and 200, and the largest model varied most at a NASC value of 200. Besides these instances, the R-squared and percent deviance explained for the different patch definitions at each NASC cutoff were within 0.1 of each other.

Within the same distance thresholds and across NASC cutoff values (i.e. patch definition A, B or C), model performance varied quite a bit. The lowest ranges in R^2 and percent deviance explained values were seen in the base model and the largest model, which had between 0.09 and 0.12 (base model range) and between 0.04 and 0.12 (largest model range). This range was much higher in the densest model, which had ranges from 0.09 to 0.29, and the shallowest model, which had ranges between 0.16 and 0.26.

A patch definition of NASC cutoff at 100, horizontal distance of 400m and vertical distance of 20 meters was chosen for all further modeling. Higher NASC cutoff values were undesirable, since they resulted in a greater number of empty grid cells containing no patches. The lowest NASC cutoff value, 50, was not used since it performed poorly in all but the base model. The chosen patch definition had consistently high explanatory power across all of the models and a relatively low NASC cutoff value. An example of patch clusters and grouping of clusters using this definition is visualized in Figure 3.

Table 3. Modeling results for the patch definitions tested. Each model took the form of nwhales ~ s(NASC, depth, area) + s(asp_wflow, asprat) + s(asp_wflow, depth) + s(ws_hours.x, k=5) + s(TOD, k=5) + s(DOY, k=5) + s(locZ, k=5) + s(meanZ, k=5), offset=log(Shape_Area), family=poisson, gamma=1.4. All patches within a grid cell, the densest, the shallowest, and the largest patches were used to build the models. The bolded line indicates the definition that was used for all further analyses. NASC: cutoff NASC value to define a patch. H dist: horizontal distance threshold. V dist: vertical distance threshold. R^2: adjusted r-square value of the model. DE: percent deviance explained of the model. N=480 data points.

				Base		Densest		Shallowest		Largest	
Patch Definition	NASC	H dist	V dist	R^2	DE	R^2	DE	R^2	DE	R^2	DE
A: literature-based	50	300m	30m	0.48	0.56	0.28	0.40	0.53	0.58	0.49	0.54
	100			0.42	0.50	0.31	0.42	0.54	0.60	0.51	0.56
	150			0.36	0.44	0.57	0.61	0.28	0.41	0.54	0.54
	200			0.45	0.53	0.34	0.46	0.34	0.46	0.49	0.52
B: decrease horizontal and vertical distances to identify tighter clusters	50	200m	20m	0.47	0.54	0.29	0.41	0.32	0.42	0.43	0.50
	100			0.42	0.50	0.28	0.42	0.52	0.57	0.48	0.56
	150			0.37	0.45	0.51	0.59	0.28	0.41	0.50	0.56
	200			0.45	0.53	0.49	0.57	0.28	0.43	0.39	0.47
C: increase horizontal distance to get more 'layered' patches	50	**400m**	**20m**	0.47	0.52	0.28	0.40	0.32	0.41	0.44	0.52
	100			**0.44**	**0.53**	**0.51**	**0.60**	**0.50**	**0.57**	**0.48**	**0.59**
	150			0.37	0.45	0.56	0.61	0.28	0.40	0.52	0.60
	200			0.45	0.54	0.46	0.56	0.49	0.57	0.56	0.61

4.4 Analysis of Patches

4.4.1 Trends over depth

Most patches were deep (70-110 meters), and these were also the largest patches. Depth had a significant effect on patch area ($F(14,465)=12.71$, $p<0.0001$) but not backscatter ($F(14,465)=1.5$, $p=0.2$). There was a general increasing trend in patch area with depth until 110 meters, at which point these variables decreased again (Figure 5). Patches at 0-10 meters were significantly smaller than all other patches ($p<0.01$). Patches at 10-50 meters depth were also significantly smaller than patches at 50-130 meters ($p<0.01$). Patches at 50-70 meters and 130-150 meters did not have a statistically significant difference in size from anything but the shallowest patches. Patches from 70-130 meters were significantly larger than patches from 0-50 meters ($p<0.01$).

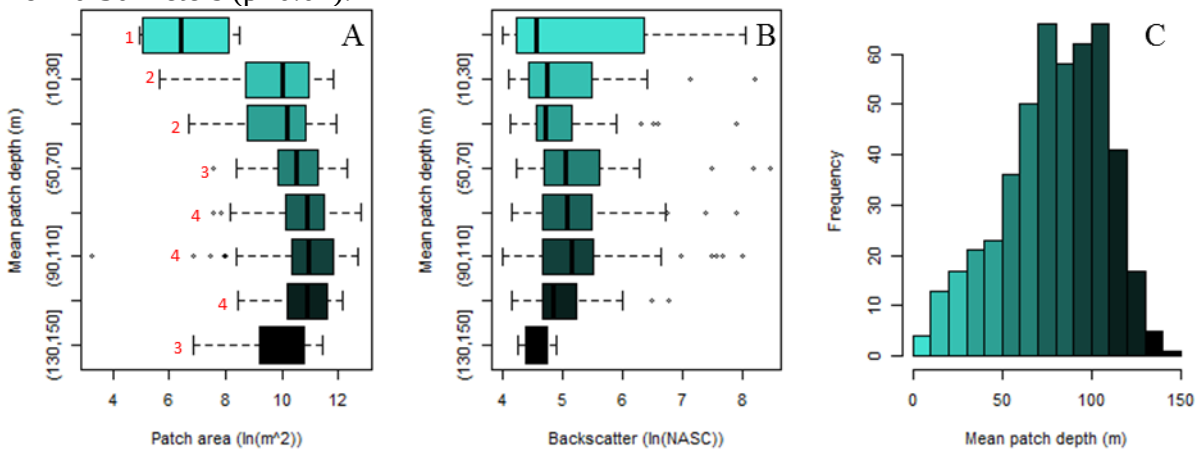

Figure 5. Trends in patch area and backscatter over depth in Frederick Sound and Lower Stephens Passage, Southeast Alaska from 2006-2008. **A**. Patch area is the total vertical area in each grid cell with NASC values greater than 100. Patch area was log-transformed. Red numbers indicate groups that are not statistically different from each other ($p>0.05$). **B.** Backscatter is the mean backscatter for all patches within a grid cell, and is log-transformed. All values are plotted against the average depth of patches in each grid cell, at 20-meter depth intervals except for patches from 0-10 meters deep. **C.** The distribution of patches over 10-meter depth intervals, with colors corresponding to the depth intervals used in **A** and **B.**

4.4.2 Seasonal trends

Patches became deeper over the course of the season. There was a significant effect of day of the year on patch depth ($F(5, 385) = 36.8$, $p<0.0001$). Patches moved downward in the water column from June to September. Patches were significantly shallower in mid-June than any other time of the year ($p<0.001$ for all comparisons). Patches in early September were significantly deeper than any other time of the year ($p<0.001$ for all comparisons except for DOY 220-240, where $p=0.003$). Days 140-160 and 180-260 were not significantly different.

The total NASC in patches in each grid cell decreased slightly in the early summer and then was fairly constant for the rest of the season. The effect of day of the year on total backscatter was significant ($F(5, 385) = 4.4$, $p=0.0007$). The total NASC for days 140 to 160 (May 19-June 8) was significantly higher than that of days 160 to 180 and 180 to 200 ($p=0.015$ and $p<0.001$, respectively) (Figure 6).

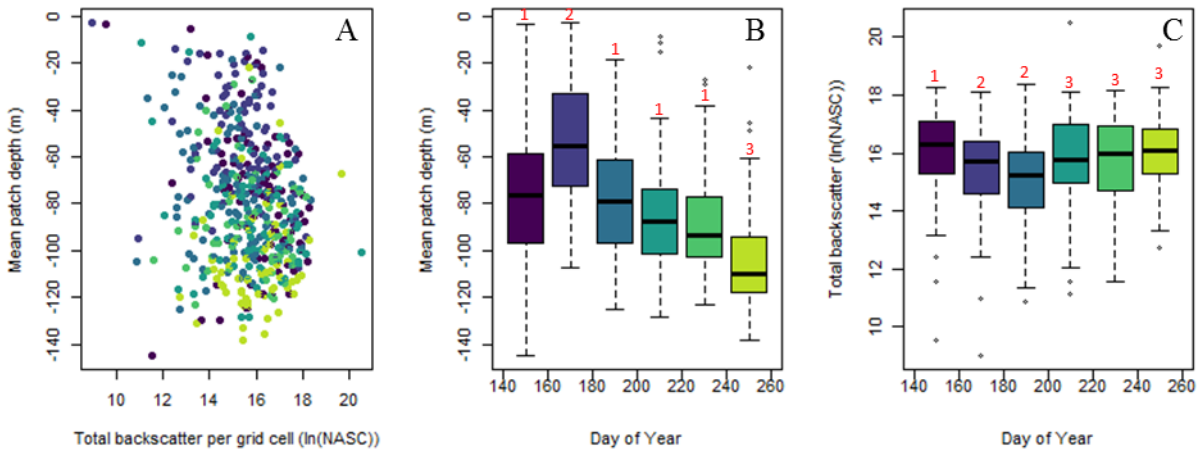

Figure 6. Seasonal trends in patch backscatter and depth in Frederick Sound and Lower Stephens Passage, Southeast Alaska from 2006-2008. All plots are colored by day of the year, with dark purple representing days 140-160 (late May) and yellow-green representing days 240-260 (early September). Each color is a 20-day period. Total backscatter is the sum of all NASC values greater than 100 in the grid cell, log-transformed after summation. All time periods with the same red number label were not significantly different from each other. **A** shows the relationship between total backscatter and patch depth, colored by season. Patches are visibly deeper at the end of the season, while trends in total backscatter are less visible. **B** shows the trend in patch depth over season. Both group 2 and 3 were significantly different from group 1 and each other. In **C,** which shows trends in total backscatter over the season, group 1 was significantly different from groups 2 and 3 ($p<0.05$).

4.5 Hot Spot Results

The results of the hot spot analysis using a 15km radius were more significant in the modeled results than using an 8km radius, although there was no great difference between the two. Therefore, the results presented going forward are for the 15 km hot spot analysis.

A. Momentary Hot Spots

Areas with high backscatter were clustered in space, with clear hot and cold spots during each survey. Hot spots were not always in the same location, although there was often a large hot spot at the confluence of Stephens Passage and Frederick Sound (Figure 7). A second, smaller hotspot sometimes appeared at the southeastern corner of the study area. The second survey in 2008 did not appear to fit any of these patterns, and instead there was a hotspot along the southeastern coast of the study area. NASC values were otherwise consistently low in the southern part of the study area. It is of note that sonar surveys were begun in the south and moved northward, taking approximately a week to complete. These are therefore not a perfect snapshot into conditions in the study area, but instead represent conditions over a week.

B. Persistent Hot Spots

The mean z-scores for all surveys indicated that the lower portion of Fredericks Sound had one large and consistent cold spot, while its upper arm and the southern portion of Stephens Passage were generally hot spots (Figure 7). The magnitude of the mean z-scores indicated that the southern cold spot was more pronounced than the hot spots. Visually, the cold spot appeared to be tightly clustered (Figure 7). The average z-scores for hot spots were not as high, and were also not as tightly clustered. Despite this, the eastern arm of Frederick Sound was the most consistently 'hot' area, and the area where Frederick Sound meets Stephens Passage included a weaker hot spot.

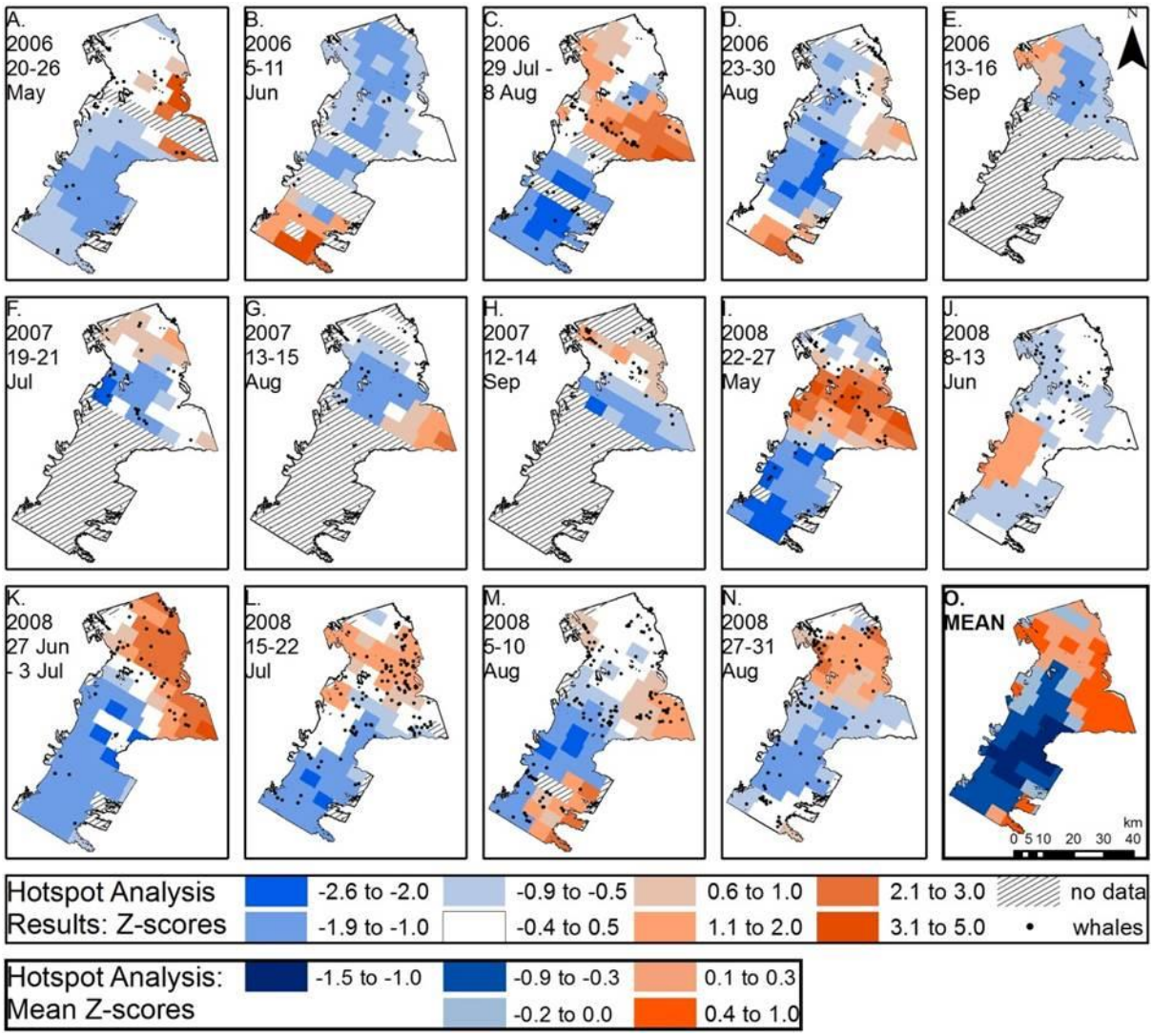

Figure 7. Results of hot spot analysis in Frederick Sound and Lower Stephens Passage, Southeast Alaska from 2006-2008. Getis Gi* statistic was calculated using average NASC values within each grid cell and all neighbors within 15 kilometers. Average NASC values were calculated by summing the NASC values of all sonar blocks in the grid cell and dividing by the number of sonar blocks. The output of the Getis Gi* statistic is Z scores, which are standardized values that can be compared between surveys. **A-N.** Momentary hot spots for each survey are presented. **O.** Persistent hotspots were calculated as the average Z score for all surveys. Note differing color ramp.

4.6 Modeling Results

The patch-explicit model had almost twice as much explanatory power as the simple model. The simple model explained only 35% of deviance and had a low R^2 value of 0.24, while the patch-explicit model explained 59% of deviance and had a higher R^2 value of 0.60. In addition, the prediction error of the patch-explicit model was lower than that of the simple model. The patch-explicit and simple models had an UBRE score of 0.64 versus 0.95, respectively (Table 4). A total of 480 grid cells were used in the models, of which 202 contained whales. According to these statistics, the patch-explicit model performed much better than the simple model.

Table 4. Generalized Additive Model (GAM) results. The simple model used horizontally averaged backscatter, while the patch-explicit model used patch-explicit backscatter variables. Values in parentheses represent linear predictors, while all other values are for smooth functions. *p*-values in italics represent terms that were not significant and were dropped from the final model. D.E.=percent of deviance explained; Adj. R^2=adjusted r-squared; UBRE=unbiased risk estimate, which represents the average prediction error. For dispersion, a value of $\alpha > 0$ indicates that the model is overdispersed if $p<0.05$. See Table 2 for a description of the predictor variables. N=480.

Model:	**Simple**			**Patch-explicit**		
Predictor:	edf (est.)	Chi-sq (z)	*p*	edf (est.)	Chi-sq (z)	*p*
Intercept	(-17.5)	(-290.5)	<2e-16	(-17.9)	(-138.7)	<2e-16
s(area, depth, NASC of all patches)	-	-	-	55.5	250.1	<2e-16
s(NASC of largest patch)	-	-	-	7.5	51.3	3.7e-8
s(total NASC)	3.2	60.1	1.8e-12	-	-	-
s(DOY)	4.1	88.5	<2e-16	5.3	76.6	3.1e-14
s(ws_hours)	4.0	62.4	4.0e-12	3.7	48.5	2.9e-9
s(tide)	2.2	10.5	0.0113	3.4	19.6	0.00053
s(meanZ)	3.7	24.5	6.2e-5	3.7	27.7	1.4e-5
s(asp_wflow, depth)	18.6	84.0	3.4e-9	13.2	54.9	6.4e-6
locZ	3.4	8	*0.1*	3.4	5	*0.3*
npatch	-	-	-	1	1.6	*0.2*
D.E.		35.1			59.2	
Adj. R^2		0.24			0.60	
UBRE		0.95			0.64	
Dispersion	z=4.0	p=2.7e-5	α=2.2	z=3.1	p=0.001	α=1.3

In the simple model, there was a highly significant and positive relationship between total backscatter and whale counts. Whale counts increased almost linearly with total backscatter until they plateaued at higher values (Figure 8A). In the middle of this range, the relationship was well-defined and standard error was low. However, there were a limited number of data points for the highest backscatter values.

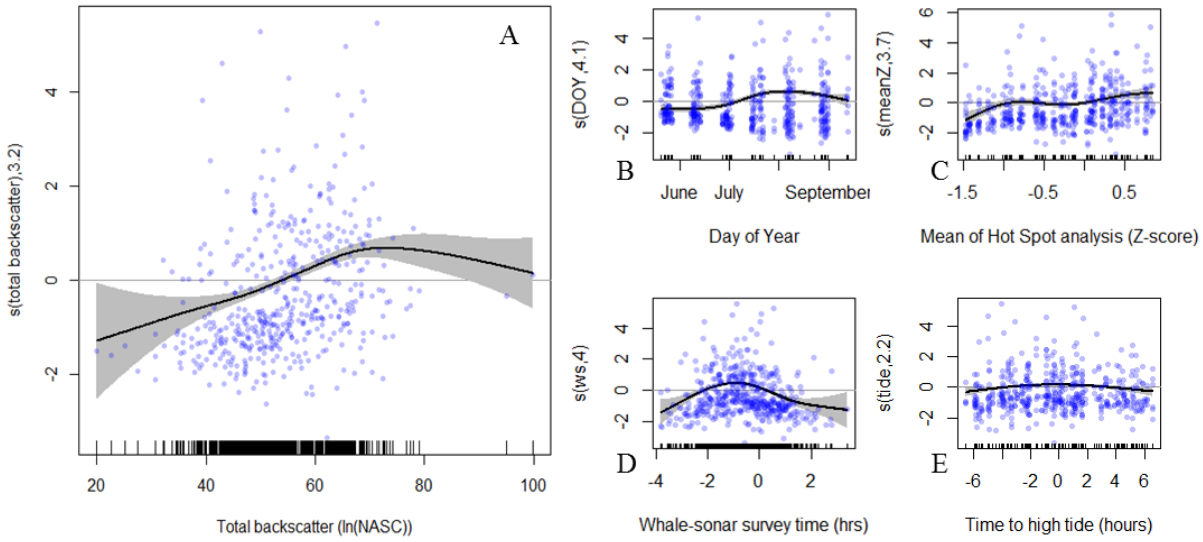

Figure 8. Smooth functions for the simple Generalized Additive Model (GAM) of whale counts. The black line represents the smooth predictor term of whale counts, with degrees of freedom in parentheses on the y axis. The grey area is the standard error of the prediction. Blue dots are the model residuals. An explanatory variable that explains much of the variation in whale counts will have residuals clustered tightly around the black line, while disperse residuals indicate that the variable is not good at explaining whale counts on its own. **A.** The relationship between horizontally averaged backscatter (a proxy for prey density) and whale counts. **B.** Seasonal effects on whale counts. **C.** Persistent hot spot effect on whale counts. **D.** Spotter bias, based on distance from grid cell when whale was spotted, and its effect on whale counts. **E.** Time to high tide's effect on whale counts. The interaction between water depth and the direction of water flow over the bottom is not shown, but was nearly identical to Figure 9G. N=480.

In the patch-explicit model, patch depth, size and backscatter intensity were very important explanatory variables. The three-way interaction between the average depth and backscatter and the total area of all the patches in the grid cell was highly significant (Figure 9A-C). The area of a patch had particularly strong explanatory power, with few whales being predicted for patches less than e^10 (≈ 22,000) m^2 in vertical area. Few whales were predicted at 0-30 meters' depth unless a very large patch was present. In the deepest portion of the water column that was surveyed, patch area did not appear to be important. At 30 meters' depth, slightly higher backscatter values were favored and then became less important important as patch depth increased. The model predicted most whales at 35-60 and then 80-100 meter deep patches. While the three-way interaction of average patch conditions in the grid cells do not indicate that whales were strongly associated with higher backscatter intensities, the backscatter of the largest patch in each grid cell had strong explanatory power. For the large patches that had a NASC value of approximately 500 or greater, there was a strong positive relationship between backscatter and whale count (Figure 9D). The number of krill patches identified in a grid cell did not have a significant explanatory effect in the model. The results of the patch-explicit model indicated that the depth and size of all patches within a grid cell as well as the backscatter intensity of the largest patch were important explanatory variables for whale count.

Identical predictor variables not related to backscatter were used in both models, and they had very similar effects. The model results are presented in (Table 4). There was a small but highly significant seasonal effect seen in the day of the year, where the predicted number of whales increased between July and August (Figure 8B and Figure 9F). Before July, the linear predicted value for day of the year was negative, and in August it was positive. Recurring hot spots (meanZ) were also significant, with a positive relationship to whale counts. There were fewer whales at mean z-scores less than -1 and more whales where z-scores were greater than 0 (Figure 8C and Figure 9E). In contrast to the positive effect of persistent hot spots on whale counts, the backscatter hot spots identified during each survey (locZ) had no effect on whale counts. The interaction between bottom depth and the angle at which water flowed over the bottom aspect was significant. Whales were predicted at shallow areas (0-120 meters deep) with water striking the bottom at -360 to -110 degrees. This corresponded mainly to grid cells with a north- to west-facing slope with water flowing in a northerly to easterly direction. The effect of tide on whale count was weak and could arguably have been dropped from the model. However, the model predicted fewer whales at peak low tide and otherwise tide had no effect on whale counts (Figure 8E and Figure 9H). The effect of the difference in time between when a whale was spotted and when the hydroacoustic survey was conducted was highly significant. The model predicted more whales between two and zero hours before the grid cell was surveyed with the sonar, with a peak around -1 hours (Figure 8D and Figure 9I).

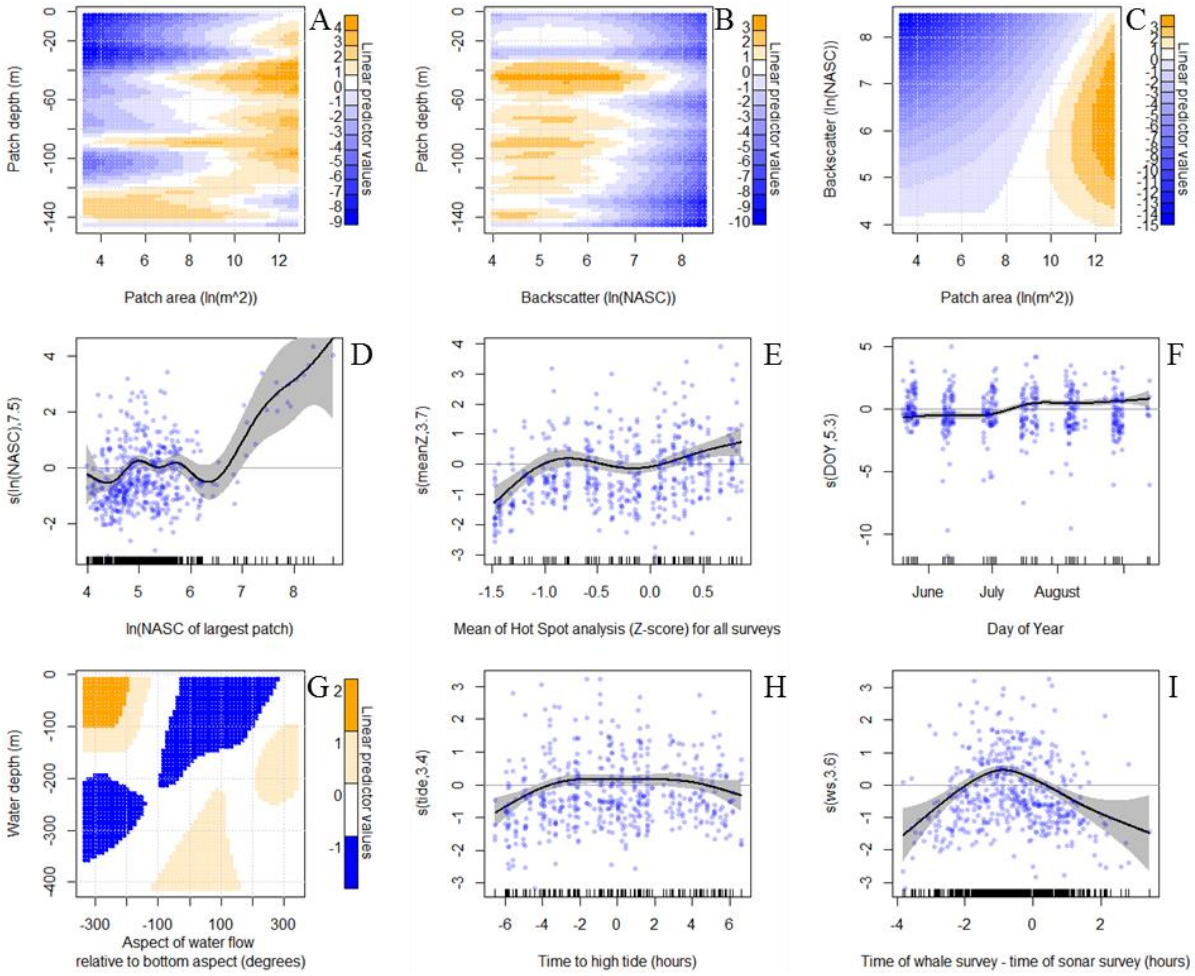

Figure 9. Smooth predictor functions for the patch-explicit GAM of whale counts. **A**, **B** and **C** show the three-way interaction between patch depth, area and backscatter for all patches within a grid cell. For interaction plots, the color of the dot represents the terms' linear predictor value for whale counts at the corresponding predictor terms' values. Orange indicates a positive contribution to predicted whale counts while blue indicates a negative contribution to predicted whale counts. For interaction terms, note differing scale bars. **D:** backscatter of the largest patch in the grid cell**, E**: effect of persistent hot spots**, F**: seasonal effects on whale counts**, H**: time to high tide's effect on whale counts, and **I:** spotter bias representing distance of whale from boat; these depict smooth functions for single terms. **G** represents the two-way interaction between water depth and the direction in which water flows over the bottom. For single terms, the black line is the smooth predictor of whale counts, with degrees of freedom in parentheses on the y axis. The grey area is the standard error. Blue dots are the model residuals. An explanatory variable that explains much of the variation in whale counts will have residuals clustered tightly around the black line, while disperse residuals indicate that the variable is not good at explaining whale counts on its own. N=480.

Models built using the shallowest, deepest or largest patch groups were not as powerful as the patch-explicit model built using averages for all patches in each grid cell. Results for these analyses are presented in Appendix S4, Figures S3-S10 and Tables S2-S3. Models built to explain the number of whale groups instead of total whales performed similarly and are not presented. Measures of spotter bias, i.e. visibility, wave height and wind speed, had no effect on the model.

4.6.1 Model Evaluation

Based on percent deviance explained, R^2 values and model error, the patch-explicit model was much more successful in explaining humpback whale locations than the simple model. The patch-explicit model was thus evaluated more thoroughly. The results of the patch-explicit model mapped against actual whale observations (Figure 10, Figure 11) indicated that the model captured general spatial trends in actual whale locations, although there was some mismatch between predicted and observed whale counts. The absolute error, calculated

as the observed whale count minus the predicted whale count, is shown for each survey in Figure 12.

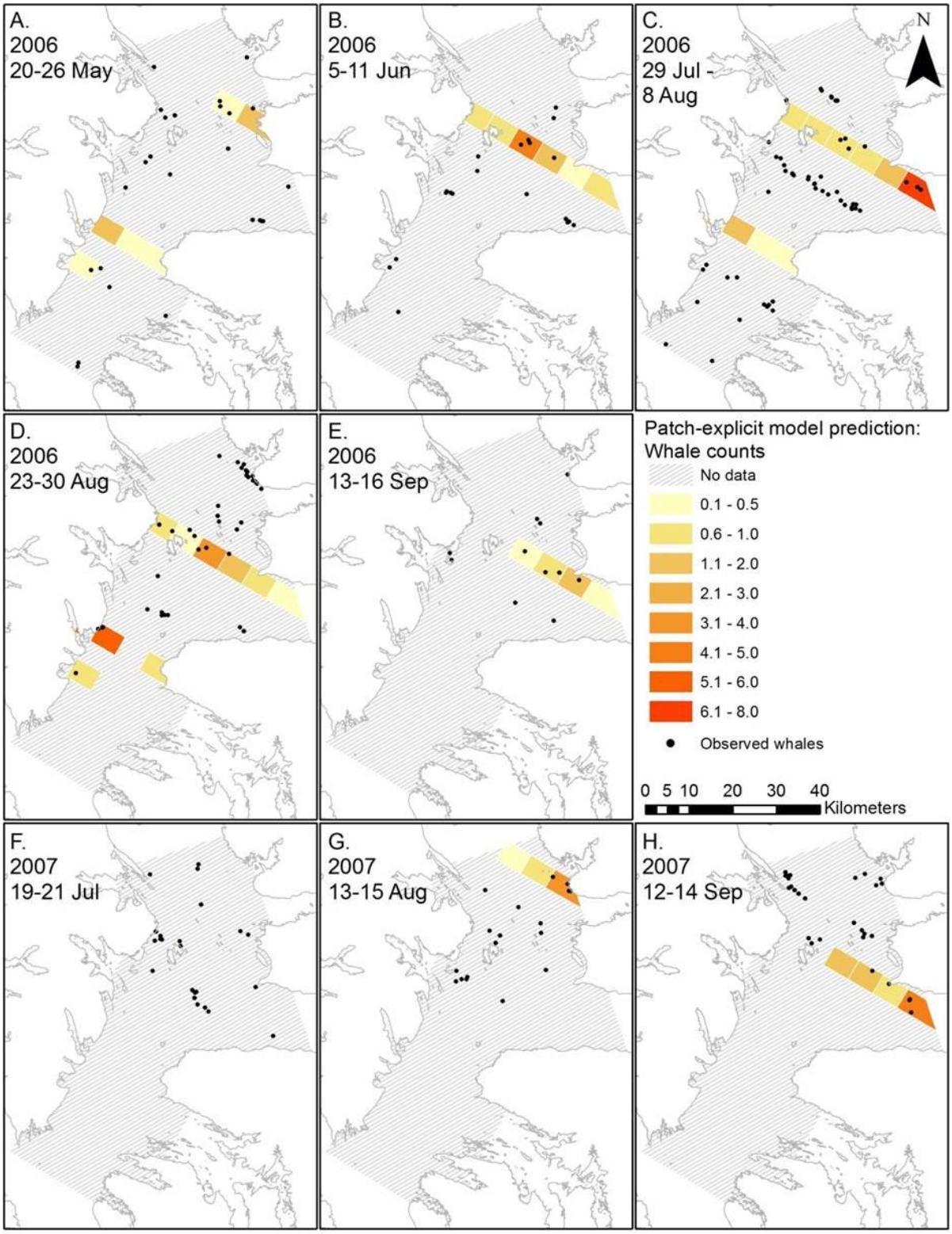

Figure 10. Actual location of observed whales (black dots) and the patch-explicit model predicted whale counts (orange grid cell values) for 2006 and 2007 in Frederick Sound and Lower Stephens Passage, Southeast Alaska. The patch explicit model used average values for all patches within each grid cell as well as bathymetric and temporal variables to predict whale counts. Only data where sonar and whales were surveyed within four hours of each other were used, leading to few data points from surveys in these years. However, the data included was sampled in an equivalent manner to that of 2008.

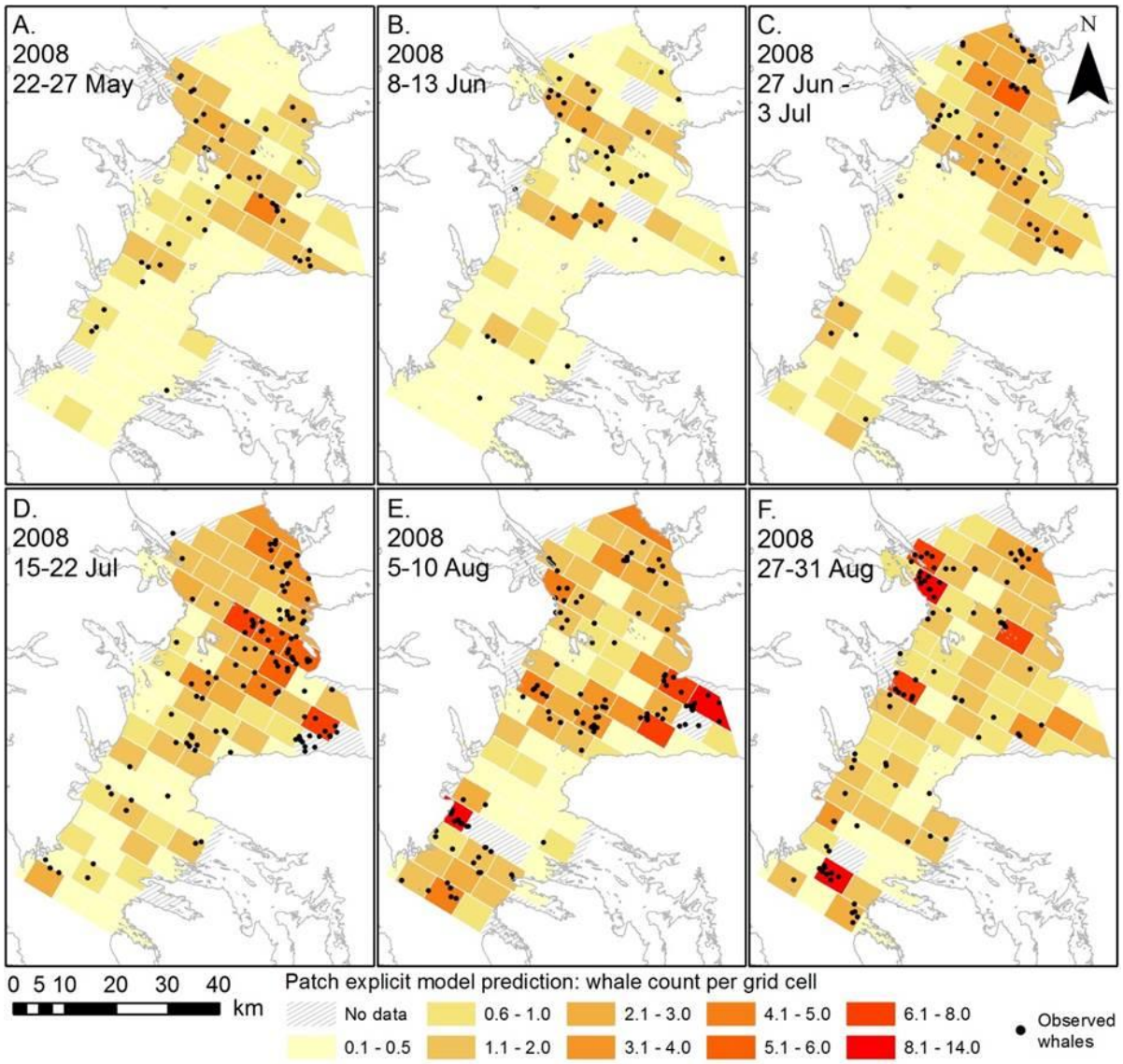

Figure 11. Actual location of observed whales (black dots) and the patch-explicit model predicted whale counts (orange grid cell values) for 2008 in Frederick Sound and Lower Stephens Passage, Southeast Alaska. The patch explicit model used average values for all patches within each grid cell as well as bathymetric and temporal variables to predict whale counts.

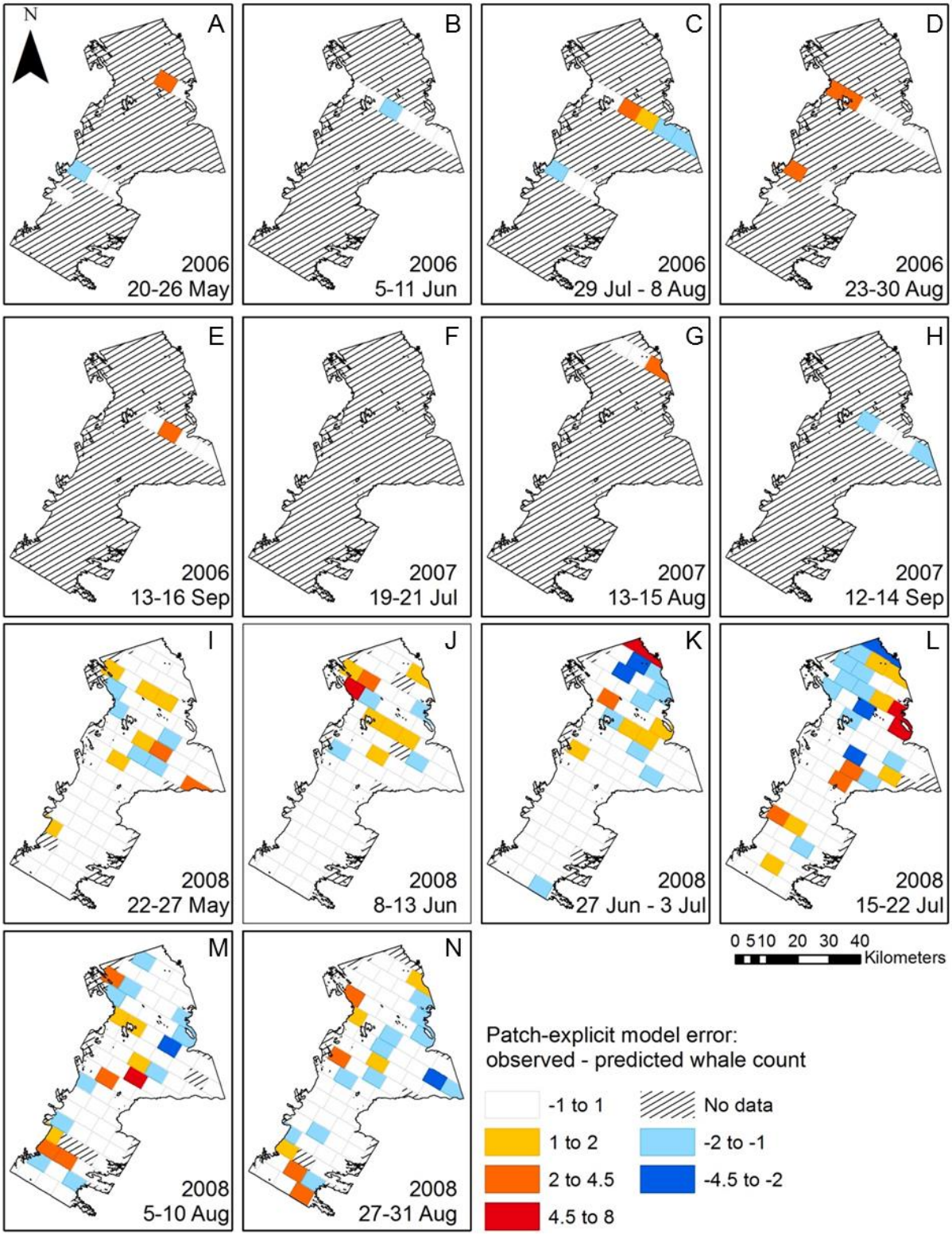

Figure 12. Model error for the patch-explicit GAM, which predicted whale counts based on the average values of all patches within a grid cell as well as bathymetric and temporal variables. Blue colors represent model over-prediction and orange colors represent model under-prediction. Few data points were used from the 2006 and 2007 surveys due to large temporal mismatches between sonar and whale surveys. The data points included for 2006 and 2007 were sampled in an equivalent manner to those from 2008.

The patch-explicit model exhibited some skewness and heterogeneity. Residuals did not follow a normal distribution (Figure 13A), which was confirmed using the Pearson Chi-square test for normality (P=80.4, p<0.0001). A quantile-quantile plot of the residuals, which plots the sorted residuals percentiles against a normal distributions' percentiles, also indicated some skew at the ends of the residual values, particularly the upper values (Figure 13B). An examination of the model residuals plotted against the fitted values (Figure 13C) indicated a slight cone shape in the residuals, suggesting heterogeneity. Finally, plotting the predicted against observed whale count showed a tendency for the model to underestimate large values and overestimate small values (Figure 13D).

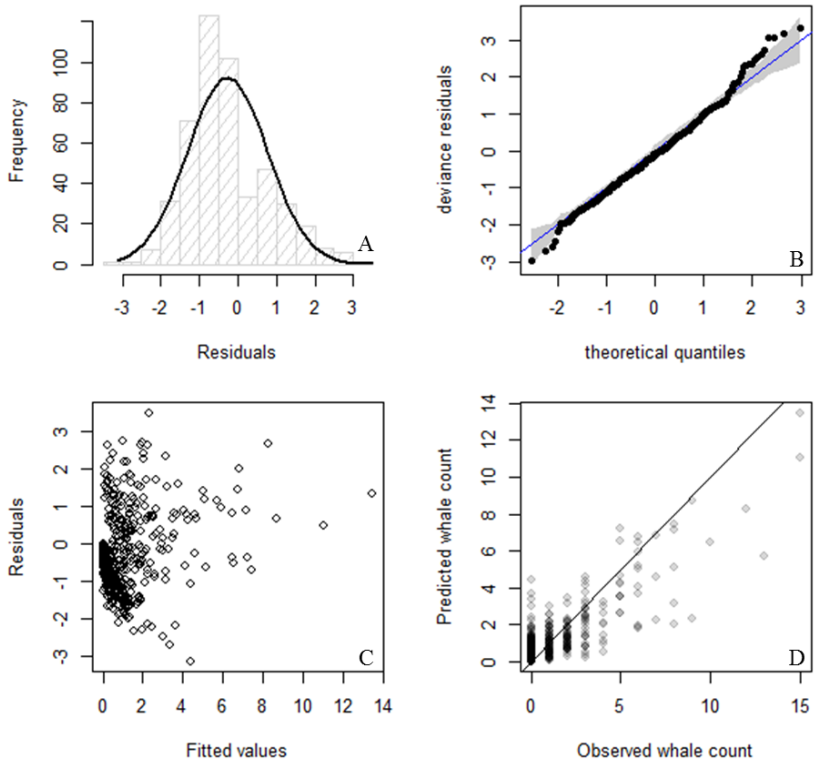

Figure 13. Evaluation of residuals and model fit for the patch-explicit model. Panels **A** and **B** show if the residuals have a normal distribution. The residuals were skewed to the left and did not have a normal distribution. Panel **C** shows whether the model exhibits homogeneity. There was some indication of a heterogeneic cone-shape. Panel **D** shows the model's predictive power. In **D**, points are transparent so that darker point clusters represent denser point groups and most data fell in the range of 0-3 observed whales. N=480 data points for each graph.

A test of model dispersion also indicated that both models were overdispersed. The models had an α between 1.4 to 1.9 (Table 4). When a negative binomial distribution was used instead, however, the model performance decreased drastically (R^2=0.29) and the model residuals were highly skewed to the right. The same was true for a quasipoisson distribution (R^2=0.40). Because of this, the Poisson distribution was retained despite leading to an overdispersed model. It was likely that one or several explanatory variables were missing, thus leading to overdispersion.

An evaluation of spatial autocorrelation using variograms indicated that there was some weak clustering of model residuals along the north-south axis (0^0) and the east-west (90^0) axis (Figure 14). However, the number of pairs for the first lag in both graphs was much lower than the remainder of the lag pairs. The map of model error concurs with this evaluation of some residual clustering, seen particularly in late July and early August of 2008 (Figure 12).

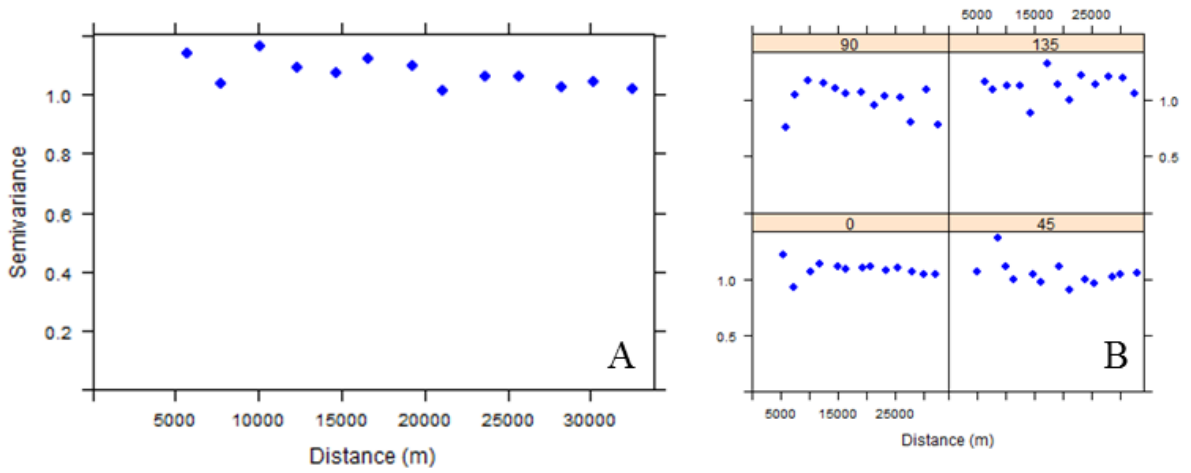

Figure 14. Variograms for the residuals of the patch-explicit model assess remaining spatial trends in the model. Variograms were created by calculating the semivariance of lag pairs starting at 5000 meters. An upward trend in semivariance indicates that closer points are more similar to each other than distant points and therefore exhibit spatial autocorrelation. Panel **A** shows the variogram for all directions, while Panel **B** assesses anisotropy in four directions: 0, 45, 90 and 135°. There were few points in the first lag pairs, and trends between the first and second point can be disregarded. N=480 data points for each graph.

A comparison of models with and without a temporal correlation structure indicated that there was no temporal autocorrelation in the models. The base model with a temporal correlation structure performed no better than the model without (AIC=2013 for no correlation structure, AIC=2015 with a correlation structure).

A visualization of the data used to generate the three-way interaction of krill patch characteristics was used to assess the model for data gaps and sensitivity to outliers. The model fit closely to outliers, with most residuals for outlying data points at or near 0 (Figure 15). The cutoff point at which the model no longer had a near-perfect fit to outlying data was at values approximately less than e^7 m^2 for area, greater than e^6.5 for NASC, and outside of the range 15-135 m for depth. These points give some indication of where the GAM has been built using a robust set of data points, and where it is simply fitting to a few, sparse data points. At these sparse data areas, it is possible that the GAM over fit the data since GAMs have a general tendency to do so (Zuur et al. 2011).

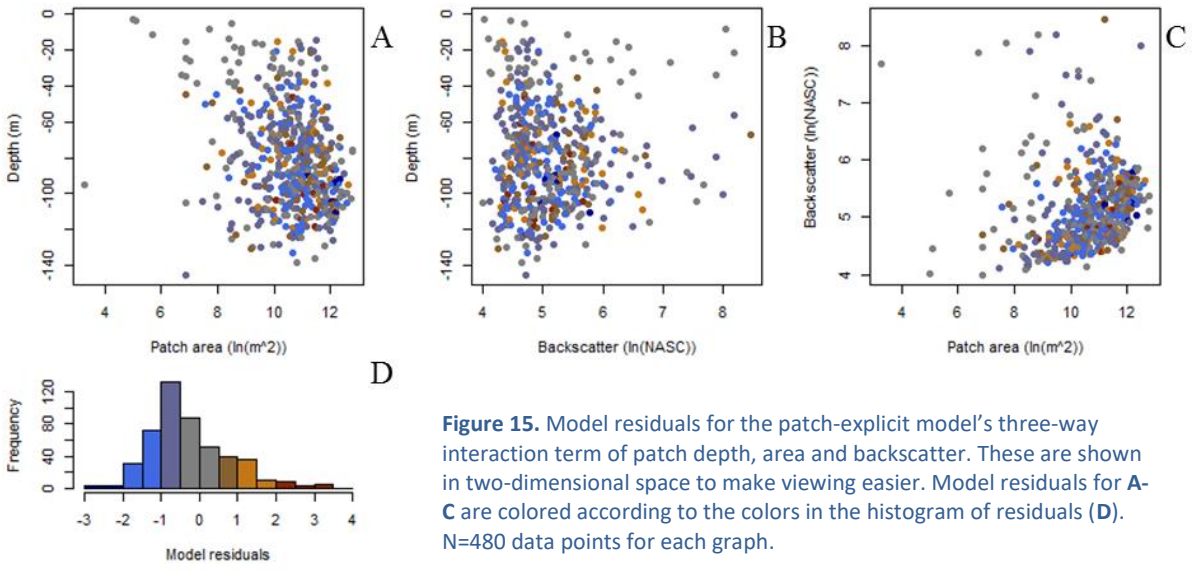

Figure 15. Model residuals for the patch-explicit model's three-way interaction term of patch depth, area and backscatter. These are shown in two-dimensional space to make viewing easier. Model residuals for **A-C** are colored according to the colors in the histogram of residuals (**D**). N=480 data points for each graph.

4.6.2 Additional Analyses

There was some spatial pattern in the interaction term of water depth and aspect of water flow relative to bottom aspect. The grid cells that predicted greater whale counts were located along the coastline, mainly in the southern part of Frederick Sound (Figure 16).

Figure 16. Location of grid cells with water flowing over the bottom aspect at -360° to -100° and with a depth of 0 to 150 meters. These cells are highlighted in orange and had a significant positive effect on whale count within the interaction term. All of these grid cells had the highest predicted whale counts of +2 for the interaction term of direction of water flow over the bottom and water depth in the patch-explicit model. See Figure 9G for this interaction term.

4.6.3 Sensitivity analysis to error in whale location

The model performed similarly with whale points that were randomized by the estimated error in whale location (Figure 17). Model performance, as estimated by R^2 and percent deviance explained, was near the mean of the output of the sensitivity analysis.

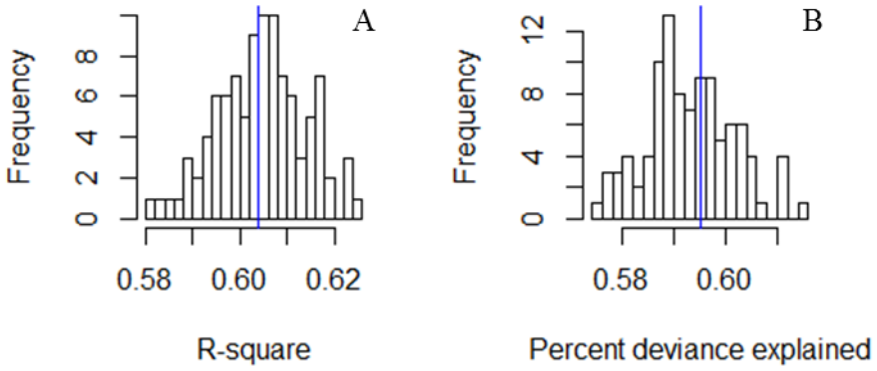

Figure 17. Sensitivity of the patch-explicit model to error in whale location. This was assessed by running the model 100 times with whale points moved randomly by the estimated error in whale locations (0.15*distance from spotter to whale). R-square and percent deviance explained represent how well the model fits to the input data. The blue line represents model performance with real data. N=480 data points in each model run.

5 DISCUSSION

This study represents a novel attempt to characterize krill patchiness and its importance for humpback whales' distribution at their feeding grounds. It is a first step towards incorporating the three-dimensional distribution of prey into marine models. The results indicate that several aspects of krill distribution that have largely been ignored in modeling studies are vital for determining humpback whales' distribution. These results point towards the significance of patchiness in the marine environment, and indicate that including variables such as depth and size of food sources can be crucial for modeling studies.

5.1 Backscatter as a proxy for krill

Backscatter values are often used as a proxy for prey located in the water column, and it is believed that the NASC values used in this study were largely representative of humpback whale prey. Net sampling performed in conjunction with the hydroacoustic surveys confirmed the presence of euphausiids in regions with strong backscatter values. A total of 155 net tows were performed in 2008, both randomly along the transect lines and at locations with strong backscatter. The euphausiid species *Thysanoessa raschii, T. longipes, T. spinifera* and *Euphausia pacifica* were caught. Of these, *T. raschii* were the most abundant (see Szabo and Batchelder (2014) for details).

In addition to net sampling, the acoustic parameters for the sonar survey were chosen to optimize the identification of potential whale prey. A 120 KHz sonar operational frequency is commonly used to sample krill because it provides a strong signal for euphausiids (Hampton 1990; Lawson et al. 2004) and will also detect small fish (Foote and Nakken 1978; MacLennan and Simmonds 2013). Individuals smaller than approximately 10mm will not be detected at 120KHz (Wiebe and Greene 1994), meaning that it is unlikely the sonar detected phytoplankton or micro zooplankton. In addition to the operational frequency, applying a threshold processing level of -65dB to the sonar data eliminated weak signals. These signals could include dense micro zooplankton or phytoplankton species or sparsely distributed regions of the target organisms that are not attractive to whales. The post-processing NASC values were most likely caused by dense aggregations of krill or small fish.

Previous studies in the area indicated that euphausiids were the main prey for foraging humpback whales, while small schooling fish were also consumed. Hydroacoustic and net-sample studies identified euphausiid scattering layers and patches of small schooling fish, including herring and pollock, in Frederick Sound and Stephens Passage (Krieger and Wing 1984). Humpback whales were found to feed mainly on these deep euphausiid scattering layers in Frederick Sound and Stephens Passage (Krieger and Wing 1986; Dolphin 1988). This has also been reported using fecal samples (Baker et al. 1992) and underwater cameras (Dolphin 1987) to identify krill as prey for humpback whales.

Due to the weight of evidence provided by net tow samples, sampling design, previous studies, and observations of whale diet, all performed in Frederick Sound and Stephens Passage, the scattering layers identified in the hydroacoustic surveys of this study were presumed to represent mainly krill. It is important to recognize that other whale prey items, namely small schooling fish, are also visible to sonar and may have attributed to the backscatter used in the analysis. Very strong signals from smaller planktonic organisms could also contribute to backscatter, although this is unlikely. Thus, NASC was an imperfect albeit the best proxy for prey density.

5.2 Evaluation of initial hypotheses

> H_1: whale distribution is dependent on krill distribution. Furthermore, the depth, density and size of krill patches are important because these factors affect the energy budget of a feeding whale.

This study provided strong support for the hypothesis that whale distribution is dependent on prey distribution during the summer feeding season. Backscatter was an important explanatory variable in both the simple and the patch-explicit model, and there was a clear pattern in which greater backscatter was correlated with higher whale counts, particularly in the simple model. The patch-explicit model showed that the depth, density and size of patches were important explanatory variables, which supported the hypothesis that krill patchiness is important for foraging whales.

5.2.1 Model using horizontally averaged prey density

The simple model, which collapsed the vertical component of backscatter to mimic the methods used by past modeling studies, gave comparable results to past studies. Friedlaender et al (2006) saw a threshold relationship between volume backscatter and whale abundance. There was a linear increase in whales until a threshold krill abundance was reached, at which point the relationship plateaued. Ressler et al (2015) found a similar shape in the relationship between whale density and euphausiid backscatter, although their study modeled larger grid cells with a 50x50 km resolution. The relationship between backscatter and whale counts seen in the simple model of this study followed the shape of these published curves closely, with an initial increase and then a plateau or potentially even a decrease at the highest observed NASC values (Figure 8A).

Although the shape of the relationship between whale counts and backscatter values was similar between this study and the literature, the explanatory power of the simple model in this study was relatively low. It explained 35% of deviance and had an R^2 value of 0.24. Friedlaender et al (2006) obtained 63% of deviance explained and an R^2 value of 0.41. They did include additional bathymetric variables relevant to their study area as well as a measure of primary productivity, which were highly significant explanatory variables in their model. Ressler et al (2015) obtained a percent deviance explained value of 71%. They included an additional variable on fish density, which was also significant in their model. Both of these studies had a much higher percent deviance explained than my model. Frederick Sound and Stephens Passage is a highly complex area that is influenced by strong tides, freshwater inputs, and varying bathymetry. These differences in explanatory power may be due to differing habitat complexities, study designs, or ecological factors.

5.2.2 Model using prey patch variables

A. Prey density

When krill patches were used in the model, however, there was a very different relationship between whales and backscatter. NASC had a slightly negative relationship with whale counts when the average backscatter of all patches in a grid cell was investigated. Given the extensive literature describing the importance of prey density for the energetic budget of lunge feeders (Goldbogen et al. 2011), this finding was surprising. The shallowest, densest and largest models gave some indication that high prey density within a patch was an important predictor of whale count, particularly for more shallow patches. However, none of these relationships were strong and sometimes conflicted with each other in different

interactions. The only clear result where prey density was important was the increasing number of whales associated with large, very dense patches (Figure 9D).

The data processing and patch definition process may have smoothed away important variation in NASC values. The NASC values used in the model were the average over an entire group of patches. Grouping all the patches together, as was done for the patch-explicit model, probably smoothed out much of the variation in NASC values between patches. The data processing method, in which sonar data were binned into 100 x 10 meter blocks, also smoothed the data and may have eliminated microscale variation in NASC to begin with. Including additional variables related to within-patch NASC values may improve modeling. This could include the maximum or top quartile of NASC values in each krill patch and the variation in NASC values within each patch.

NASC values may not have been sufficiently representative of prey quality within a patch to be important for the model. As mentioned above, NASC is a measure of suspended particles in the water column and does not take into account species, size, orientation or density of particles. The study area contained diverse micro-conditions, owing to its coastal and highly tidal nature. Different areas could be characterized by different prey species, water flow patterns, and oceanographic conditions. For example, schooling fish are known to aggregate near the Five Fingers Islands (Krieger and Wing 1984). Different life stages of krill may exhibit ontogenetic migration, which results in life stage specific spatial segregation (Pillar et al. 1989; Trathan et al. 1993; Tarling et al. 1999). Patches of different depth and caloric content may have been present in different locations because of this.

B. Prey patch size

Whales in this study clearly preferred large prey patches. There was a threshold patch area at approximately 22,000 m^2, above which whales were expected to be found in increasing numbers. Feeding on large prey patches reduces the amount of searching and traveling time for a predator. First, it is more likely to find a larger patch. Second, when prey density is held constant, larger patches contain more food and it takes longer to exhaust the prey in a larger patch. The predator will be able to devote time and energy to feeding rather than to traveling (Charnov 1976). Although the krill density of these large patches was not important when patches were grouped at the grid cell level, the largest patches in each grid cell that also had extremely high krill densities often contained many whales. This suggests that large, very dense prey patches are preferred by foraging whales.

C. Prey depth

The effect of prey depth on whale distribution was complex. There is some indication that whales preferred krill patches occurring at approximately 40 meters' depth, and were rarely found where patches were shallower than this (Figure 9A and B). Many whales were also located at patches at approximately 90 meters deep, which is where patches occurred most frequently and were the largest.

Few whales were located at prey patches in the upper 30 meters of the water column. Only seven percent of all patches occurred at this depth range. The densest patches in this shallow layer were small, and the largest patches were not very dense. Shallow prey patches in the study area may not have been of sufficient quality or quantity to attract a foraging whale.

The most whales were predicted by the model at patches with a depth of approximately 35-60 meters. Overall patch characteristics were not different at this depth from patches at other depths, and there were relatively few patches located at this depth. This suggests that prey patches distributed at approximately 40 meters' depth were optimal for humpback whales due to depth alone, rather than the effect of prey density or patch size.

The model predicted more whales at patches with a depth of 80-100 meters, regardless of patch size. Patches occurred most frequently at this depth and these patches had significantly higher area and total NASC values than the average values across all patches. Because of the high rate of occurrence at this depth, whales could have optimized their search patterns to find patches at the most commonly found depths. Due to a higher potential rate of discovery of these patches, more whales may have been located near them, regardless of how large the patches were.

The model predicted that whales would also be found at small and deep patches (130-150 meters). There were relatively few data points contributing to this relationship, and the presumed relationship may disappear given a larger sample size. If this is not the case, however, there may be an explanatory variable missing from the model. It is also possible that some of the krill patches were cut off by filtering out sonar data at depths greater than 150 meters, although after visually examining the sonar data there were few patches that appeared to be cut off in the middle.

In general, it appears that whales prefer mid-depth krill patches but are often associated with deeper prey because patches occur more frequently at depth.

5.2.3 Momentary prey hot spots

> H_2: spatial trends in krill distribution (i.e. clustering and hot spots) are important for foraging whales, since the travel costs associated with a hot spot are lower.

My model rejected the hypothesis that spatial trends in krill distribution across a 2,400 km^2 feeding area affected humpback whale distribution. Measures of local krill conditions surrounding a grid cell did not influence whale counts in any of the models I built, such that hotspots were not predicted to contain more whales and conversely, cold spots were not predicted to have fewer whales. Hot and cold spots did not capture any additional information when krill patch characteristics were used in the model. They were also not important in the simple model. This suggested that foraging whales were searching for favorable hyperlocal conditions within this feeding area. When local conditions were accounted for, the surrounding conditions were not important for the whale.

It is likely that the scale used to identify hot and cold spots was not important for foraging whales. Whales may perceive Fredericks Sound and Lower Stephens Passage as a single, large hot spot. If the study area were expanded, hot and cold spots may have been an important explanatory variable in the model, which would then support this hypothesis.

5.2.4 Persistent prey hot spots

> H_3: trends in krill distribution over time (i.e. persistent hot spots) are important for foraging whales, since these whales are long-lived, return to the same areas year after year, and presumably have a good memory for where food has been available in the past

Weak support existed for the hypothesis that long-term trends in krill distribution affect humpback whale distribution. Averaged hot spot values at each grid cell were a significant explanatory variable for whale locations, although their explanatory value was generally quite weak and the linear predictor value of the smooth function of mean hot spot values never went outside the range of -1 to 1 (Figure 9E). In general, the model indicated that consistently ‘hot’ krill areas had more whales. This suggests that whales have learned where prey is located and visit these places. However, I would be cautious to accept this

finding because it was such a weak explanatory variable. It could reflect some other variable that was not included in the model.

5.3 Other model variables

While variations in krill had the strongest explanatory power in all of the models, temporal and bathymetric variables also helped to explain the presence of whales. Variables not related to prey were expected to have a small contribution to the model. It is important for whales on their feeding grounds to consume enough calories to sustain long migratory and fasting periods. Therefore, prey is arguably the most important factor affecting whale distribution in this study. The additional explanatory power of temporal, bathymetric and water flow variables may indicate that the krill variables used in the mode did not adequately represent prey conditions. This may be due to imperfections in sampling design and gaps in the study area that were not surveyed. It may also be due to imperfect definitions of krill patches. With a better prey patch definition, additional explanatory variables may no longer contribute to the model.

5.3.1 Day of the Year

This study supported the generally accepted trends in humpback whale abundance in Southeast Alaska. Humpback whale numbers in Southeast Alaska increase markedly from spring to fall (Dahlheim et al. 2009), and this trend has also been observed specifically in Frederick Sound and Stephens Passage (Baker et al. 1985; Straley et al. 1994; Dahlheim et al. 2009). The model showed a seasonal increase in whales, which supports these findings.

The modeled increase in whales in Frederick Sound did not begin until July (Figure 9F), suggesting that some other factor beyond migratory arrival was most likely involved. Based on calculations of migratory rates, humpback whales from Hawaii could arrive at their feeding grounds in southeast Alaska as early as March. Whales begin leaving Hawaii in late February and early March, and are largely absent by April (Craig et al. 2003). The trip from Hawaii to Alaska is estimated to take about thirty days (Gabriele et al. 1996; Mate et al. 1998), which would place them in Alaska beginning in late March.

It is not well known where whales are coming from when they arrive at Fredericks Sound. Movement of whales between feeding grounds or within the inner channels of Southeast Alaska are unlikely to completely explain the seasonal increase in whale abundance. Rates of movement between feeding grounds are low for the species, although there is some large-scale exchange of whales between Southeast Alaska and both British Columbia and northern feeding grounds (Calambokidis et al. 2008; Witteveen et al. 2011). Movement within the feeding ground may have contributed to increased abundance. Despite general site fidelity, humpback whales visit many areas within Southeast Alaska, possibly following attractive food sources (Straley et al. 1994). However, since abundance is lower throughout the feeding ground in the spring, it is not likely that this is the only factor at play. Whales may also arrive from unmonitored areas, such as offshore waters. Offshore waters in Southeast Alaska are part of the overall feeding ground, with movement between inshore and offshore areas (Witteveen et al. 2011).

It is difficult to determine why whales arrived in the study area later in the season. Measurements of backscatter were not enough to explain increased whale counts. There were small seasonal changes to krill patch characteristics (Figure 6), but it is unknown if these significantly affected the prey quality in Frederick Sound and Stephens Passage. There was some indication that krill patches became deeper from May to September. Krill patch area increased early in the season and then was constant. It is unclear if this shift either affected the quality of prey patches directly or was indicative indirectly of some other change.

Changing conditions elsewhere rather than at the study site could have contributed to the increased number of whales. It is possible that whales were at another feeding site that they left as its quality deteriorated and then went to Frederick Sound and Stephens Passage, where prey conditions are relatively constant. It is difficult to examine this relationship with the available data, as this study did not sample outside Frederick Sound and Stephens Passage. Significant traveling during the feeding season is not uncommon in rorqual whales. Croll et al (2005) proposed that NE Pacific blue whales travel long distances seasonally between high-density, ephemeral euphausiid aggregations, arriving at feeding grounds during known blooms. Similar migratory behavior has been seen in humpback whales, which aggregate in foraging areas but may undertake long journeys during the feeding season (Dalla Rosa et al 2008, Kennedy et al 2014).

5.3.2 Spotter Bias

The most likely time to spot a whale was zero to two hours before the grid cell was surveyed for krill, with a peak in sightings one hour before the hydroacoustic survey. This was believed to be a product of the sampling design in 2008, which accounted for the vast majority of data points (439 out of 480). The boat drove along transect lines while conducting the hydroacoustic survey with whale spotters on board and looking forward. Whales were unlikely to be spotted behind the boat (positive values in *ws_hours*) or more than 15-20 kilometers in front of the boat (values less than -2). The *ws_hours* variable is thus accounting for spotter bias, rather than any real temporal lag between krill conditions and whale presence.

5.3.3 Bathymetry and Currents

A. Tide

The effect of tide on whale count was weak, although fewer whales were seen at peak low tide and the two hours following, and slightly more whales were seen in the hour before and after high tide. This was not believed to be a spotter bias, since wave height and tide were not correlated in the data.

Shallow-water bathymetry has been shown to modify tidal water flow and aggregate prey through a diversity of mechanisms, for example in island wake systems (Johnston et al. 2005; Johnston et al. 2007), underwater banks (Cotté and Simard 2005), and at headlands (Chenoweth et al. 2011). These effects are usually highly localized and may be in effect during ebb or flow and at different tidal velocities. It is possible that tidal effects were similar enough throughout a large enough portion of the study area that this showed up in the model. However, since currents in the area are poorly understood, it is difficult to draw any conclusions from this.

B. Bathymetry

Bathymetric variables about water depth and the angle at which water hit the bottom with respect to the direction the bottom sloped helped to explain whale location. The conditions that predicted the most whales were found close to shore in the southern portion of the study site. This was a complex interaction involving three variables. With any such interaction term, it is important to consider whether the GAM was overfitting or using this variable to fill in for something missing in the model. It is difficult to conclude from the existing data whether bathymetry was accounting for a missing explanatory variable.

Krill patches are influenced by water movement and bathymetry, and it is possible that bathymetry acted as a fill-in for persistent conditions in areas where krill were poorly sampled. Bathymetry influences water flow such that recurring krill retention zones are

created, and marine predators can exploit these predictable foraging grounds (Cotté and Simard 2005; Croll et al. 2005; Johnston et al. 2005; Johnston et al. 2007; Chenoweth et al. 2011; Santora and Reiss 2011). Krill retention zones may have bottom-up effects on a trophic system and attract small fish (Cotté and Simard 2005). If these patches were not directly sampled, bathymetric variables may have accounted for persistent conditions.

Where water flows from the eastern arm of Frederick Sound into the north-south channel, it strikes water flowing in another direction and potentially creates a very turbulent environment. The coastline is complex, with many bays and inlets. In addition, The Brothers Islands and the Five Fingers Islands in Lower Stephens Passage may influence water flow patterns. Chenoweth et al. (2011) found that headland wake systems in nearby Glacier Bay and Icy Strait were important habitats for foraging humpback whales. These occur in near-shore areas and locally modify water flow in a predictable manner, creating eddies and changing current velocities. Similar conditions may exist in this study area. Again, little work has been done to characterize water flow patterns in the area and it is difficult to draw any conclusions without further study of flow patterns.

5.4 Tendency to underestimate high values, overestimate low values

All models exhibited a strong tendency to underestimate counts that were greater than approximately six whales. This suggested that some other factor contributed to the large number of whales present in some areas. In general, conditions with high whale numbers were not appreciably different from other locations with fewer whales. Social groups are characterized by fission-fusion (Clapham 2000). Foraging whales may join other whales through a process known as local enhancement. This process has been well documented in seabirds foraging on krill and fish (Sakamoto et al 2009, Davoren et al 2010, Bairos-Novak et al 2015). Humpback whales are known to vocalize during feeding (D'Vincent et al. 1985; Parks et al. 2014; Fournet et al. 2015), providing a method by which feeding whales could be located by other individuals from fairly long distances. This could have occurred in this study and could account for the model overdispersion.

All models also had a strong tendency to overestimate whale counts in grid cells where zero whales were spotted. There is a chance that some of these points represent false zeros, but it is unlikely that such a high number of false zeros were recorded. This may indicate that the study site had not reached saturation and could support additional foraging whales, at least in accordance with the model output. However, the hydroacoustic survey failed to capture specific euphausiid characteristics such as size, species composition and caloric content. Humpback whales have been shown to prefer certain krill size classes (Santora et al 2010), and this preferential behavior may mean that high NASC areas identified by the sonar are not good prey. Further work characterizing euphausiid biology in the area must be undertaken to answer these questions.

5.5 Model shortcomings

As with any ecological study, a compromise between survey effort and sampling area was made for this study. Sonar transect lines were taken on average every 4.8 km, leaving much of the study area un-sampled. Rather than attempting a messy three-dimensional interpolation that would likely introduce quite a bit of error into the data, conditions at the transect lines were assumed to be representative of the entire grid cell. This assumption allowed for a much neater data analysis that avoided many of the complexities associated with three-dimensional data, as krill was viewed in its own two-dimensional space with distance traveled along the x-axis and depth along the y-axis. However, it was highly unlikely that this sampling design captured all of the relevant information in the study area and important prey patches were

indubitably missed. This is particularly relevant for bait balls, which are small but extremely dense schools of fish.

Some transect lines were left unsampled, and the total number of surveys varied by year. Mechanical failures in 2007 led to large data gaps and a diminished sampling area for this year. Only the northern half of the study area was sampled in 2007. Because of this, the hotspot analysis was most likely more robust for the northern portion of the study area.

In addition, as mentioned above, specific variables related to euphausiid species composition and caloric content were not captured by the study. The NASC values obtained from hydroacoustic surveys represent the signal from objects in the water column that scatter sound. The size, density and acoustic properties of objects in the water column all influence the backscatter intensity (Lawson et al. 2004). Sonar instruments cannot identify the agents responsible for reflecting sound. While NASC values were corrected for objects presumed to be too large to be whale prey, and weak signals were removed, it is still possible that suspended particles and other species with a similar acoustic signature contributed to the NASC. In addition, it was not possible to identify specific characteristics related to taxonomy and life stages. Because of this, NASC values must be treated as an imperfect proxy for krill.

5.6 Future work

5.6.1 Analysis of spatial and temporal trends in krill

Due to time constraints, the analysis of krill was limited. A better characterization of krill patches is a necessary first step in this process. Understanding krill conditions in the study area would allow for a more complete interpretation of the modeling results. The correlation of krill to certain bathymetric features and water flow patterns would be useful. It was apparent that certain areas in Frederick Sound and Stephens Passage were consistent krill hot spots, and future work should explore why this was. A better understanding of how prey conditions in the area change over time is also necessary. To analyze krill conditions, a smaller analysis scale should be used. Trends in backscatter values and patch area should be made using individual patches, not patches grouped at the grid cell level.

5.6.2 Backscatter patch methodology

The definition of a patch in this study was shaped by what was deemed statistically and ecologically important for modeling whale counts. The threshold values were developed to reflect how humpback whales perceive their environment, and therefore differed from a classic krill patch definition. Most studies on krill patches implement the method developed by Coetzee (2000) with automated software to detect patches from raw sonar files. It identifies any signals within a predetermined vertical and horizontal distance and intensity at fine scales of centimeters to meters. This study attempted to identify and summarize krill patches from post-processed sonar files, which have a much coarser resolution. Because of this, the focus was on mesoscale aggregations (10s to 100s of meters). Renting the software required to process sonar data is prohibitively expensive, and constrained the processing that was performed. Few studies have defined krill patches from such data, and this process involved extensive experimentation.

While this study represents a first step in defining krill patches relevant to foraging whales, additional parameters to identify a patch should be explored in the future. More distance threshold values should be tested when identifying patches, as this study did not include an exhaustive list. The effect of using different threshold processing levels (i.e. -75dB, -65dB, etc.) should also be examined more thoroughly. One of these processing levels may optimally eliminate weak signals representing non-relevant, sparse prey aggregations while including only the aggregations at densities that are important for foraging whales.

The statistics that were calculated for each krill patch should be expanded. Measures such as patch distance from the bottom may also be included. Other variables about patchiness within a grid cell could be calculated, such as the density of krill patches, the horizontal area covered by krill patches, and the distance between krill patches. The shape of patches could be represented in a simple length:thickness ratio. Patch area, length and thickness were collinear and could not be used together in the model, but using the ratio would most likely deal with this issue.

Further development is required to eliminate flaws in the patch grouping method. Patches were combined based on depth to create depth-stratified groups. Additional weighting factors based on patch size and distance from each other would create more ecologically relevant groups. However, this may group dissimilar patches from a whale's perspective.

This study showed that using only the densest, largest, or shallowest patch was not as successful in modeling whale counts as using overall prey conditions within each grid cell. This suggests that patches suitable for a foraging whale do not fit into a single criterion, such as being shallow or dense. Instead, it is likely several factors interact to define ideal prey patches. Multiple categories of patches may also be favorable for the whale. Future work could involve clustering krill patches based on characteristics such as depth, density, thickness and vertical area. Instead of simply using the shallowest/densest/largest krill patches for a model, the patches deemed most attractive for a whale should be identified. If the ideal patch in each grid cell is identified, it is expected to be more successful for modeling whale counts than using average conditions of all patches in the grid cell.

Despite shortcomings in the patch definition methodology, this study moves a step forward in answering questions on how different summary statistics of a krill patch affect whale distribution. Most likely because a single definition for an ideal krill patch was not identified, the average conditions for all patches in the grid cell resulted in the best model for this study. Although identifying the ideal krill patch will likely improve models, it is of note that the average conditions are easier to calculate and represent much less work on the part of the modeler. In this respect, very little additional work can contribute to a much better model.

5.6.3 Modeling whale distribution

Improved krill patch definitions are likely to improve the model's ability to explain humpback whale distribution on their feeding grounds, while increased understanding of krill trends in the area will help to interpret the output of the model. This study is a starting point for analyses of whale distribution in patchy environments, and future work will require careful definition of prey patches and identification of the aspects of patchiness that are most important to a foraging whale.

5.7 Applications

This model moves a step forwards in understanding humpback whale foraging decisions and the prey characteristics that are most important to foraging whales. The model also helps to identify areas with high whale densities in Frederick Sound and Stephens Passage. This information can be used for conservation and marine planning. First, boat traffic in the area should take into account the areas with high whale densities when planning routes, since humpback whales are at high risk for ship collision. Second, the development of marine conservation areas should account for where krill conditions are favorable and the model predicted high whale counts. These areas support a number of predators in addition to humpback whales. Krill form the basis of the marine food chain at high latitudes, and the areas where krill are attractive to whales are likely also areas where other marine predators can be found at high densities.

6 CONCLUSION

This study modeled humpback whale distribution across a feeding site in Frederick Sound and Stephens Passage, Southeast Alaska. The best model included patch specific variables on the depth, size and density of prey. This indicates that using variables on prey patches greatly improves spatial models of humpback whale distribution as compared to traditional models that have collapsed prey densities into horizontal space.

The model indicated that humpback whales were most likely to be found at large prey patches, regardless of the average prey density within these patches. They may be searching for hyperlocal, dense prey aggregations within these larger patches. Furthermore, whales were found at patches that were located at the most frequently occurring depth across the feeding area. They may optimize their search patterns based on the depth at which prey is most likely to be found. More humpback whales were found in consistent prey 'hot spots', although this relationship was weak. Variables related to prey species and life stages would most likely improve the model.

The model consistently over-predicted whale counts in areas with zero or one whale and under-predicted whale counts in areas with greater than six whales. This suggests that using backscatter values alone does not fully explain whale distribution. Whale behavior, including searching strategies and grouping behavior, was not included in the model and may account for the skewed predictive abilities of the model.

Future work on modeling marine predators should include measures of patchiness. The marine environment is widely recognized as being characterized by patchiness on many spatial and temporal scales, and it is an oversimplification not to include this information in ecological models. This study is a first step towards modeling cetacean distribution using patch-explicit measures of prey.

7 REFERENCES

Baird, R. W., and S. M. Burkhart. 2000. Bias and variability in distance estimation on the water: implications for the management of whale watching. In *IWC Meeting Document SC/52/WW1*.

Baker, C. S., L. M. Herman, A. Perry, W. S. Lawton, J. M. Straley, and J. H. Straley. 1985. POPULATION CHARACTERISTICS AND MIGRATION OF SUMMER AND LATE-SEASON HUMPBACK WHALES (MEGAPTERA NOVAEANGLIAE) IN SOUTHEASTERN ALASKA. *Marine Mammal Science,* 1**:** 304-323.

Baker, C. S., J. M. Straley, and A. Perry. 1992. Population characteristics of individually identified humpback whales in southeastern Alaska: summer and fall 1986. *Fishery Bulletin,* 90**:** 429-437.

Barange, M. 1994. Acoustic identification, classification and structure of biological patchiness on the edge of the Agulhas Bank and its relation to frontal features. *South African Journal of marine science,* 14**:** 333-347.

Barlow, J., M. C. Ferguson, E. A. Becker, J. V. Redfern, K. A. Forney, I. L. Vilchis, P. C. Fiedler, T. Gerrodette, et al., 2009. Predictive modeling of cetacean densities in the eastern Pacific Ocean. Report. [in Swedish, English summary]

Benoit-Bird, K. J., B. C. Battaile, S. A. Heppell, B. Hoover, D. Irons, N. Jones, K. J. Kuletz, C. A. Nordstrom, et al. 2013. Prey patch patterns predict habitat use by top marine predators with diverse foraging strategies. *PLoS One,* 8**:** e53348.

Bivand, R., J. Hauke, and T. Kossowski. 2013. Computing the Jacobian in Gaussian Spatial Autoregressive Models: An Illustrated Comparison of Available Methods. *Geographical Analysis,* 45**:** 150-179. DOI: 10.1111/gean.12008

Bivand, R., and G. Piras. 2015. Comparing implementations of estimation methods for spatial econometrics. American Statistical Association.

Brinton, E., and J. G. Wyllie. 1976. *Distributional atlas of euphausiid growth stages off southern California, 1953 through 1956*. Marine Life Research Program, Scripps Institution of Oceanography.

Brower, A. A., M. C. Ferguson, S. V. Schonberg, S. C. Jewett, and J. T. Clarke. 2017. Gray whale distribution relative to benthic invertebrate biomass and abundance: Northeastern Chukchi Sea 2009–2012. *Deep Sea Research Part II: Topical Studies in Oceanography,* 144**:** 156-174. DOI: 10.1016/j.dsr2.2016.12.007

Burrows, J. A., D. W. Johnston, J. M. Straley, E. M. Chenoweth, C. Ware, C. Curtice, S. L. DeRuiter, and A. S. Friedlaender. 2016. Prey density and depth affect the fine-scale foraging behavior of humpback whales Megaptera novaeangliae in Sitka Sound, Alaska, USA. *Marine Ecology Progress Series,* 561**:** 245-260. DOI: 10.3354/meps11906

Cade, D. E., A. S. Friedlaender, J. Calambokidis, and J. A. Goldbogen. 2016. Kinematic Diversity in Rorqual Whale Feeding Mechanisms. *Curr Biol,* 26**:** 2617-2624. DOI: 10.1016/j.cub.2016.07.037

Calambokidis, J., E. A. Falcone, T. J. Quinn, A. M. Burdin, P. Clapham, J. Ford, C. Gabriele, R. LeDuc, et al. 2008. SPLASH: Structure of populations, levels of abundance and status of humpback whales in the North Pacific. *Unpublished report submitted by Cascadia Research Collective to USDOC, Seattle, WA under contract AB133F-03-RP-0078 [available from the author]*.

Charnov, E. L. 1976. Optimal foraging, the marginal value theorem. *Theoretical population biology,* 9**:** 129-136.

Chenoweth, E. M., C. M. Gabriele, and D. F. Hill. 2011. Tidal influences on humpback whale habitat selection near headlands. *Marine Ecology Progress Series,* 423**:** 279-289.

Clapham, P. J., and J. G. Mead. 1999. Megaptera novaeangliae. *Mammalian Species***:** 1-9.

Coetzee, J. 2000. Use of a shoal analysis and patch estimation system (SHAPES) to characterise sardine schools. *Aquatic Living Resources,* 13**:** 1-10. DOI: https://doi.org/10.1016/S0990-7440(00)00139-X

Cohen, J. H., and R. B. Forward. 2016. Zooplankton Diel Vertical Migration -- A Review of Proximate Control. In *Oceanography and Marine Biology: An Annual Review,* eds. R. N. Gibson, R. J. A. Atkinson, and J. D. M. Gordon, 77-110. CRC Press.

Cotté, C., and Y. Simard. 2005. Formation of dense krill patches under tidal forcing at whale feeding hot spots in the St. Lawrence Estuary. *Marine Ecology Progress Series,* 288**:** 199-210.

Craig, A. S., L. M. Herman, C. M. Gabriele, and A. A. Pack. 2003. Migratory timing of humpback whales (Megaptera novaeangliae) in the central North Pacific varies with age, sex and reproductive status. *Behaviour,* 140**:** 981-1001.

Croll, D. A., B. Marinovic, S. Benson, F. P. Chavez, N. Black, R. Ternullo, and B. R. Tershy. 2005. From wind to whales: trophic links in a coastal upwelling system. *Marine Ecology Progress Series,* 289**:** 117-130. DOI: 10.3354/meps289117

D'Vincent, C. G., R. M. Nilson, and R. E. Hanna. 1985. Vocalization and coordinated feeding behavior of the humpback whale in southeastern Alaska. *Scientific Reports of the Whales Research Institute,* 36**:** 41-47.

Dahlheim, M. E., P. A. White, and J. M. Waite. 2009. Cetaceans of Southeast Alaska: distribution and seasonal occurrence. *Journal of Biogeography,* 36**:** 410-426.

Dalla Rosa, L., J. K. B. Ford, and A. W. Trites. 2012. Distribution and relative abundance of humpback whales in relation to environmental variables in coastal British Columbia and adjacent waters. *Continental Shelf Research,* 36**:** 89-104. DOI: 10.1016/j.csr.2012.01.017

Dalla Rosa, L., E. Secchi, Y. Maia, A. Zerbini, and M. Heide-Jørgensen. 2008. Movements of satellite-monitored humpback whales on their feeding ground along the Antarctic Peninsula. *Polar Biology,* 31**:** 771-781.

Dolphin, W. 1987. Prey densities and foraging of humpback whales, Megaptera novaeangliae. *Cellular and Molecular Life Sciences,* 43**:** 468-471.

Dolphin, W. F. 1988. Foraging dive patterns of humpback whales, Megaptera novaeangliae, in southeast Alaska: a cost–benefit analysis. *Canadian Journal of Zoology,* 66**:** 2432-2441.

Falk-Petersen, S., W. Hagen, G. Kattner, A. Clarke, and J. Sargent. 2000. Lipids, trophic relationships, and biodiversity in Arctic and Antarctic krill. *Canadian Journal of Fisheries and Aquatic Sciences,* 57**:** 178-191.

Falk-Petersen, S., C. Hopkins, and J. Sargent. 1990. Trophic relationships in the pelagic Arctic food web. In *Trophic relationships in the marine environment,* eds. M. Barnes, and R. N. Gibson, 315-333. Aberdeen, Scotland: Aberdeen University Press.

Fock, H., H. Von Westernhagen, F. Uiblein, and F. Köster. 2002. Biodiversity and species-environment relationships of the demersal fish assemblage at the Great Meteor Seamount (subtropical NE Atlantic), sampled by different trawls. *Marine Biology,* 141**:** 185-199. DOI: 10.1007/s00227-002-0804-y

Foote, K. G., and O. Nakken. 1978. Dorsal aspect target strength functions of six fishes at two ultrasonic frequencies.

Fournet, M. E., A. Szabo, and D. K. Mellinger. 2015. Repertoire and classification of non-song calls in Southeast Alaskan humpback whales (Megaptera novaeangliae). *The Journal of the Acoustical Society of America,* 137**:** 1-10.

Franks, J. S. P. 1992. Sink or swim: accumulation of biomass at fronts. *Marine Ecology Progress Series***:** 1.

Friedlaender, A. S., P. N. Halpin, S. S. Qian, G. L. Lawson, P. H. Wiebe, D. Thiele, and A. J. Read. 2006. Whale distribution in relation to prey abundance and oceanographic processes in shelf waters of the Western Antarctic Peninsula. *Marine Ecology Progress Series,* 317**:** 297-310.

Friedlaender, A. S., E. L. Hazen, D. P. Nowacek, P. N. Halpin, C. Ware, M. T. Weinrich, T. Hurst, and D. Wiley. 2009. Diel changes in humpback whale Megaptera novaeangliae feeding behavior in response to sand lance Ammodytes spp. behavior and distribution. *Marine Ecology Progress Series,* 395**:** 91-100. DOI: 10.3354/meps08003

Gabriele, C. M., J. M. Straley, L. M. Herman, and R. J. Coleman. 1996. Fastest documented migration of a North Pacific humpback whale. *Marine Mammal Science,* 12**:** 457-464.

Genin, A. 2004. Bio-physical coupling in the formation of zooplankton and fish aggregations over abrupt topographies. *Journal of Marine Systems,* 50**:** 3-20. DOI: 10.1016/j.jmarsys.2003.10.008

Goldbogen, J., J. Calambokidis, E. Oleson, J. Potvin, N. Pyenson, G. Schorr, and R. Shadwick. 2011. Mechanics, hydrodynamics and energetics of blue whale lunge feeding: efficiency dependence on krill density. *Journal of Experimental Biology,* 214**:** 131-146.

Goldbogen, J. A., J. Calambokidis, D. A. Croll, J. T. Harvey, K. M. Newton, E. M. Oleson, G. Schorr, and R. E. Shadwick. 2008. Foraging behavior of humpback whales: kinematic and respiratory patterns suggest a high cost for a lunge. *J Exp Biol,* 211**:** 3712-3719. DOI: 10.1242/jeb.023366

Goldbogen, J. A., A. S. Friedlaender, J. Calambokidis, M. F. McKenna, M. Simon, and D. P. Nowacek. 2013. Integrative Approaches to the Study of Baleen Whale Diving Behavior, Feeding Performance, and Foraging Ecology. *BioScience,* 63**:** 90-100. DOI: 10.1525/bio.2013.63.2.5

Goldbogen, J. A., E. L. Hazen, A. S. Friedlaender, J. Calambokidis, S. L. DeRuiter, A. K. Stimpert, B. L. Southall, and D. Costa. 2015. Prey density and distribution drive the three-dimensional foraging strategies of the largest filter feeder. *Functional Ecology,* 29**:** 951-961. DOI: 10.1111/1365-2435.12395

Goldbogen, J. A., J. Potvin, and R. E. Shadwick. 2010. Skull and buccal cavity allometry increase mass-specific engulfment capacity in fin whales. *Proc Biol Sci,* 277**:** 861-868. DOI: 10.1098/rspb.2009.1680

Hamner, W. M. 1984. Aspects of schooling in Euphausia superba. *Journal of Crustacean Biology,* 4**:** 67-74.

Hamner, W. M. 1995. Predation, cover, and convergent evolution in epipelagic oceans. *Marine and Freshwater Behaviour and Physiology,* 26**:** 71-89. DOI: 10.1080/10236249509378930

Hamner, W. M., and P. P. Hamner. 2000. Behavior of Antarctic krill (Euphausia superba): schooling, foraging, and antipredatory behavior. *Canadian Journal of Fisheries and Aquatic Sciences,* 57**:** 192-202.

Hampton, I. 1990. Measurements of differences in the target strength of Antarctic krill (Euphausia superba) swarms at 38 kHz and 120 kHz. *Selected scientific papers***:** 75-86.

Hazen, E. L., A. S. Friedlaender, M. A. Thompson, C. R. Ware, M. T. Weinrich, P. N. Halpin, and D. N. Wiley. 2009. Fine-scale prey aggregations and foraging ecology of humpback whales Megaptera novaeangliae. *Marine Ecology Progress Series,* 395**:** 75-89. DOI: 10.3354/meps08108

Healey, M. C., R. E. Thomson, and J. F. Morris. 1990. Distribution of commercial troll fishing vessels off southwest Vancouver Island in relation to fishing success and oceanic water properties and circulation. *Canadian Journal of Fisheries and Aquatic Sciences,* 47**:** 1846-1864.

Heywood, K. J. 1996. Diel vertical migration of zooplankton in the Northeast Atlantic. *Journal of Plankton Research,* 18**:** 163-184. DOI: 10.1093/plankt/18.2.163

Hsuesh, Y., and J. J. O'Brien. 1971. Steady coastal upwelling induced by an along-shore current. *Journal of Physical Oceanography,* 1**:** 180-186.

Isaacs, J. D., and R. A. Schwartzlose. 1965. Migrant Sound Scatterers: Interaction with the Sea Floor. *Science,* 150**:** 1810-1813.

Johnston, D., L. Thorne, and A. Read. 2005. Fin whales Balaenoptera physalus and minke whales Balaenoptera acutorostrata exploit a tidally driven island wake ecosystem in the Bay of Fundy. *Marine Ecology Progress Series,* 305**:** 287-295.

Johnston, D. W., M. E. Chapla, L. E. Williams, and D. K. Matthila. 2007. Identification of humpback whale Megaptera novaeangliae wintering habitat in the Northwestern Hawaiian Islands using spatial habitat modeling. *Endangered Species Research*. DOI: 10.3354/esr00049

Kennedy, A. S., A. N. Zerbini, O. V. Vásquez, N. Gandilhon, P. J. Clapham, and O. Adam. 2014. Local and migratory movements of humpback whales (Megaptera novaeangliae) satellite-tracked in the North Atlantic Ocean. *Canadian Journal of Zoology,* 92**:** 9-18. DOI: 10.1139/cjz-2013-0161

Kim, Y. J., and C. Gu. 2004. Smoothing spline Gaussian regression: more scalable computation via efficient approximation. *Journal of the Royal Statistical Society: Series B (Statistical Methodology),* 66**:** 337-356.

Krieger, K. J., and B. L. Wing. 1984. *Hydroacoustic surveys and identification of humpback whale forage in Glacier Bay, Stephens Passage, and Frederick Sound, southeastern Alaska, summer*

1983. National Oceanic and Atmospheric Administration, National Marine Fisheries Service, Northwest and Alaska Fisheries Center, Auke Bay Laboratory.
Krieger, K. J., and B. L. Wing. 1986. *Hydroacoustic monitoring of prey to determine humpback whale movements*. National Oceanic and Atmospheric Administration, National Marine Fisheries Service, Auke Bay Laboratory [Northwest and Alaska Fisheries Center].
Lampert, W. 1989. The Adaptive Significance of Diel Vertical Migration of Zooplankton. *Functional Ecology,* 3**:** 21-27. DOI: 10.2307/2389671
Lawson, G. L., P. H. Wiebe, C. J. Ashjian, S. M. Gallager, C. S. Davis, and J. D. Warren. 2004. Acoustically-inferred zooplankton distribution in relation to hydrography west of the Antarctic Peninsula. *Deep Sea Research Part II: Topical Studies in Oceanography,* 51**:** 2041-2072.
Mackas, D. L., K. L. Denman, and M. R. Abbott. 1985. Plankton patchiness: biology in the physical vernacular. *Bulletin of Marine Science,* 37**:** 652-674.
MacLennan, D. N., and E. J. Simmonds. 2013. *Fisheries Acoustics*. Springer Netherlands.
Mate, B. R., R. Gisiner, and J. Mobley. 1998. Local and migratory movements of Hawaiian humpback whales tracked by satellite telemetry. *Canadian Journal of Zoology,* 76**:** 863-868.
Mateos, M., G. M. Arroyo, A. Rodríguez, D. Cuenca, and A. De La Cruz. 2010. Calibration of visually estimated distances to migrating seabirds with radar measurements. *Journal of Field Ornithology,* 81**:** 302-309.
Mauchline, J. 1980. The Biology of Mysids and Euphausiids. In *Advances in Marine Biology,* ed. J. H. S. Blaxter, 373-677. Academic Press.
Miller, T. W., R. D. Brodeur, G. Rau, and K. Omori. 2010. Prey dominance shapes trophic structure of the northern California Current pelagic food web: evidence from stable isotopes and diet analysis. *Marine Ecology Progress Series,* 420**:** 15-26.
Moloney, C. L., A. Jarre, S. Kimura, D. L. Mackas, O. Maury, E. J. Murphy, W. T. Peterson, J. A. Runge, et al. 2010. Dynamics of marine ecosystems: ecological processes. In *Marine Ecosystems and Global Change,* eds. M. Barange, J. G. Field, R. P. Harris, E. E. Hofmann, R. I. Perry, and F. Werner. Oxford: Oxford University Press.
Murphy, E., J. Watkins, P. Trathan, K. Reid, M. Meredith, S. Thorpe, N. Johnston, A. Clarke, et al. 2007. Spatial and temporal operation of the Scotia Sea ecosystem: a review of large-scale links in a krill centred food web. *Philosophical Transactions of the Royal Society of London B: Biological Sciences,* 362**:** 113-148.
Murphy, E. J., D. J. Morris, J. L. Watkins, and J. Priddle. 1988. Scales of interactions between Antarctic krill and the environment. In *Antarctic Ocean and Resources Variability,* ed. D. Sarhage, 120-130. Berlin: Springer.
Nicol, S., and Y. Endo. 1999. Krill fisheries: development, management and ecosystem implications. *Aquatic Living Resources,* 12**:** 105-120.
Ogawa, T., and T. Shida. 1950. On the sensory tubercles of lips and oral cavity in the sei and fin whale. *Sci. Rep. Whales Res. Inst,* 3**:** 1-16.
Parks, S. E., D. A. Cusano, A. K. Stimpert, M. T. Weinrich, A. S. Friedlaender, and D. N. Wiley. 2014. Evidence for acoustic communication among bottom foraging humpback whales. *Scientific reports,* 4.
Pebesma, E. J. 2004. Multivariable geostatistics in S: the gstat package. *Computers & Geosciences,* 30**:** 683-691.
Piatt, J. F., and D. A. Methven. 1992. Threshold foraging behavior of baleen whales. *Marine Ecology Progress Series***:** 205-210.
Pillar, S., D. Armstrong, and L. Hutchings. 1989. Vertical migration, dispersal and transport of Euphausia lucens in the southern Benguela Current. *Marine Ecology Progress Series***:** 179-190.
Pivorunas, A. 1979. The Feeding Mechanisms of Baleen Whales: Since Robert Sibbald first described baleen whales in 1692, we have come to distinguish three types—the right whales, grazers on copepods; the finner whales, engulfers of krill and fish; and the gray whale, a forager of the sea bottom. *American Scientist,* 67**:** 432-440.
Price, H. J. 1989. Swimming behavior of krill in response to algal patches: a mesocosm study. *Limnology and Oceanography,* 34**:** 649-659.

Reid, K., A. S. Brierley, and G. A. Nevitt. 2000. An initial examination of relationships between the distribution of whales and Antarctic krill Euphausia superba at South Georgia. *Journal of Cetacean Research and Management*, 2**:** 143-149.

Santora, J. A., and C. S. Reiss. 2011. Geospatial variability of krill and top predators within an Antarctic submarine canyon system. *Marine Biology*, 158**:** 2527-2540. DOI: 10.1007/s00227-011-1753-0

Santora, J. A., C. S. Reiss, A. M. Cossio, and R. R. Veit. 2009. Interannual spatial variability of krill (Euphausia superba) influences seabird foraging behavior near Elephant Island, Antarctica. *Fisheries Oceanography*, 18**:** 20-35. DOI: 10.1111/j.1365-2419.2008.00490.x

Santora, J. A., C. S. Reiss, V. J. Loeb, and R. R. Veit. 2010. Spatial association between hotspots of baleen whales and demographic patterns of Antarctic krill Euphausia superba suggests size-dependent predation. *Marine Ecology Progress Series*, 405**:** 255-269. DOI: 10.3354/meps08513

Services, N. N. O. 2017. Tide Predictions at 9451785, THE BROTHERS, STEPHENS PASSAGE AK. Retrieved 2017, from https://tidesandcurrents.noaa.gov/noaatidepredictions.html?id=9451785.

Simmard, Y., G. Lacroix, and L. Legendre. 1986. Diel vertical migrations and nocturnal feeding of a dense coastal krill scattering layer (Thysanoessa raschi and Meganyctiphanes norvegica) in stratified surface waters. *Marine Biology*, 91**:** 93-105.

Simon, M., M. Johnson, and P. T. Madsen. 2012. Keeping momentum with a mouthful of water: behavior and kinematics of humpback whale lunge feeding. *J Exp Biol*, 215**:** 3786-3798. DOI: 10.1242/jeb.071092

Slijper, E. J., and R. J. Harrison. 1979. *Whales*. Cornell University Press.

Sourisseau, M., Y. Simard, and F. Saucier. 2006. Krill aggregation in the St. Lawrence system, and supply of krill to the whale feeding grounds in the estuary from the gulf. *Marine Ecology Progress Series*, 314**:** 257-270.

Sourisseau, M., Y. Simard, and F. J. Saucier. 2008. Krill diel vertical migration fine dynamics, nocturnal overturns, and their roles for aggregation in stratified flows. *Canadian Journal of Fisheries and Aquatic Sciences*, 65**:** 574-587. DOI: 10.1139/f07-179

Stimpert, A. K., D. N. Wiley, W. W. L. Au, M. P. Johnson, and R. Arsenault. 2007. 'Megapclicks': acoustic click trains and buzzes produced during night-time foraging of humpback whales (Megaptera novaeangliae). *Biology Letters*, 3**:** 467-470. DOI: 10.1098/rsbl.2007.0281

Straley, J. M., C. M. Gabriele, and C. S. Baker 1994. Seasonal characteristics of humpback whales(Megaptera novaeangliae) in southeastern Alaska. PhD Thesis University of Alaska Fairbanks

Szabo, A. 2015. Immature euphausiids do not appear to be prey for humpback whales (Megaptera novaeangliae) during spring and summer in Southeast Alaska. *Marine Mammal Science*, 31**:** 677-687. DOI: 10.1111/mms.12183

Szabo, A. R. 2011. Aspects of the foraging Ecology of Humpback Whales (Megaptera novaeangliae) in Frederick Sound and Stephens Passage, Southeast Alaska. PhD Thesis Oregon State University

Szabo, A. R., and H. P. Batchelder. 2014. Late spring and summer patterns of euphausiid reproduction in Southeast Alaska fjord waters. *Marine Ecology Progress Series*, 516**:** 153-161. DOI: 10.3354/meps11003

Tarling, G., J. Cuzin-Roudy, and F. Buchholz. 1999. Vertical migration behaviour in the northern krill Meganyctiphanes norvegica is influenced by moult and reproductive processes. *Marine Ecology Progress Series***:** 253-262.

Tarling, G. A., T. Klevjer, S. Fielding, J. Watkins, A. Atkinson, E. Murphy, R. Korb, M. Whitehouse, et al. 2009. Variability and predictability of Antarctic krill swarm structure. *Deep Sea Research Part I: Oceanographic Research Papers*, 56**:** 1994-2012. DOI: 10.1016/j.dsr.2009.07.004

R: A language and environment for statistical computing. 3.1.2, R Foundation for Statistical Computing, Vienna, Austria.

Trathan, P., J. Priddle, J. Watkins, D. Miller, and A. Murray. 1993. Spatial variability of Antarctic krill in relation to mesoscale hydrography. *Marine Ecology Progress Series***:** 61-71.

Ware, C., A. S. Friedlaender, and D. P. Nowacek. 2011. Shallow and deep lunge feeding of humpback whales in fjords of the West Antarctic Peninsula. *Marine Mammal Science,* 27**:** 587-605. DOI: 10.1111/j.1748-7692.2010.00427.x

Weingartner, T., L. Eisner, G. L. Eckert, and S. Danielson. 2009. Southeast Alaska: oceanographic habitats and linkages. *Journal of Biogeography,* 36**:** 387-400. DOI: 10.1111/j.1365-2699.2008.01994.x

Weinrich, M. 1998. Early experience in habitat choice by humpback whales (Megaptera novaeangliae). *Journal of Mammalogy,* 79**:** 163-170.

Wiebe, P. H., and C. H. Greene. 1994. The use of high frequency acoustics in the study of zooplankton spatial and temporal patterns. In *Proc. NIPR Symp. Polar Biol*, 133-157.

Williams, R., R. Leaper, A. N. Zerbini, and P. S. Hammond. 2007. Methods for investigating measurement error in cetacean line-transect surveys. *Journal of the Marine Biological Association of the UK,* 87**:** 313. DOI: 10.1017/s0025315407055154

Witteveen, B. H., J. M. Straley, E. Chenoweth, C. S. Baker, J. Barlow, C. Matkin, C. M. Gabriele, J. Neilson, et al. 2011. Using movements, genetics and trophic ecology to differentiate inshore from offshore aggregations of humpback whales in the Gulf of Alaska. *Endangered Species Research,* 14**:** 217-225.

Wood, S. N. 2006. *Generalized Additive Models: An Introduction with R*. CRC Press.

Wood, S. N. 2011. Fast stable restricted maximum likelihood and marginal likelihood estimation of semiparametric generalized linear models. *Journal of the Royal Statistical Society: Series B (Statistical Methodology),* 73**:** 3-36.

Woodson, C., and M. McManus. 2007. Foraging behavior can influence dispersal of marine organisms. *Limnology and Oceanography,* 52**:** 2701-2709.

Zeileis, A., and C. Kleiber. 2008. AER: applied Econometrics with R. *R package version 0.9-0, URL http://CRAN. R-project. org/package= AER*.

Zuur, A. F., E. N. Ieno, and C. S. Elphick. 2010. A protocol for data exploration to avoid common statistical problems. *Methods in Ecology and Evolution,* 1**:** 3-14.

Zuur, A. F., E. N. Ieno, N. J. Walker, A. A. Saveliev, and G. M. Smith. 2011. *Mixed Effects Models and Extensions in Ecology with R*. Springer.

8 APPENDIX

S1. Location of transect lines of sonar surveys and results of whale survey

Whale and sonar surveys were completed fourteen times in the study area. Figure S1shows the transect lines used in the sonar survey. A stratified random sampling design was employed, and this is why the lines are not evenly spaced and are in different locations within each strata for each survey. Figure S2 depicts the strata that were surveyed for whales over the fourteen surveys of the study, and the location of all whales that were spotted.

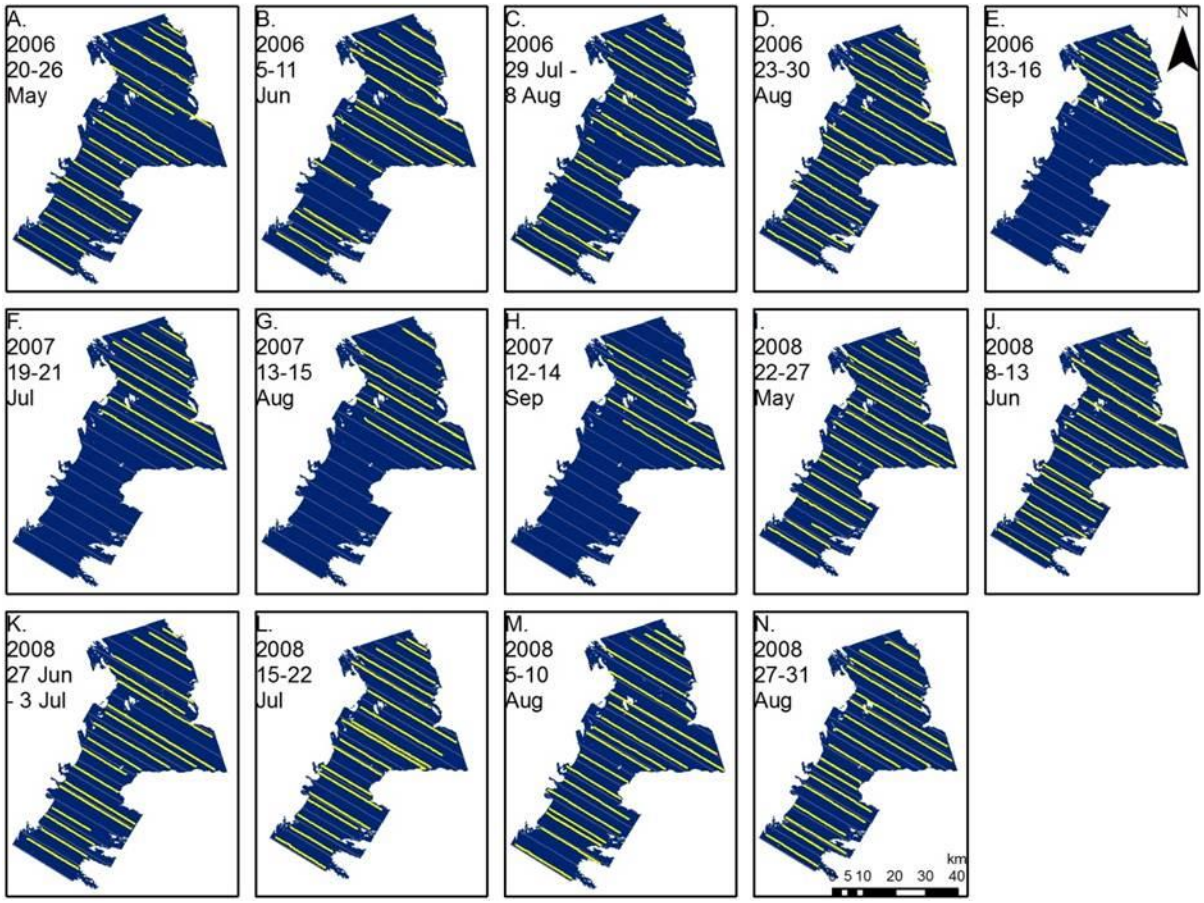

Figure S1. Sonar sampling transect lines. Yellow lines represent boat path for each survey. Study area was sampled from south to north over the course of approximately five days. Most inconsistencies are because sampling was weather-dependent.

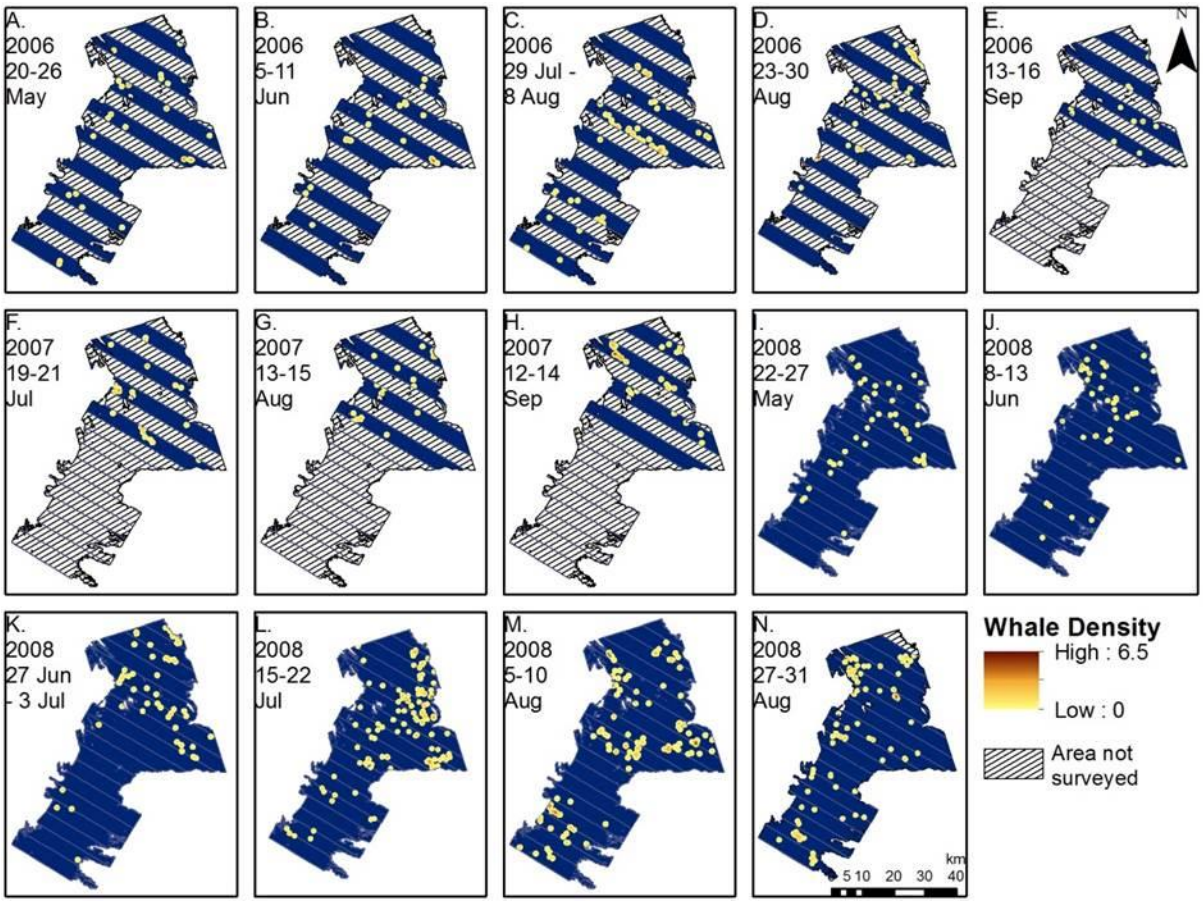

Figure S2. Results of whale surveys. Resighted whales and whales outside the stratum being surveyed were removed from the dataset and are not shown. The whale spotting vessel was driven down the center of the stratum for 2006 and 2007. In 2008, the whale spotters were on board the sonar surveying vessel. See Figure S1 for location of the 2008 transect lines.

S2. Methodology to correct sonar data for single targets

Conversion of single targets' target strength (TS) values to NASC values was done using the following equations. Variables used in the equations are reported in Table S1.

Table S1. Variables used in sonar equations

Variable	Value	Description
φ	$10^{(-\frac{21}{10})}$	Equivalent beam angle of sonar (beam width)
α	-0.51	
C	$2 \times \alpha$	Calibration factor, dependent on transducer sensitivity and electronic components of echo integrator
c	1473.59 m/s	Speed of sound in water
T_p	0.000256 sec	Pulse duration of a single ping
TS	Varies	Target strength of a single target
$target\ range$	Varies	Distance to the single target
$beam\ volume$	Varies	Beam volume at integrated echo depth
$thickness$	Varies	Thickness (height) of insonified volume at integrated echo depth

$$Calibrate = 10 \times \log_{10} \frac{c \times T_p \times \varphi}{2} \text{ [calibration factor, specific to sonar]}$$

$$LogR20 = 20 \times \log_{10}(target\ range) \text{ [time varied gain correction factor]}$$

$$s_{v,single} = TS - LogR20 - Calibrate + C \text{ [single target backscatter, in dB]}$$

$$linear_{sv\_single} = 10^{\frac{s_{v,single}}{10}} \text{ [single target backscatter, linearized]}$$

$$E_{total} = linear_{sv\_single} \times n \text{ [total backscatter]}$$

$$E_{mean} = \frac{E_{total}}{beam\ volume} \text{ [volume backscatter]}$$

$$NASC_{single\_target} = 4\pi \times 1852^2 \times E_{mean} \times thickness \text{ [NASC]}$$

S3. R scripts to define krill patches and patch groups

A. Krill patch definition

The following code was used to define a krill patch in R. The function defined all patches within a transect, and patches were then 'cut' into the grid cell they were located in. The function was thus applied in a loop of each survey and each transect within each survey.

```
lyrs=function(df,cut,dist_thr,vert_scale){
  #df: the data frame containing data from one transect
  #cut: the NASC cutoff value for defining a layer
  #dist_thr: the distance between points for defining a layer
  #vert_scale: the amount the vertical (depth) is scaled to be equivalent
with horizontal distance
  require(sp)
  require(rgdal)

  df_cut=df[which(df$NASC_corrected>=cut),]

  if (length(df_cut[,1]>1)){
    x=df_cut$Dist_M
    y=df_cut$Depth_mean * vert_scale
```

```
xy=SpatialPointsDataFrame(matrix(c(x,y),ncol=2),data.frame(ID=df_cut$mergeI
D))

      chc=hclust(dist(data.frame(rownames=rownames(xy@data),
      x=coordinates(xy)[,1], y=coordinates(xy)[,2])), method='single')

    chc.330=cutree(chc, h=dist_thr)

    xy@data=data.frame(xy@data, Clust=chc.330)
    out=xy@data
    df_clus=merge(df, out, by.x='mergeID', by.y='ID', all.x=TRUE)
    return(df_clus)
  }
  else {
    df_clus=df[0,]
    df_clus$Clust=integer(0)
    return(df_clus)
  }
}
```

B. Krill patch grouping

The following code was used to group krill patches by depth. All krill patches within a grid cell with a mean depth that was within 35 meters of one another were grouped together using the first function, first_clustergroup(). If the group consisted of patches that spanned more than 35 vertical meters (identified using the function group_range()), the group was split along the greatest separation distance using the function split_groups(). This process was repeated twice to ensure that all groups spanned the correct range.

```
first_clustergroup = function(depths,ids){
  ids=seq(1,length(depths), by=1)   #these are their id values
  group_df=as.data.frame(cbind(depths, ids))
  group_df$UID=U_ids
  group_df$ids2=NA
  colnames(group_df)=c('depths', 'ids', 'UID', 'ids2')
  c1=clusters(depths, 35)   #group the patches
  c1_num=length(c1)         #find the initial number of groups
  if(c1_num>0){
    #find how many of the points have been placed in a cluster
    n_inclust=0
    for(j in 1:length(c1)){
      n_inclust=length(c1[[j]])+n_inclust
    }

    #find how many points there are total
    n_tot=nrow(cl2)

    #find how many points are not in a cluster
    n_notinclust=n_tot - n_inclust

    #create vector of all points not in a cluster
    p_independent=NA   #points not in a cluster
    p_incluster=numeric()   #points in a cluster
    p_incluster_ind=numeric()   #index of points in a cluster
    #find points in a cluster
    for(j in 1:length(c1)){
      p_incluster=append(p_incluster, c1[[j]])
    }
```

```
    #create index of points in a cluster
    for(j in 1:length(p_incluster)){
      p_incluster_ind=append(p_incluster_ind,
which(depths==p_incluster[j]))
    }
    #find points not in a cluster
    p_independent=depths[-unique(p_incluster_ind)]   #this is a list of all
the points not initially in the cluster
    #give all points not in a cluster a unique id
    j=0
    if(length(p_independent)>0){
      for(j in 1:length(p_independent)){
        group_df$ids2[which(depths==p_independent[j])]=j
      }
    }
    #give all points in a cluster the cluster id
    clusnum=j
    if(c1_num>0){
      for(j in 1:c1_num){
        clusnum=clusnum+1
        cl_0=c1[[j]]
        p_inclust_ind0=as.numeric()
        for(k in 1:length(cl_0)){
          p_inclust_ind0=append(p_inclust_ind0, which(depths==cl_0[k]))
        }
        group_df$ids2[unique(p_inclust_ind0)]=clusnum
      }
    }

    # write clustering to original file
    return(group_df$ids2)
    #cl$grouping[wind]=group_df$ids2
    #cl2$grouping=group_df$ids2
  }
  else {
    return(seq(1, length(depths), by=1))
    #cl$grouping[wind]=seq(1, length(wind), by=1)
    #cl2$grouping=seq(1, length(wind), by=1)
  }
}

group_range = function(cl2, un_groups){
  for(j in un_groups){
    gr_ind=which(cl2$grouping==j)
    gr_i=cl2[gr_ind,]
    gr_range=max(gr_i$depth_av)[1] - min(gr_i$depth_av)[1]
    for(k in gr_ind){
      cl2$range1[k]=gr_range
    }
  }
  return(cl2)
}

split_groups=function(cl2, un_groups){
  for(j in un_groups){
    new_id1=j
    new_id2=j+0.01
    while(new_id2 %in% un_groups){
      new_id2=new_id2+0.01
    }
    gr_ind=which(cl2$grouping==j)
```

```
    gr_i=cl2[gr_ind,]
    npts=nrow(gr_i)
    if(gr_i$range1[1]>35){
      ord=order(gr_i$depth_av)
      d2=gr_i$depth_av[ord]
      #didn't write anything for i2
      brks=rep(NA, npts)
      for (p in 1:(npts-1)){    #calculate distance between each patch
(already sorted)
        brks[p]=d2[p+1]-d2[p]
      }
      brks_max=which(brks==max(brks, na.rm=TRUE))[1]   #find maximum
distance between patches
      clus_group1=rep(new_id1, brks_max)        #assign all pts before
break to cluster 1
      clus_group2=rep(new_id2, (npts - brks_max))  #assign all pts after
break to cluster 2
      clus_group0=c(clus_group1, clus_group2)   #combine the two clusters
      clus_group0_sort=rep(NA,npts)       #initialize vector to hold
cluster assignments in proper order
      for (q in 1:npts){                  #re-sort clusters to original
order
        clus_group0_sort[ord[q]]=clus_group0[q]
      }
      gr_i$grouping2=clus_group0_sort
    }
    else{
      gr_i$grouping2=gr_i$grouping
    }
    cl2$grouping2[gr_ind]=gr_i$grouping2
  }
  return(cl2)
}
```

S4. Additional model results

The four models that were built to test the importance of the density, quantity and depth of prey for foraging humpback whales were the base model, the densest model, the largest model and the shallowest model. The base model explained 53% of deviance and had an adjusted R^2 value of 0.50 (Table S2). The shallowest, largest and densest models explained 47%, 41% and 38% of deviance and had adjusted R^2 values of 0.34, 0.31 and 0.24, respectively (Table S3). A total of 480 grid cells were used in the model, of which 202 contained whales.

Comparison of model using all patches, shallowest, largest and densest patch

All four final models used similar predictor variables, although there were some differences in interaction terms. For the base model, the interaction terms related to backscatter had the greatest explanatory value (Table S2) and were highly significant ($p<0.0001$, Table S2). The smooth functions of the base model are presented in Figure S4. Those of the other three models were very similar to the base model as well as being nearly identical to one another, so only the shallowest model smooth functions are presented (Figure S5). There was a small but highly significant seasonal effect, where the predicted number of whales increased between July and August (Figure S4A**,** Table S2**,** $p<0.0001$). Before July, the linear predicted value for day of the year (DOY) was negative, and in August it was positive. The effect of time between when a whale was spotted and they hydroacoustic survey was also highly significant ($p<0.0001$, Table S2). The model predicted more whales between two and zero hours before the grid cell was surveyed with the sonar (Figure S4B). The effect of tide on whale count was weak and could arguably have been dropped from the model ($p=0.005$, Table S2). However, the model predicted fewer whales at peak low tide and otherwise tide had no effect on whale counts (Figure S4C). Finally, the z-value of the hot-spot analysis averaged over all surveys (meanZ) was highly significant ($p<0.0001$, Table S2), with an increasing linear effect (Figure S4D). Time of day (TOD) and the local conditions surrounding a grid cell (locZ) had no predictive value and were dropped from the model (Table S2).

Base Model

In the base model, backscatter variables were very important for explaining whale counts while bathymetry had a smaller role. The interaction terms related to backscatter had the greatest predictive value (Figure S3A, B and C) and were highly significant ($p<0.0001$, Table 8). The area of a patch had particularly strong predictive effects, with few whales being predicted for patches less than 22,000 m2 ($e^{10} \approx 22{,}000$) in vertical area. Few whales were predicted where patches were at 110-150 meters' depth; most whales were predicted at patches with 20-110 meters' depth and large areas. The effect of NASC was less clear, although there was a cutoff value below which no whales were predicted when looking at the relationship between NASC magnitude and patch area. This relationship did not exist between NASC and patch depth, and if anything higher NASC values led to lower whale predictions with respect to density and depth.

The interaction between bottom depth and water flow direction relative to bottom aspect was significant for the base model ($p=0.00006$, Table S2), although its predictive value was not as strong as the interactions of backscatter variables (Figure S3D). At shallow areas (0-120 meters) with water striking the bottom at -360 to -110 degrees, whales were predicted. This corresponded mainly to grid cells with a north- to west-facing slope with water flowing in a northerly to easterly direction.

Shallowest Model

For the shallowest model, interaction terms related to backscatter and bathymetry were both important for predicting whales. When the three-way interaction between NASC, patch area and patch depth was simplified into three two-way interactions, it became evident that the interaction between patch depth and NASC was not important for the model. The AIC score was 1418 for the three-way interaction term, 1382 for the three two-way interactions, and 1382 when the interaction between depth and NASC was dropped; the interaction was not significant ($p=0.11$). The interaction between depth and NASC was therefore dropped. While the interaction between patch area and backscatter was not highly significant ($p=0.046$), it was still important for the model (AIC=1399 without it).

The effect of depth and patch area together were important for predicting whales in the shallowest model ($p=0.0005$, Table S3). Depth had a negative effect on predicted whale counts, while patch area had a positive effect (Figure 9A). More whales were predicted at either shallow or large patches, but not at deep and small patches. Patch area and NASC did not affect whale predictions as strongly, although more whales were predicted at either very dense or very large patches (Figure 9B). The relationship of water flow direction to bathymetry and depth were very different from the base model, although it was highly significant ($p<0.0001$, Table S3). Water with a depth of 0-200 meters was unfavorable for whales, while areas below 200 meters deep were favorable (Figure 9C). The direction that water hit the bottom had a modifying effect on this, with peaks in predicted whale counts at three locations: where water flowed northeast over a southwest facing slope (-210^0), water flowed westward to northward over northeast to southeast facing slopes (60^0), and water flowed in a southwest to northwest direction over slopes facing the same direction (260^0). The interaction between depth and surface roughness was also very significant ($p<0.0001$, Table S3), although the interaction was once again dominated by depth (Figure 9D). The model predicted most whales at around 50 to 200 meters' depth, with more whales above a rougher surface.

Largest Model

The predictive value of the backscatter variables was much lower for the largest GAM model, although they were still highly significant ($p<0.0001$, Table 5). Their forms can be seen in Figure 10, and while more whales were predicted at very large, shallow patches (Figure 10A) and large, dense patches (Figure 10C), whales were also predicted at small and sparse patches and small and deep patches. The interaction of water depth and bottom roughness was similar to that of the shallowest model, as was the interaction between water depth and water flow direction over the bottom (Figure 10D and E).

Densest Model

The three-way interaction for backscatter variables was once again highly significant for the densest model ($p<0.0001$, Table S3). The most important part of this interaction was a prediction for more whales at shallow patches with high backscatter (Figure 11B). The model also predicted more whales at shallow patches with a large area (Figure 11A). There was also a prediction for more whales at very small patches and fewer whales at very high and very low backscatter values. The two-way interaction between bottom roughness and the direction of water flow over the bottom was highly significant ($p<0.0001$, Table S3), and more whales were predicted at the same peaks as seen in the shallowest model. Rougher bottoms also had higher whale predictions. The interaction between water depth and bottom roughness was highly significant ($p<0.0001$, Table S3), but the relationship between the two is rather unclear besides a general increase in the number of whales predicted with increasing depth (Figure 11E).

Model Evaluation

Based on percent deviance explained, R^2 values and model error, the base model was most successful in explaining humpback whale locations. AIC values could not be compared between the models since different explanatory variables were used. The results of the base model mapped against actual whale observations (Figure 10, Figure 11) indicated that the model captured general spatial trends in actual whale locations, although there was clearly some mismatch between predicted and observed whale counts. The absolute error, calculated as the observed whale count minus the predicted whale count, is shown for each survey in Figure 12.

The base model residuals did not follow a normal distribution (Figure 13A), which was confirmed using the Pearson Chi-square test for normality ($P=78.9$, $p<0.0001$). A quantile-quantile plot of the residuals, which plots the sorted residuals percentiles against a normal distributions' percentiles, also indicated some skew at the ends of the residual values, particularly the upper values (Figure 13B). An examination of the model residuals plotted against the fitted values (Figure 13C) indicated a slight cone shape in the residuals, suggesting heterogeneity. Finally, plotting the predicted against observed whale count showed a tendency for the model to underestimate large values and overestimate small values (Figure 13D). These patterns were also true for the shallowest, largest and densest models (see Appendix S4).

A test of model dispersion also indicated that all models were overdispersed. The models had an α between 1.4 to 1.9 (Table S2, Table S3). When a negative binomial distribution was used instead, however, the model performance decreased drastically ($R^2=0.26$) and the model residuals were highly skewed to the right. The same was true for a quasipoisson distribution ($R^2=0.33$). Because of this, the Poisson distribution was retained despite leading to an overdispersed model. It was likely that one or several explanatory variables were missing, thus leading to overdispersion.

Table S2. GAM results using all patches. Effective degrees of freedom (edf) represents model smoothness, with a lower edf representing a less flexible model. Smoothing functions are represented by s(). P-values in italics correspond to terms not included in the final model. See Table 2 for a description of the predictor variables. A value of $\alpha > 0$ indicates that the model is overdispersed.

Layer definition:	**Base model**		
Predictor:	Edf (estimate)	Chi-sq (z-value)	*p*
Intercept	(-17.8)	(-149)	<2e-16
s(area, depth, NASC)	53.7	264	<2e-16
s(DOY)	4.8	94	<2e-16
s(ws_hours)	3.6	52	5.6e-10
s(tide)	2.5	13	0.0052
s(meanZ)	1	17	5.6e-10
s(asp_wflow, depth)	13.8	50	6.4e-5
s(TOD)	1	0	*0.99*
s(locZ)	1	0.4	*0.5*
D.E.		52.8	
Adj. R^2		0.502	
UBRE			
RMSE		1.36	
MAE		0.87	
Dispersion	*z*=4.2	*p*=1.5e-5	α=1.46

Table S3. Model results of three separate GAMs built using the densest, shallowest or largest patch as an explanatory variable. Edf: Effective degrees of freedom; smoothing functions are represented by s(); D.E.: percent deviance explained; RMSE: root mean square error; MAE: mean absolute error. P-values in italics correspond to terms not included in the final model. See Table 5 for a description of the predictor variables. A value of $\alpha > 0$ indicates that the model is overdispersed.

Layer definition:	**Shallowest**			**Largest**			**Densest**		
Predictor:	edf (est.)	Chi-sq (z)	*p*	edf (est.)	Chi-sq (z)	*p*	edf (est.)	Chi-sq (z)	*p*
Intercept	(-17.7)	(-183)	<2e-16	(-17.7)	(-244)	<2e-16	(-17.6)	(-241)	<2e-16
s(area, depth, NASC)	-	-	-	10.9	67	1.2e-9	9.0	39	1.2e-5
s(area, depth)	20.8	58	0.0005	-	-	-	-	-	-
s(area, NASC)	11.4	25	0.046	-	-	-	-	-	-
s(NASC,depth)	-	-	-	-	-	-	-	-	-
s(DOY)	3.4	70	4.7e-14	3.4	78	8.2e-16	3.6	93	<2e-16
s(ws_hours)	3.6	60	4.8e-12	4.2	59	3.5e-11	3.6	72	1.4e-14
s(tide)	2.3	14.8	0.0017	2.6	18	0.0005	2.3	13	0.005
s(meanZ)	1	30	3.8e-8	1	30	4.7e-8	1	24	1.2e-6
s(asp_wflow, depth)	19.3	75	6.2e-8	14.6	41	0.0018	-	-	-
s(arearat, depth)	19.2	76	4.0e-8	15.3	29	0.06	17.2	61	4.7e-6
s(arearat, asp_wflow)	-	-	-	-	-	-	15.5	65	4.9e-7
s(TOD)	1	0.5	*0.5*	1	4	*0.04*	1	2.3	*0.13*
s(locZ)	1	0	*0.98*	1	0	*0.95*	1.9	0.7	*0.7*
D.E.		46.7			41			37.7	
Adj. R^2		0.34			0.314			0.238	
UBRE									
RMSE		1.56			1.71			1.74	
MAE		0.98			1.0			1.1	
Dispersion	z=5.3	p=5.7e-8	α=1.5	z=4.6	p=2.4e-6	α=1.5	z=5.0	p=2.5e-7	α=1.9

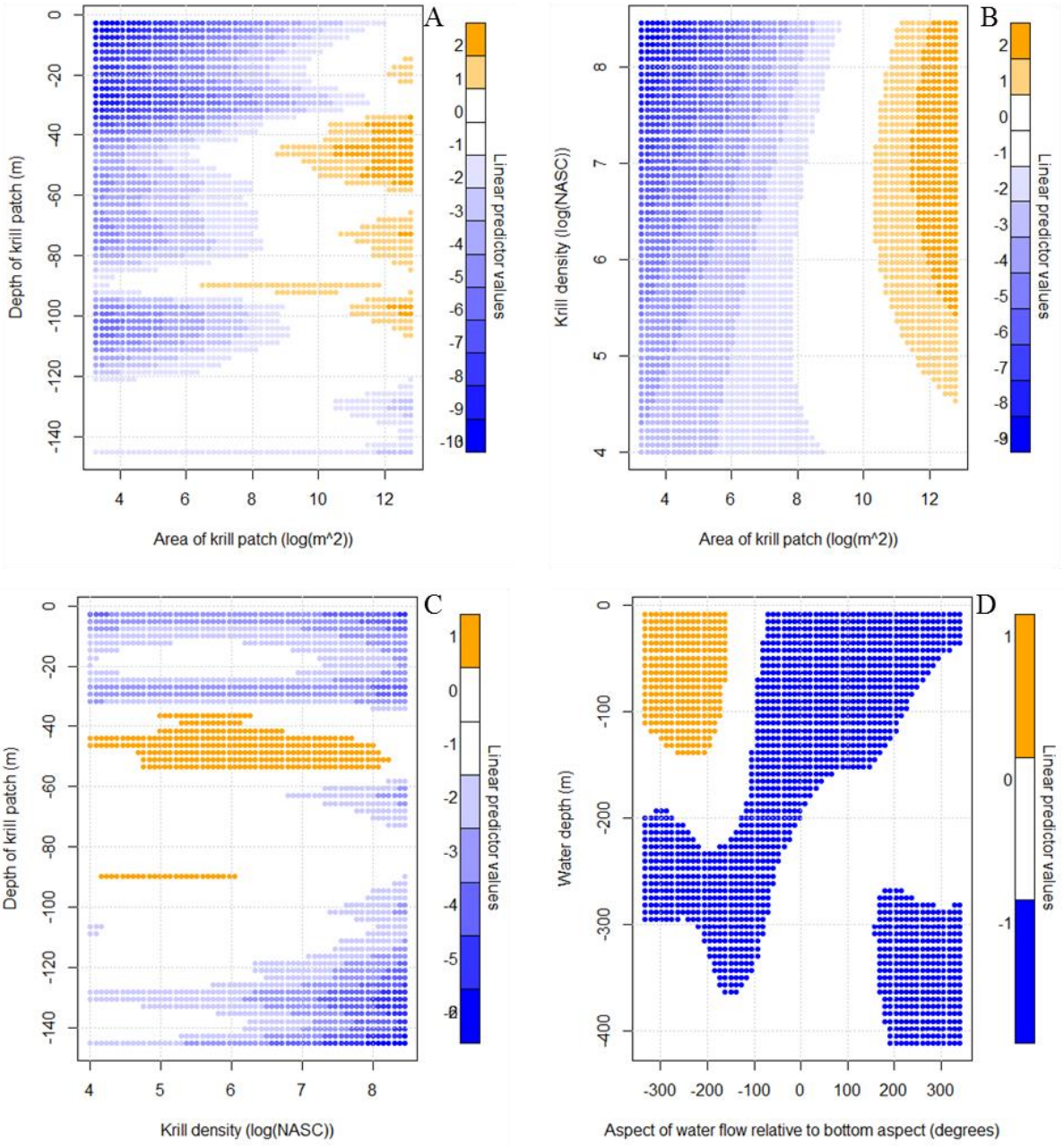

Figure S3. Interaction terms for the GAM base model. Panels A, B, and C depict the three-way interaction between patch depth, patch area, and backscatter. Panel D depicts the two-way interaction between water depth and the angle at which water flows against the bottom aspect. The linear predictor value is the value of the smooth function and shows the direction (orange is positive, blue is negative) and magnitude of the interaction term's contribution to predicting whale values. Note differing scale on color bars.

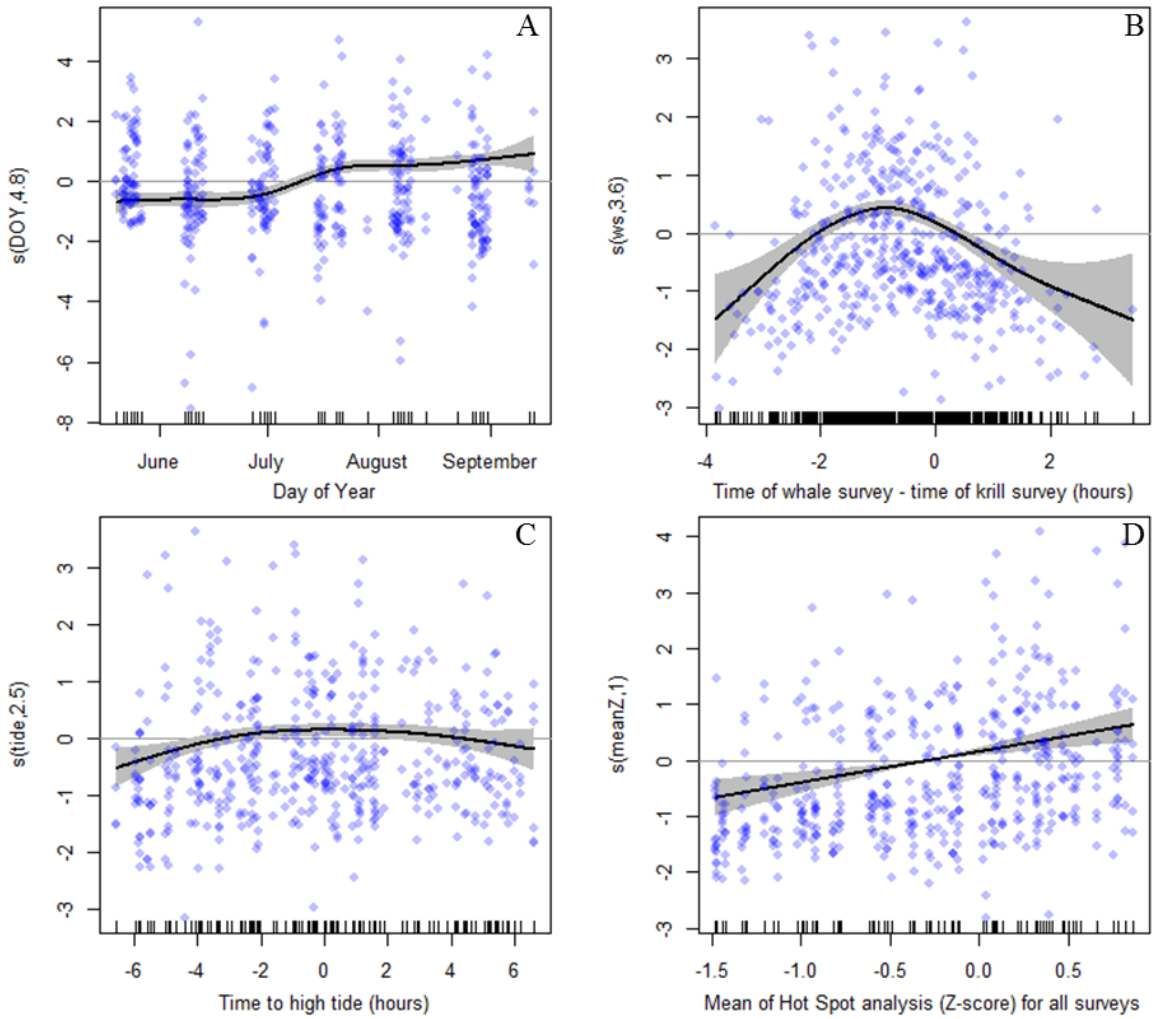

Figure S4. Single interaction terms of the GAM base model. The y-axis represents the terms of the smooth function (i.e. linear predictor values) for each predictive variable. A negative value has a negative effect on the number of predicted whales while a value above zero has a positive effect. The dark line is the smooth function, the gray band represents a 95% confidence interval, the blue dots are the model residuals, and the rug on the x-axis represents the input data points.

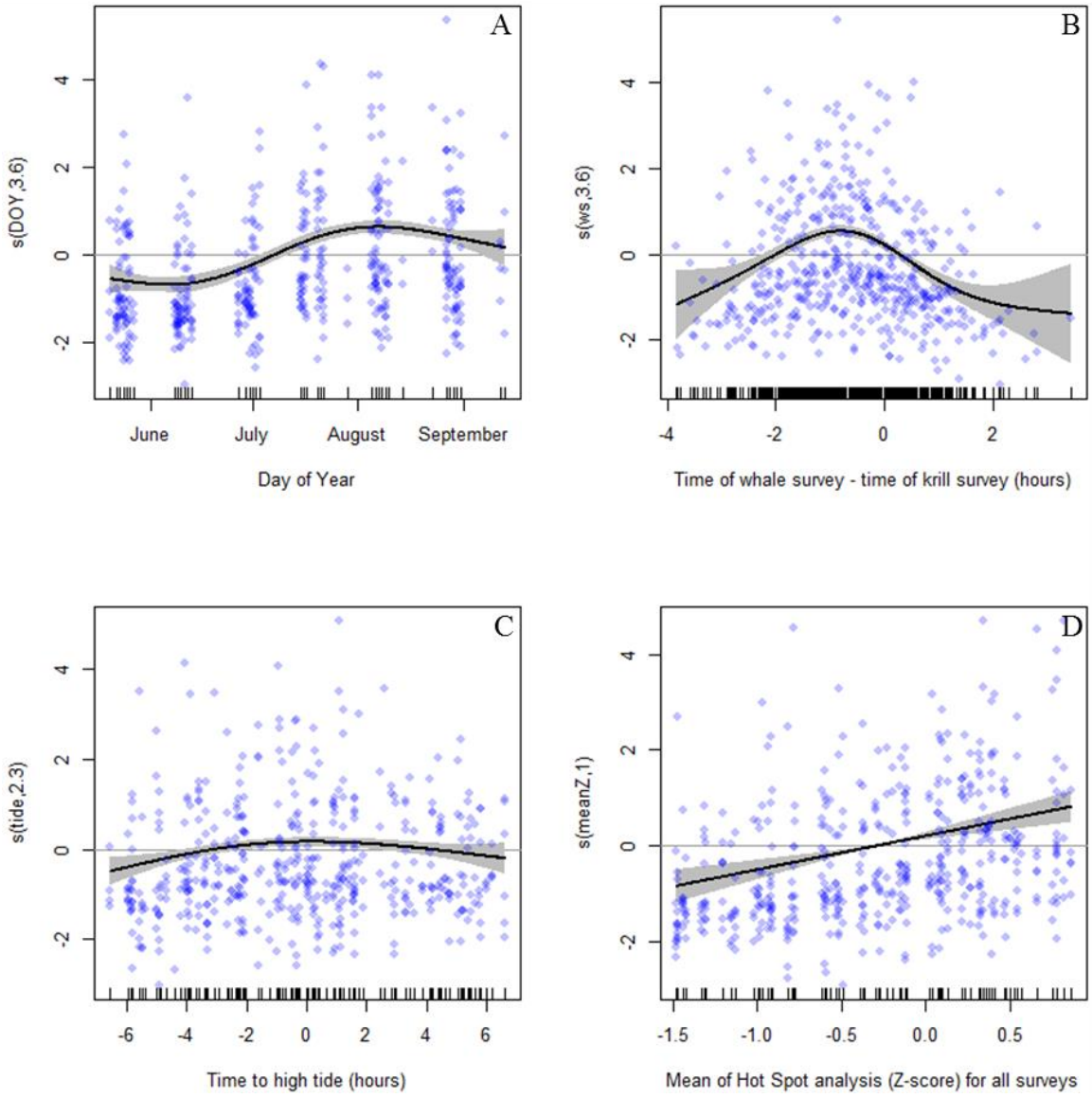

Figure S5. Modeled smooth functions for the predictor variables of the densest model. The smooth functions for the shallowest and largest models are nearly identical to this and are therefore not depicted.The y-axis represents the terms of the smooth function (i.e. linear predictor values) for each predictive variable. A negative value has a negative effect on the number of predicted whales while a value above zero has a positive effect. The dark line is the smooth function, the gray band represents a 95% confidence interval, the blue dots are the model residuals, and the rug on the x-axis represents the input data points.

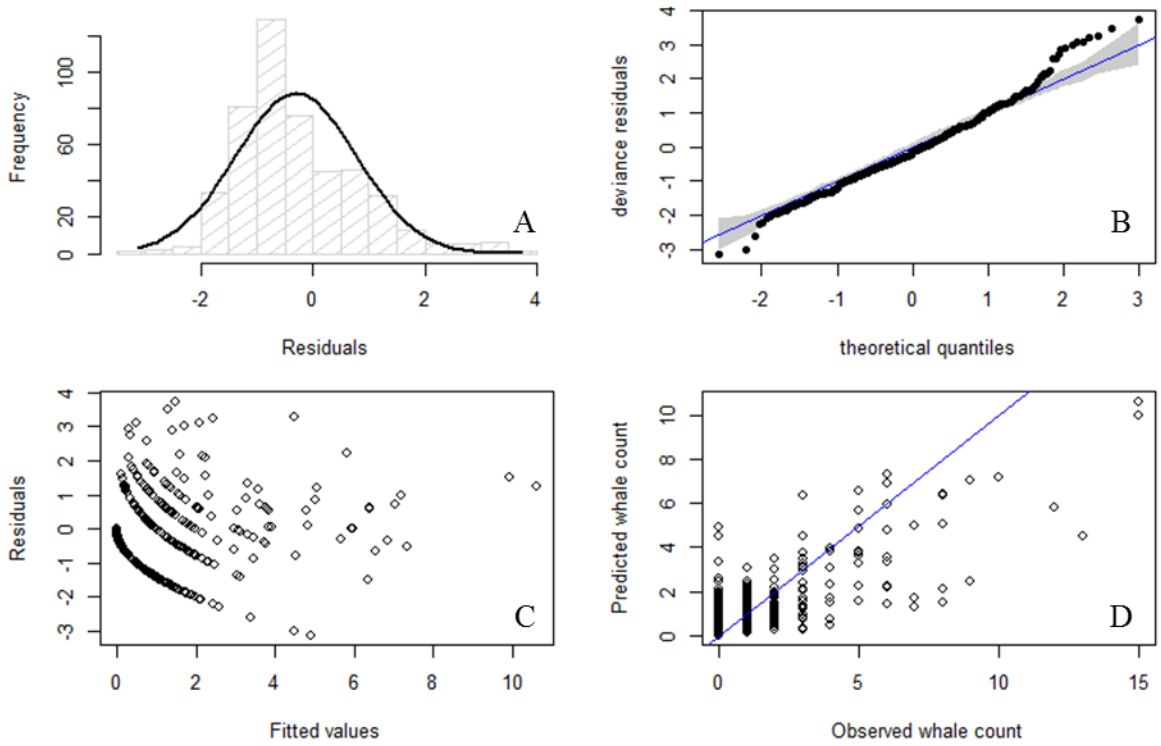

Figure S6. Evaluation of residuals and model fit for the base model. Panels A and B assess if the residuals have a normal distribution. The residuals were skewed to the left and did not have a normal distribution. Panel C assesses whether the model exhibits homogeneity. There was some indication of a heterogeneic cone-shape, with the model fitting very well to larger values. Panel D shows the model's predictive power.

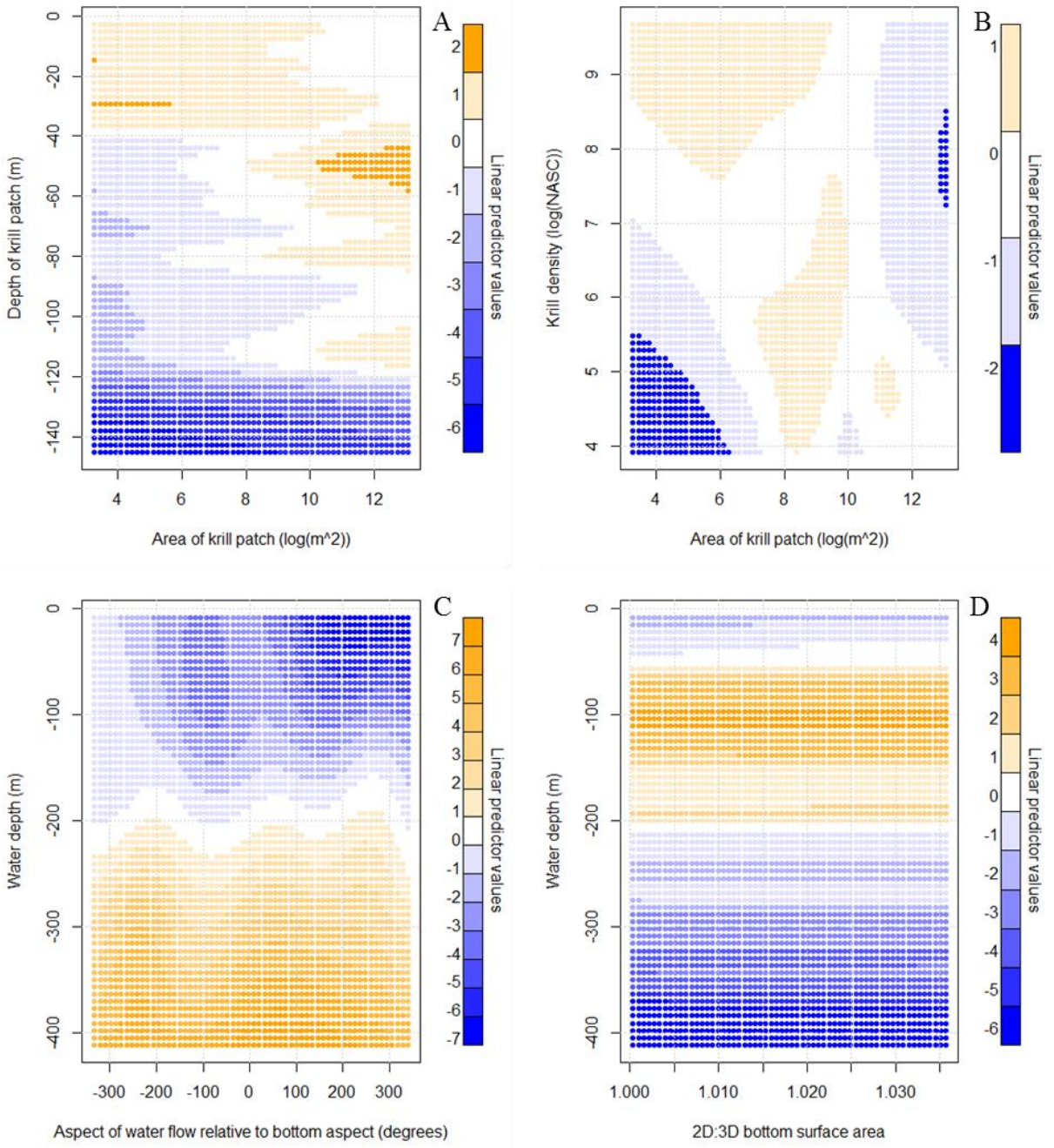

Figure S7. Shallowest GAM interaction terms. All panels depict two-way interactions. The linear predictor value is the value of the smooth function and shows the direction (orange is positive, blue is negative) and magnitude of the interaction term's contribution to predicting whale values. Note differing scale on color bars.

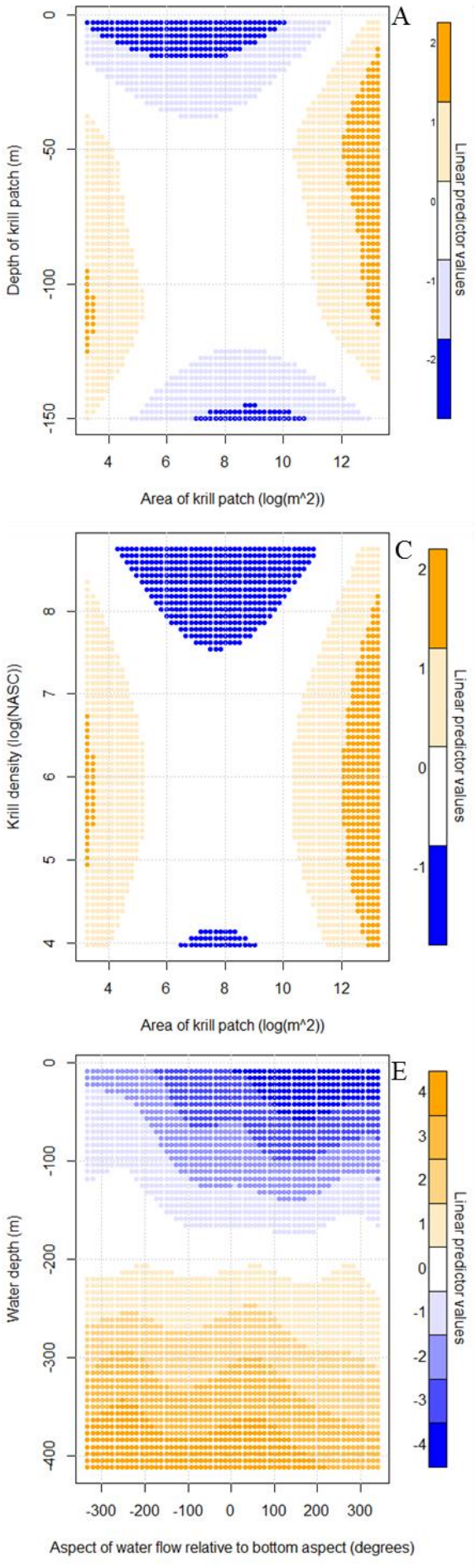

Figure S8. Largest GAM interaction terms. Panels A, B, and C depict the three-way interaction between patch depth, patch area, and backscatter. Panel D and E depict two-way interactions between water depth with bottom surface roughness (D) or with the angle at which water flows against the bottom aspect (E). The linear predictor value is the value of the smooth function and shows the direction (orange is positive, blue is negative) and magnitude of the interaction term's contribution to predicting whale values. Note differing scale on color bars.

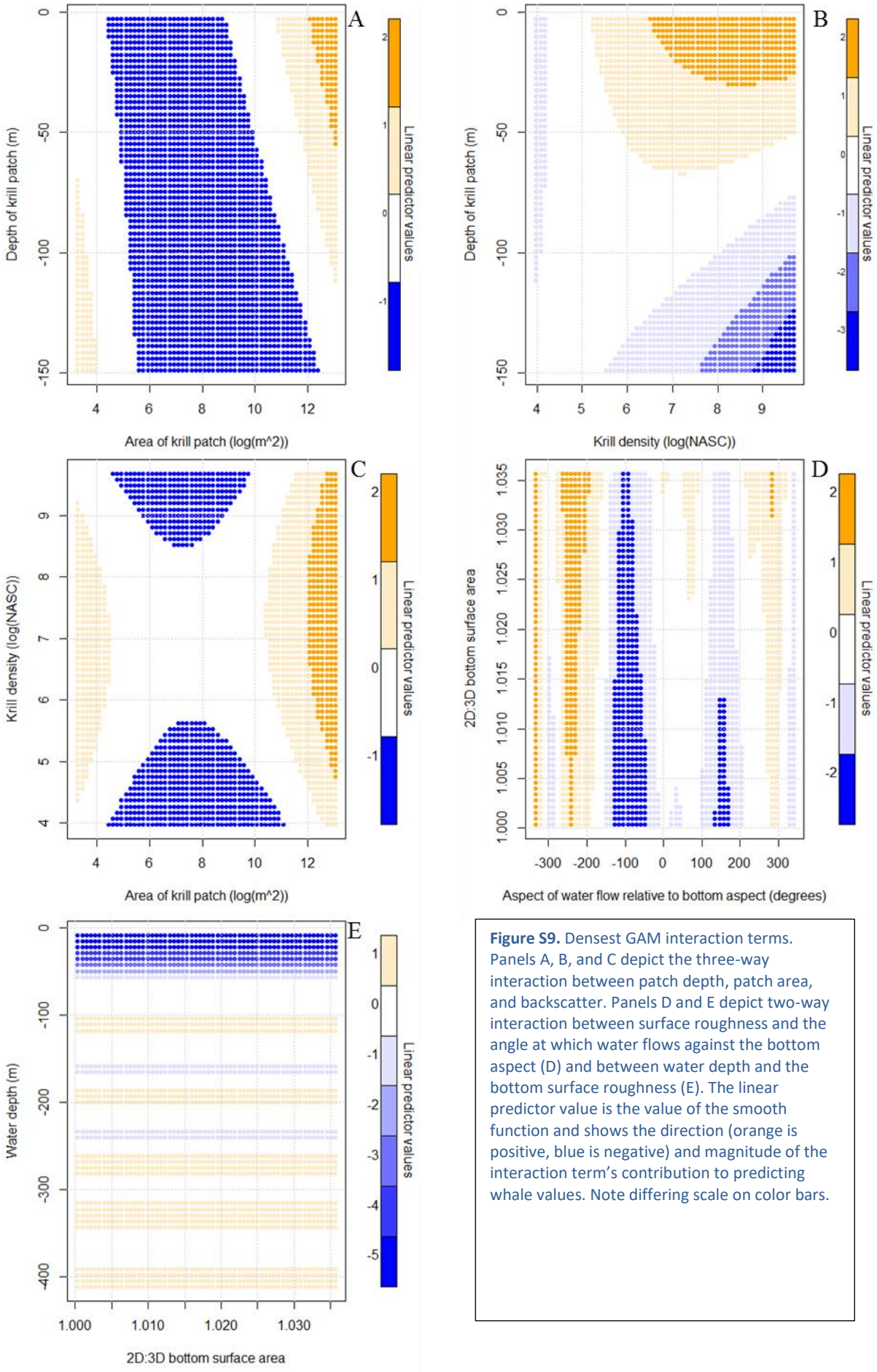

Figure S9. Densest GAM interaction terms. Panels A, B, and C depict the three-way interaction between patch depth, patch area, and backscatter. Panels D and E depict two-way interaction between surface roughness and the angle at which water flows against the bottom aspect (D) and between water depth and the bottom surface roughness (E). The linear predictor value is the value of the smooth function and shows the direction (orange is positive, blue is negative) and magnitude of the interaction term's contribution to predicting whale values. Note differing scale on color bars.

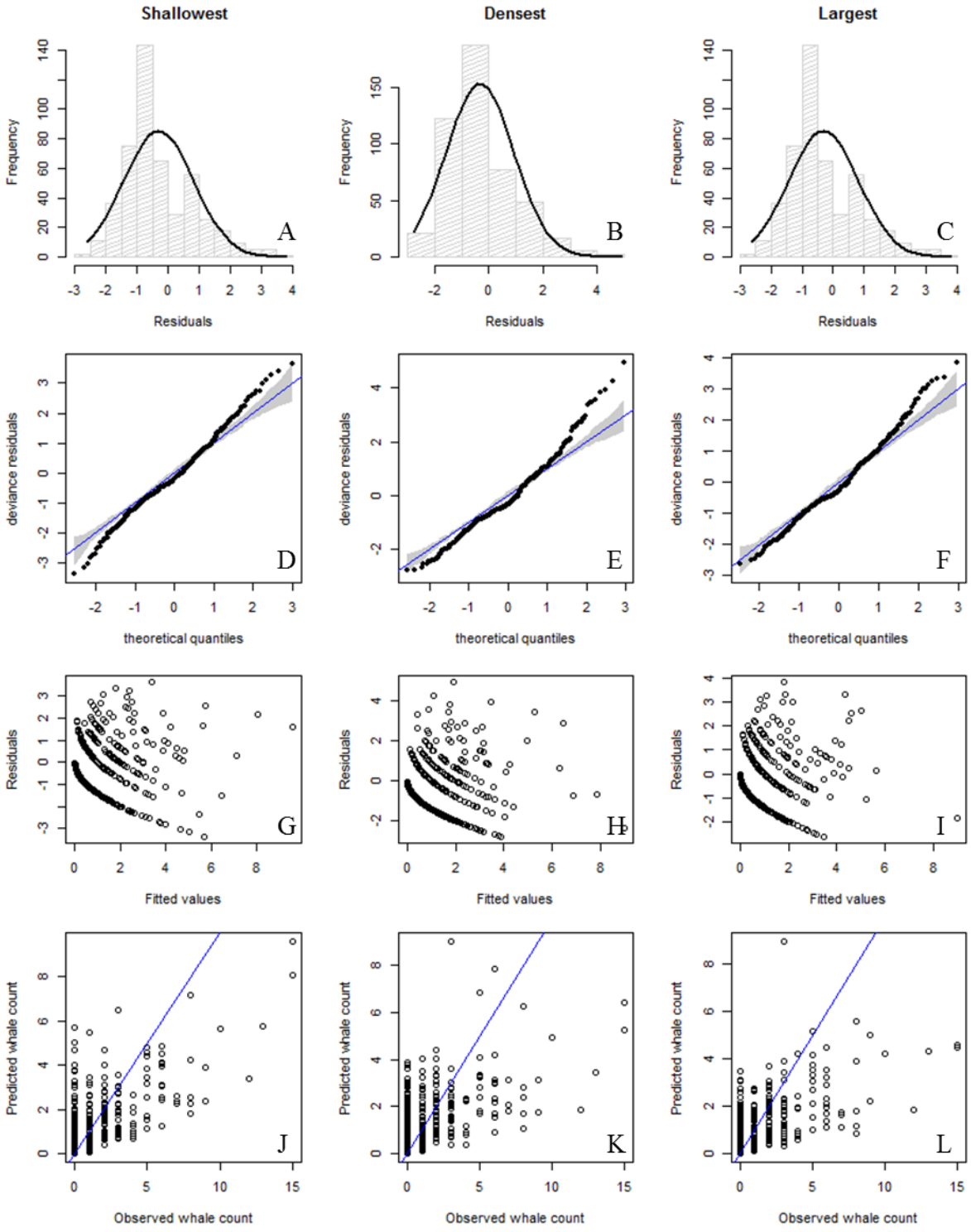

Figure S10. Evaluation of model residuals and model fit for the shallowest, densest and largest model. **A-F** show if the residuals have a normal distribution. The residuals were skewed to the left and did not have a normal distribution. **G-I** show whether the model exhibits homogeneity. There was some indication of a heterogeneic cone-shape, particularly in the densest and largest models. **J-L** shows the model's predictive power.